Title

CAL/APT Program: Test Results from Accelerated Pavement Test on Pavement Structure Containing Asphalt Treated Permeable Base (ATPB) Section 500RF

Authors

Harvey, John T.
du Plessis, Louw
Long, Fenella
et al.

Publication Date

1997-06-01

CAL/APT PROGRAM: TEST RESULTS FROM ACCELERATED PAVEMENT TEST ON PAVEMENT STRUCTURE CONTAINING ASPHALT TREATED PERMEABLE BASE (ATPB) SECTION 500RF

Report Prepared for

CALIFORNIA DEPARTMENT OF TRANSPORTATION

by

John T. Harvey, Louw du Plessis, Fenella Long, John A. Deacon, Irwin Guada, David Hung, Clark Scheffy

June 1997
Pavement Research Center
Institute of Transportation Studies
University of California, Berkeley

Technical Report Documentation Page

1. Report No. RTA-65W485-3	2. Government Accession No.	3. Recipient's Catalog No.
4. Title and Subtitle CAL/APT Program: Test Results From Accelerated Pavement Test On Pavement Structure Containing Asphalt Treated Permeable Base (ATPB)–Section 500RF		5. Report Date June 1997 6. Performing Organization Code
7. Authors John T. Harvey, Louw du Plessi, Fenella Long, John A. Deacon, Irwin Guada, David Hung and Clark Scheffy		8. Performing Organization Report No.
9. Performing Organization Name and Address Pavement Research Center: CAL\APT Program Institute of Transportation Studies University of California at Berkeley Berkeley, CA 94720		10. Work Unit No. 11. Contract or Grant No.
12. Sponsoring Agency Name and Address Division of New Technology and Research California Department of Transportation Sacramento, CA 94273-0001		13. Type of Report and Period Covered Interim Report, 1995-96 14. Sponsoring Agency Code
15. Supplementary Notes This 5 year project is being performed in cooperation with the US Department of Transportation, Federal Highway Administration		

16. Abstract. This report is the **second** in a series which describe the results of tests on full-scale pavements constructed at the Richmond Field Station (RFS) which have been designed and constructed according to Caltrans procedures. It contains a summary of the results and their interpretation of the Heavy Vehicle Simulator (HVS) tests on the *first* of *four* pavement test sections, an asphalt-concrete section containing an asphalt-treated permeable base (ATPB), designated section 500RF. The tests on the four test sections have been performed as part of Goal 1 of the CAL/APT Strategic Plan. Results of the test and their analysis indicate the following: 1 The HVS testing environment at the Richmond Field Station with respect to fatigue performance is more benign relative to moisture effects but provides a slightly more severe temperature environment than that which might be expected in natural California settings. 2. The importance of mix compaction on pavement performance has been conclusively demonstrated and the current Caltrans mix compaction specification has been shown to permit excessive air-void contents. Improved pavement performance that could result from tightening the specification has been demonstrated by the results obtained from Section 500RF. Such a change in the specification has the potential to result in large (and quantifiable) savings to the State. 3. The fatigue analysis and design system developed during the SHRP program and refined within the CAL/APT program has been used to explain the difference between the design estimate for Section 500RF of approximately 1×10^6 ESALs and the HVS measurement of approximately 112×10^6 ESALs. Although some of the discrepancy remains unaccounted for (possibly as a result of difficulties in modeling the bonding between the two lifts of asphalt concrete), the overall agreement helps to validate both the analysis and design system as a mechanism for structural design and the current Caltrans design methodology.
4. The weak bond observed between asphalt-concrete lifts in Section 500RF has been found to significantly degrade pavement performance. While the extent to which weak bonding may be prevalent in California pavements is unknown, the fact that the HVS test pavement was constructed according to standard Caltrans procedures suggests possible problems within pavements in service. If additional investigations confirm such possible problems, remedial action such as the application of suitable tack coats will result in significant improvements in pavement performance. 5. The Asphalt Institute's subgrade strain criterion for controlling subgrade rutting has been confirmed by the 500RF test. While additional validation is necessary, this criterion enables a mechanistic/empirical analysis of subgrade rutting to supplement routine Caltrans design procedures in special investigations. 6. Results of the 500RF test suggest that the Caltrans structural design procedure is conservative, presumably because it must accommodate a wide variety of mixes, climates, construction practices, etc. The likely result in many instances is overdesign. The economic consequences of this overdesign can, conceptually at least, be evaluated by life-cycle cost models. The analysis and design system, being developed and refined in part within the CAL/APT program, will provide a basis for more accurate structural designs compatible with acceptable levels of reliability.

17. Key Words Heavy Vehicle Simulator (HVS), asphalt concrete pavement, asphalt-treated permeable base, asphalt concrete, fatigue cracking, pavement performance		18. Distribution Statement No restrictions. This document is available to the public.	
19. Security Classif. (of this report) Unclassified	20. Security Classif. (of this page) Unclassified	21. No. of Pages 112	22. Price

DISCLAIMER

The contents of this report reflect the views of the authors who are responsible for the information and the accuracy of the data presented herein. The contents do not necessarily reflect the official views of policies of the California Department of Transportation or the Federal Highway Administration. The report does not constitute a standard, specification, or regulation.

FINANCIAL DISCLOSURE STATEMENT

This research has been funded by the Division of New Technology and Research of the State of California Department of Transportation (contract No. RTA-65W485). The total contract amount for the five year period (1 July 1994 through 30 June 1999) is $5,751,159. This report presents the results of the first HVS test completed in November 1995 on a pavement section containing asphalt treated permeable base. The report provides an analysis of the test results and conclusions which contain implications for Caltrans pavement design and pavement construction practices.

IMPLEMENTATION STATEMENT

Results of the first HVS test demonstrate the importance of mix compaction on pavement performance (both fatigue and permanent deformation) and the fact that the current Caltrans compaction specification permits excessive air-void contents at the time of pavement construction. Improved pavement performance that used results from tightening the specifications would result in very large, quantifiable savings to the State.

A weak bond was observed between the asphalt-concrete lifts in the section and was found to significantly degrade pavement performance. While the extent to which weak bonding may be prevalent in California pavements is unknown, the fact that the HVS test pavements were constructed according to standard Caltrans procedures suggests possible problems within pavements in service. If additional investigations confirm such problems, remedial action such as the application of suitable tack coats will result in significant improvements in pavement performance and, hence, reduction in cost. If weak bonding is pervasive, remedial action could result in huge savings.

ACKNOWLEDGMENTS

Financial support for this project was provided by the State of California Department of Transportation as part of the CAL/APT Project. Mr. Wesley Lum of the Division of New Technology and Research is the CAL/APT Project Manager and Mr. William Nokes, Office of Project Planning and Design, is the Contract Monitor for the University of California, Berkeley contact.

TABLE OF CONTENTS

LIST OF FIGURES

LIST OF TABLES

EXECUTIVE SUMMARY

This report is the **second** in a series which describe the results of tests on full-scale pavements constructed at the Richmond Field Station (RFS) which have been designed and constructed according to Caltrans procedures. It contains a summary of the results and their interpretation of the Heavy Vehicle Simulator (HVS) tests on the *first* of *four* pavement test sections, an asphalt-concrete section containing an asphalt-treated permeable base (ATPB), designated section 500RF. The tests on the four test sections have been performed as part of Goal 1 of the CAL/APT Strategic Plan (*1*).

One objective of the test program [described in Reference (*2*)] is to develop data to quantitatively verify existing Caltrans pavement design methodologies for Asphalt Treated Permeable Base (ATPB) pavements and conventional Aggregate Base (AB) pavements with regard to failure under trafficking at moderate temperatures (Goal 1), while preparing a uniform platform on which overlays (Goal 3 of the Strategic Plan) will be constructed which also will be trafficked. The objective of the program includes:

- quantification of the effective elastic moduli of the various pavement layers, based on an ad-hoc use of layered elastic analysis;
- quantification of the stress dependence of the pavement layers;
- determination of the failure mechanisms of the various layers; and
- determination and comparison of the fatigue lives of the two types of pavement structure.

HVS loading on this pavement section was initiated in May 1995 and completed in early November 1995 after the application of more than 2.5×10^6 load repetitions. The first load

associated (fatigue) cracks were observed at approximately 650,000 load repetitions. At 2.57×10^6 load repetitions cracking had reached a level which, according to Caltrans pavement management criteria, resembled a newer pavement that had failed by alligator cracking. The average maximum vertical rut depth at the centerline of the test section at this point was 15 mm, considered failure due to rutting by Caltrans criteria. It was noted that the cracks were hairline (less than 1/32 inch) and pumping was not observed in contrast to typical field sections.

Chapter 2 describes the test program for section 500RF. The test section, designed according to Caltrans procedures (*3*) for a Traffic Index of 9.0 (1.0 million ESALs), consists of a clay subgrade, aggregate subbase (ASB), aggregate base (AB), the ATPB, and asphalt concrete (AC). Design thicknesses of the pavement components are: ASB-229 mm (0.75 ft); AB-183 mm (0.60 ft); ATPB-76 mm(0.25 ft); and AC-137 mm (0.45 ft). Actual thicknesses at the loading site of the AB and ATB are close to the design values while the ASB is 137 mm (0.45 ft) and the AC is 150 mm (0.49 ft).

Table 2.1 summarizes the data collection program for section 500RF. Loading, applied by dual bias-ply tires inflated to a pressure of 690 kPa (100 psi), consisted of 150,000 repetitions of a 40 kN (9000 lb) load followed by 50,000 repetitions of a 80 kN (18,000 lb) and then by about 2.37 million repetitions of a 100 kN (22,500 lb) load. At the termination of loading, about 2.57 million total repetitions, fatigue cracking was visible throughout the test section. Lateral wander of the wheels over the one meter (3.3 ft) width of the section was programmed as seen in Figure 2.4.

Pavement response measurements were obtained using Multi-Depth Deflectometers (MDDs), the Road Surface Deflectometer (RSD), the laser profilometer, and a straight edge. Fatigue crack development was monitored using photographs. Thermocouples were used to

measure the air temperature and pavement temperatures at various depths in the asphalt concrete. Chapter 3 summarizes the data obtained during the course of loading.

A significant observation reported in Chapter 3 is that cracking appears to have occurred in only the top lift of the AC layer. Moreover, it was observed from a limited coring program that there appeared to be little or no bond between the two lifts used to achieve the constructed thickness of the AC layer. In addition, measurements indicate that the lower AC lift was compacted to an average air void content of 3.9 percent while the upper lift was not as well compacted, i.e. an average air void content of about 6.5 percent.

The 2.57 million repetitions actually applied to test section 500RF corresponds to about 112 million ESALs (based on the Caltrans load equivalency factor of 4.2). Chapter 4 provides a detailed analysis of the test results using multilayered elastic analysis to explain the observed behavior.

Results of the analysis reported in Chapter 4 indicate a rather good correspondence between the Caltrans design estimate of approximately 1,000,000 ESALs and the HVS test measurement of approximately 112,000,000 ESALs. The major impediment to reconciling these two estimates seems to be the inability to accurately quantify effects of the layer interface condition. The following findings of this aspect of the study are considered to have been reasonably well demonstrated and to represent appropriate hypotheses for future inquiry and validation:

1. The protected environment of HVS testing at the Richmond Field Station is different from that experienced in natural California settings. With regard to fatigue distress, the moisture environment is likely to be more benign in the testing enclosure at RFS while

the temperature environment is slightly more severe than comparable, unprotected locations for the 500RF test.

2. Based on the performance of Section 500RF under accelerated HVS loading, Caltrans flexible pavement designs for TI=9.0 pavements with ATPB layers that are relatively undamaged by water appear to be reasonably reliable, eliminating the risk of premature fatigue failure by providing reliability levels up to 90 percent or more. At the same time, some specific conditions have been identified in prior analysis where California pavement designs may be particularly susceptible to fatigue cracking (*9*).

3. Fatigue life measurements under full-scale accelerated loading are typically expected to exceed design estimates because design estimates must incorporate a safety factor to minimize the risk of premature failure while accommodating, at the same time, expected variabilities in testing, in construction, in traffic, and in mix design. For a design reliability level of 90 percent, the computed ratio of simulated HVS ESALs to design ESALs estimated using the fatigue analysis and design system was approximately 3.7.

4. The mixture fatigue analysis and design system proved to be an effective tool for explaining fatigue performance of the HVS pavement. The relatively good agreement between the simulation estimate and actual HVS measurement suggests that the analysis and design system may eventually prove useful for structural design as well as for mixture design. The analysis suggests no need for recalibrating the analysis and design system based on the performance of this HVS test pavement.

5. According to the Asphalt Institute's subgrade strain criterion, severe subgrade rutting in the HVS pavement would not be expected. Testing of HVS Section 500RF generally confirmed the Asphalt Institute's criterion.

6. The analysis reported herein corroborates prior work showing the importance of good compaction of the asphalt concrete surface to superior fatigue performance. Good compaction of the mix also reduces the magnitude of subgrade rutting.
7. Loss of bonding at the interface between asphalt-concrete lifts can cause a significant degradation in fatigue life and an increase in subgrade rutting.
8. Different mixes, even with similar binders, can result in significantly different fatigue performance. The importance and effectiveness of laboratory fatigue testing and simulation to quantitatively estimate differences in fatigue performance in-situ was demonstrated by the analyses presented in Chapter 4.

Chapter 5 provides the conclusions which are as follows:

1. The HVS testing environment at the Richmond Field Station with respect to fatigue performance is more benign relative to moisture effects but may provide a slightly more severe temperature environment than that which might be expected in natural California settings.
2. The importance of mix compaction on pavement performance has been conclusively demonstrated and the current Caltrans mix compaction specification has been shown to permit excessive air-void contents. Improved pavement performance that could result from "tightening" the specification has been demonstrated by the results obtained from Section 500RF. Such a change in the specification has the potential to result in large (and quantifiable) savings to the State.

3. The fatigue analysis and design system developed during the SHRP program and refined within the CAL/APT program has been used to explain the difference between the design estimate for Section 500RF of approximately 1×10^6 ESALs and the HVS measurement of approximately 112×10^6 ESALs. Although some of the discrepancy remains unaccounted for (possibly as a result of difficulties in modeling the bonding between the two lifts of asphalt concrete), the overall agreement helps to validate both the analysis and design system as a mechanism for structural design and the current Caltrans design methodology.
4. The weak bond between asphalt-concrete lifts in Section 500RF has been found to significantly degrade pavement performance. While the extent to which weak bonding may be prevalent in California pavements is unknown, the fact that the HVS test pavement was constructed according to standard Caltrans procedures suggests possible problems within pavements in service. If additional investigations confirm such possible problems, remedial action such as the application of suitable tack coats will result in significant improvements in pavement performance.
5. The Asphalt Institute's subgrade strain criterion for controlling subgrade rutting has been confirmed by the 500RF test. While additional validation is necessary, this criterion enables a mechanistic/empirical analysis of subgrade rutting to supplement routine Caltrans design procedures in special investigations.
6. Results of the 500RF test suggest that the Caltrans structural design procedure is conservative, presumably because it must accommodate a wide variety of mixes, climates, construction practices, etc. The likely result in many instances is overdesign. The economic consequences of this overdesign can, conceptually at least, be evaluated by life-cycle cost models. The analysis and design system, being developed and refined is

part within the CAL/APT program, will provide a basis for more accurate structural designs compatible with acceptable levels of reliability.

CHAPTER 1

INTRODUCTION

This report is the **second** in a series which describe the results of tests on full-scale pavements constructed at the Richmond Field Station (RFS) which have been designed and constructed according to Caltrans procedures. It contains a summary of the results and their interpretation of the Heavy Vehicle Simulator (HVS) tests on the first of four pavement test sections, an asphalt-concrete section containing an asphalt-treated permeable base (ATPB), designated section 500RF.

HVS loading on this pavement section was initiated in May 1995 and completed in early November, 1995 after the application of more than 2.5×10^6 load repetitions. The tests on the four test sections are being performed as part of Goal 1 of the CAL/APT Strategic Plan (*1*).

The first report in this series, entitled: *Initial CAL/APT Program: Site Information, Test Pavements Construction, Pavement Materials Characterizations, Initial CAL/HVS Test Results, and Performance Estimates* contains detailed information on the construction details as well as results of tests to define the properties of the various pavement components of the four pavement test sections (*2*). To minimize the length of this report, information utilized herein and contained in the above noted report will only be referenced.

1.1 BACKGROUND AND OBJECTIVES

The test results described herein are the first from a series of tests on four pavement test sections described in the experimental test plan for completion of Goals 1 and 3 of theStrategic Plan for Phase II of the CAL/APT Program (1). One objective of this test plan, described in

Reference (2) is to develop data to quantitatively verify existing design methodologies for Asphalt Treated Permeable Base (ATPB) pavements and conventional Aggregate Base (AB) pavements with regard to failure under trafficking at moderate temperatures (Goal 1), while preparing a uniform platform on which overlays (Goal 3) will be constructed which also will be trafficked. This objective includes:

- quantification of the effective elastic moduli of the various pavement layers, based on an ad-hoc use of layered elastic analysis;
- quantification of the stress dependence of the pavement layers;
- determination of the failure mechanisms of the various layers; and
- determination and comparison of the fatigue lives of the two types of pavement structure.

This report together with the reports on each of the four sections, associated special reports and a final report will complete this test plan objective and the work included in Goal 1 of the Strategic Plan CAL/APT.

1.2 PURPOSE AND SCOPE

The scheduled sequence of HVS testing of the four test sections is: drained ATPB site (500RF), undrained AB site (501RF), drained ATPB site (502CT), and undrained AB site (503RF). The purpose of this report is to present the results of tests on Section 500RF. The information is presented herein in as brief a form as possible but in sufficient detail to provide a basis for the recommendations which result from this initial test, recommendations which suggest changes be made in Caltrans' construction and construction control procedures.

1.3 ORGANIZATION OF REPORT

Chapter 2 of the report contains a complete description of the test program performed on Section 500RF, including the loading sequence, instrumentation, and data collection scheme. Chapter 3 presents a summary and discussion of the data collected during the test including pavement performance and temperatures. In Chapter 4 the actual pavement performance is then compared with the fatigue life predicted for the test section by the Caltrans thickness design procedure. Analyses are presented which attempt to provide an explanation for the substantially longer fatigue life exhibited by the test section as compared to that for which it was designed. Analyses are also presented which demonstrate how an even longer fatigue life could have potentially been obtained. Chapter 5 summarizes the results of the test. Conclusions regarding the performance of the pavement are presented which reflect the analyses presented in Chapter 4. Based on the conclusions, recommendations are made for changes to Caltrans construction requirements to improve asphalt concrete pavement performance.

CHAPTER 2

TEST PROGRAM

2.1 TEST SECTION LAYOUT

The test pavement is approximately 70 m (231 ft) long by 8 m (26 ft) wide and consists of two pavement sections, one drained and the other undrained, Figure 2.1. Test site 500RF is one of the drained sections, meaning that it includes a layer of asphalt treated permeable base (ATPB). The grade along the length of the test pavement is 0.75 percent to the south, with a transverse cross-slope of 2.0 percent to the east. Each test section is 8 m (26.4 ft) long by 1 m (3.3 ft) wide and is subdivided into sixteen 0.5 m long by 1.0 m wide subsections, distinguished by markers numbering 0 to 16.

The pavement structure (Figure 2.2) was designed following Caltrans procedures (*3*) and consists of a clay subgrade (AASHTO A-7-6), aggregate subbase (ASB), aggregate base (AB), the ATPB, and asphalt concrete (AC). A summary of the construction control data for this section is contained in Reference (*2*). For this pavement the design thickness of the ASB is 229 mm; however, due to the longitudinal slope of the subgrade and the 2 percent cross-slope across the test pavement, the thickness of the ASB varied from 125 mm (0.40 ft) on the north end to 305 mm (1.0 ft) on the south end. At section 500RF, the subbase thickness is 137 mm (0.45 ft). The design thicknesses of the other pavement components are: AB, 183 mm (0.60 ft); ATPB, 76 mm (0.25 ft); and AC, 137 mm (0.45 ft). Exact layer thicknesses of each of the HVS test sites will be determined from measurements in test pits after the overlay testing is completed. Construction measurements and data from several cores next to 500RF indicate that the AB and ATPB

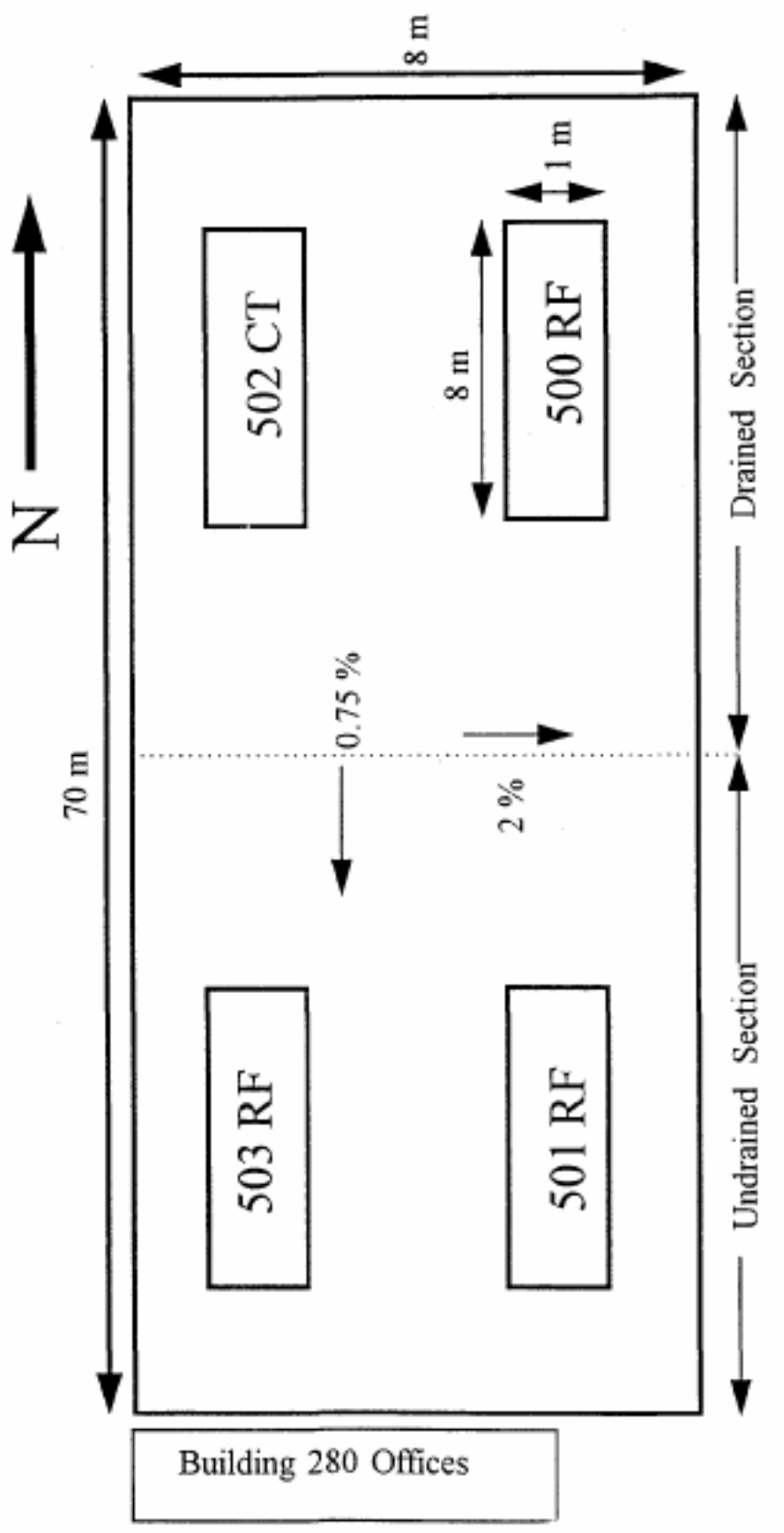

Figure 2.1 Test Pavement at Richmond Field Station with Test Sections

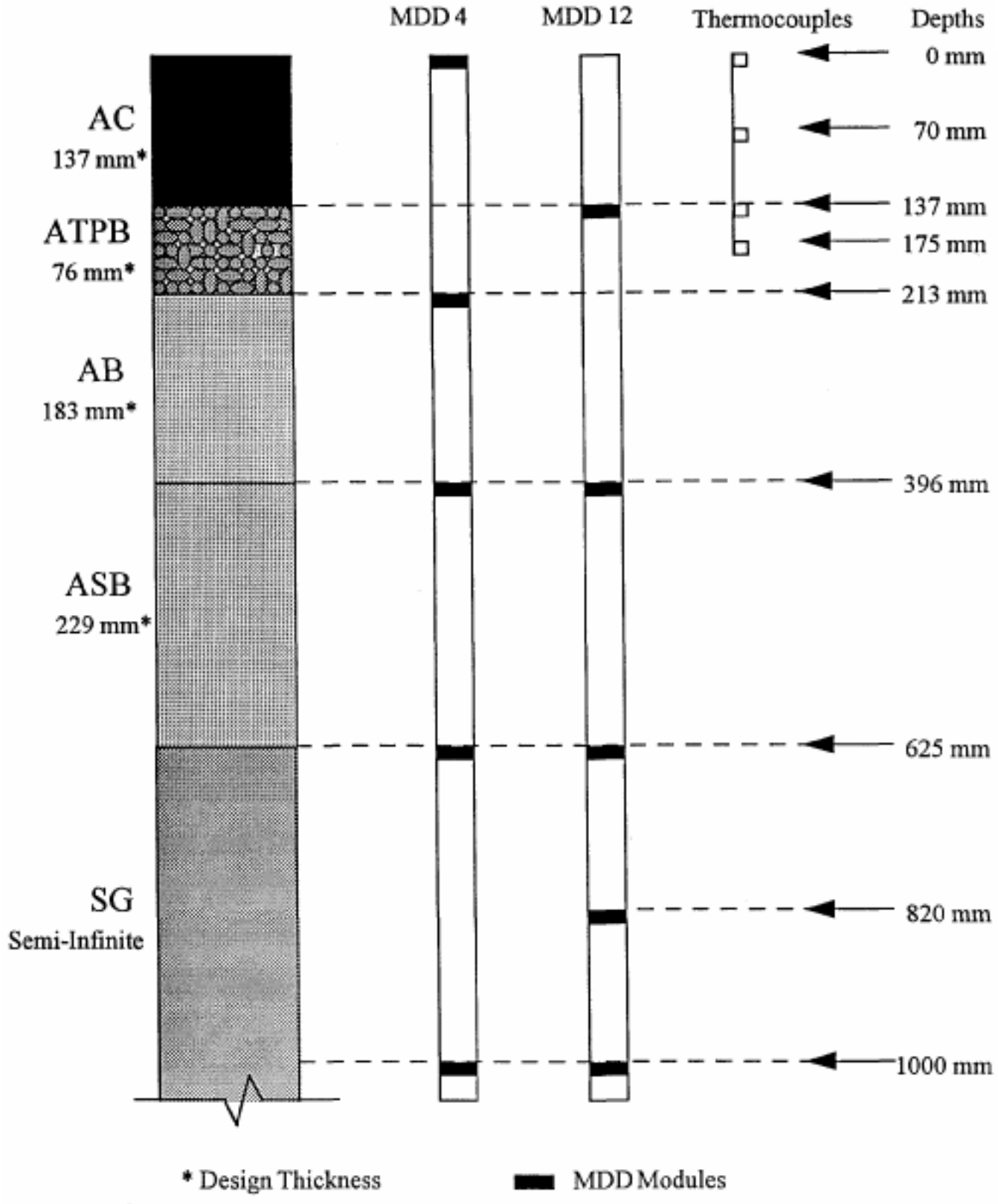

Figure 2.2 500RF Pavement Structure with MDD and Thermocouple Positioning

thicknesses are approximately equal to the design thicknesses, and the thickness of the AC is about 150 mm.

2.2 TEST PROGRAM

The HVS test program followed for section 500RF is summarized in Table 2.1. This table shows the data collection schedule during the course of the test. Depths at which the multidepth deflectometers (MDDs) and thermocouples were placed are shown in Figure 2.2, while their locations on the surface of the test section are shown in Figure 2.3. Positions at which deflections were measured with the road surface deflectometer are also shown in Figure 2.3. As will be noted in Table 2.1, intervals between measurements, in terms of load repetitions, were selected to insure adequate characterization of the pavement as damage developed.

2.2.1 Loading Program

For this experiment the HVS was equipped with dual truck tires, representing one-half of a single axle. Load is applied through two Goodyear bias-ply truck tires inflated to a pressure of 690 kPa (100 psi).

The test wheel trafficks the length of the 8 m test section. Lateral wander over the 1 m (3.3 ft) width of the test section is programmed, as shown in Figure 2.4, to simulate traffic wander on a typical highway lane [3.7 m (12 ft) wide][1]. The one square meter areas

[1]Appendix A contains a discussion of the lateral load distribution (wander) used in this test.

Table 2.1 Data Collection Program for Test Section 500RF

Repetitions	Trafficking Load kN	Rut Profiles	MDD				RSD											
							Centerline				200 mm Left[1]				200 mm Right[1]			
			Test Wheel Load, kN				Test Wheel Load, kN				Test Wheel Load, kN				Test Wheel Load, kN			
			40	60	80	100	40	60	80	100	40	60	80	100	40	60	80	100
10	40	X	X				X				X				X			
10,000 to 50,000 (10,000 incr)	40	X	X				X				X				X			
100,000	40	X	X				X				X				X			
125,000	40	X	X				X				X				X			
150,000	40680	X	X	X	X		X	X	X		X	X	X		X	X	X	
175,000	80	X	X		X		X		X		X		X		X		X	
200,000	806100	X	X	X	X	X	X	X	X	X	X	X	X	X	X	X	X	X
225,000	100	X	X			X	X			X	X			X	X			X
250,000	100	X	X		X		X		X		X		X		X		X	
300,000 to 800,000 (50,000 incr)	100	X	X			X	X			X	X			X	X			X
Crack appearance (647,499)	100	X	X		X	X	X		X	X	X		X	X		X	X	X
800,000 to 2,100,000 (50,000 incr)	100	X	X			X	X			X								
850,000 to 2,100,000 (100,000 incr)	100	X	X			X												
2,100,000 to Final (100,000 incr)	100	X	X			X	X			X								
Final (2,572,732)	100	X	X	X	X	X	X	X	X	X	X	X	X	X	X	X	X	X

[1] Looking in direction of increasing longitudinal reference points (0-16)

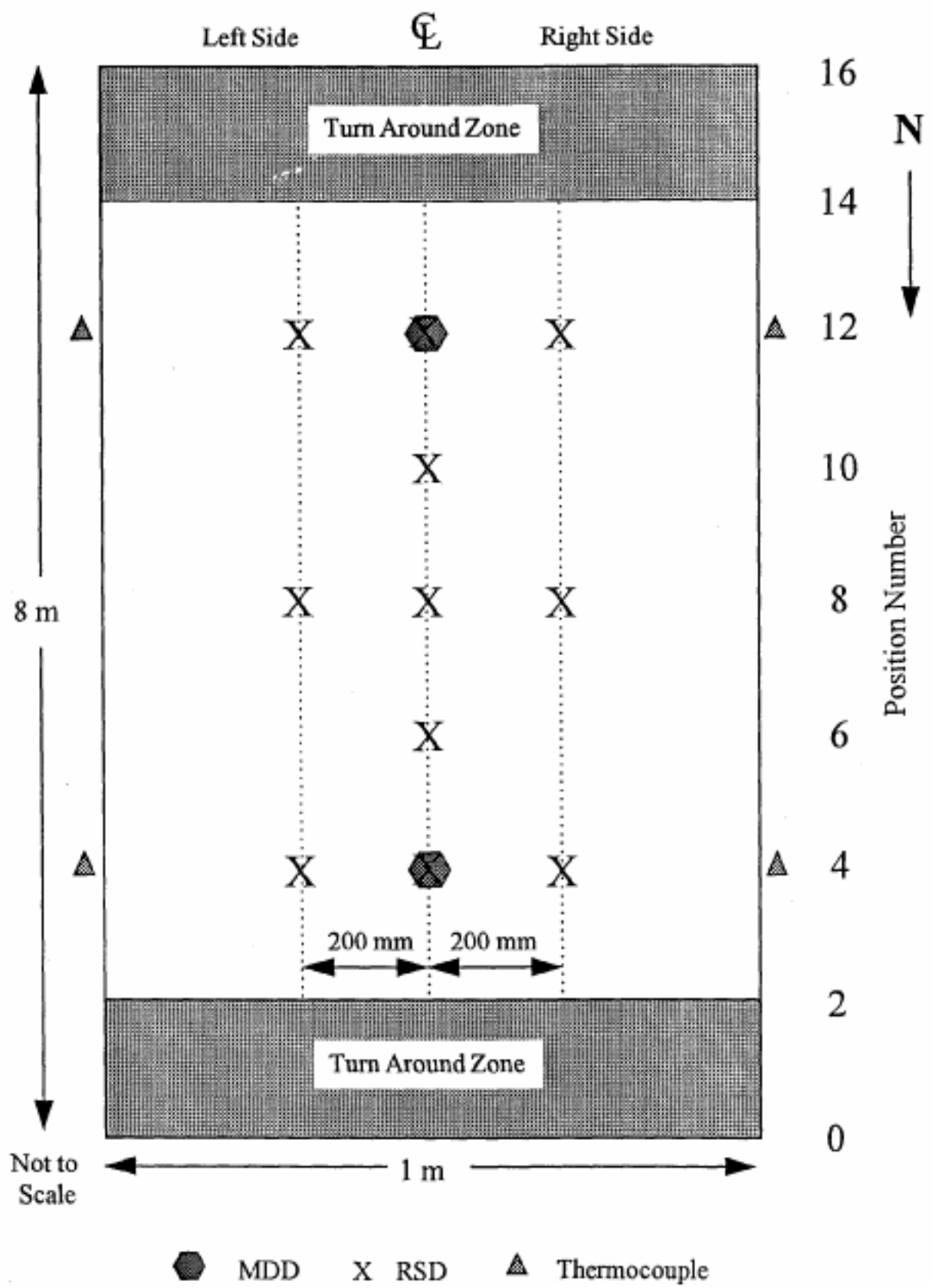

Figure 2.3 Plan View of Test Section and Location of Instruments for Data Collection

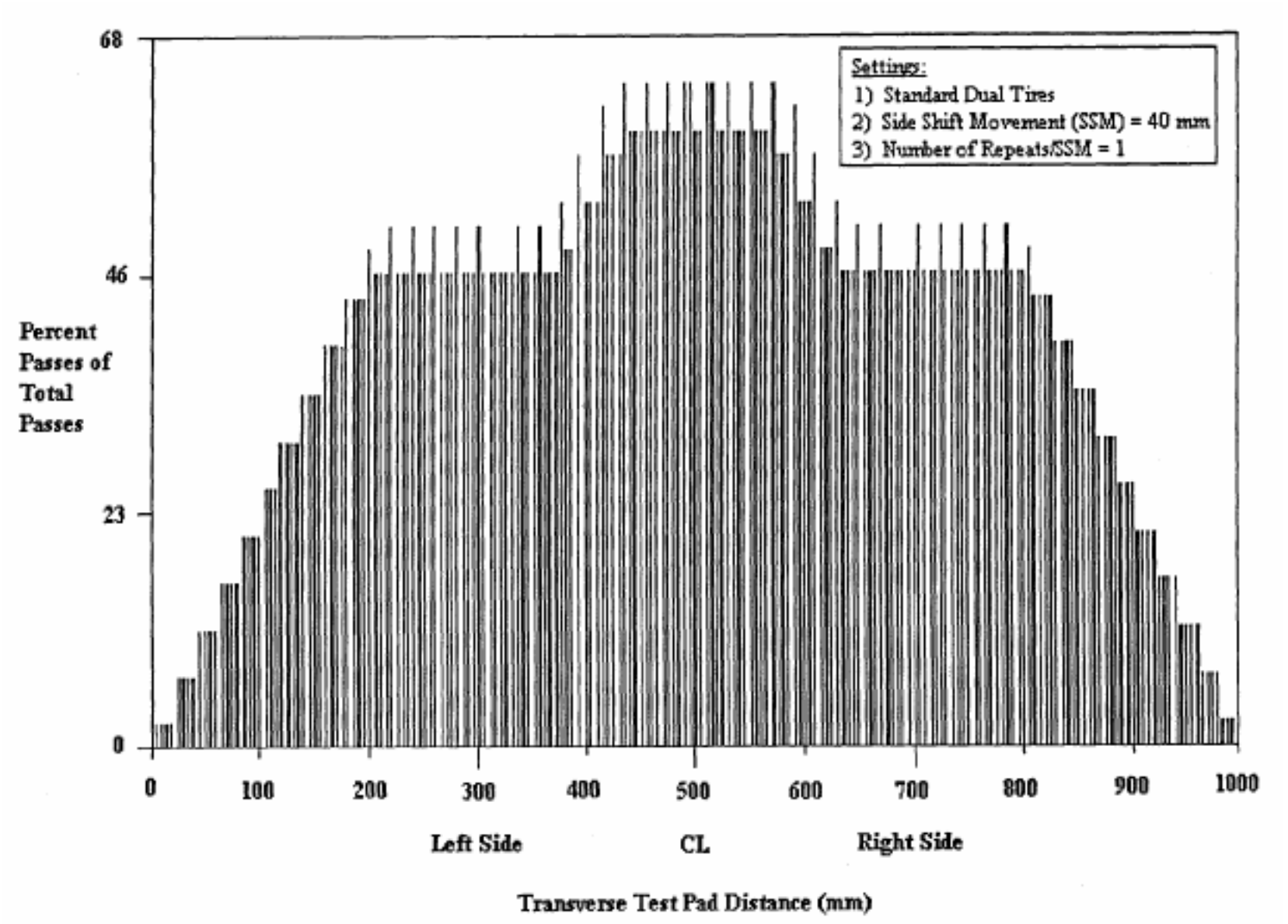

Figure 2.4 Transverse Load Distribution for HVS

at both ends serve as turnaround zones in which the test wheel decelerates and accelerates; the 6 m length between reference points 2 and 14 is the portion of the test section in which performance is evaluated.

As seen in Table 2.1, a load of 40 kN was used to traffic the section for the first 150,000 repetitions to prevent excessive damage to the newly constructed asphalt concrete. After 150,000 repetitions, the load was increased to 80 kN for 50,000 repetitions. From 200,000 repetitions the trafficking load was increased to 100 kN; this load was maintained for the remainder of the test to accelerate pavement cracking. A total of 2.57 million repetitions were applied before termination of trafficking, at which time cracking was visible throughout the test section.

2.2.2 Measurements

To evaluate pavement response during HVS testing of section 500RF, measurements were obtained using the Multi-Depth Deflectometer (MDD), the Road Surface Deflectometer (RSD), the laser profilometer, and a straight edge. Fatigue crack development was monitored using photographs. Thermocouples were used to measure the air temperature and pavement temperatures at various depths in the asphalt concrete. Detailed descriptions of the instrumentation and the various measuring equipment are included in References (*2*) and (*4*)

RSD surface deflection data were obtained at the reference points shown in Figure 2.3 along the centerline of the section and at locations 200 mm (8 in.) on each side of the centerline. These latter measurements, taken off of the centerline where the wander pattern results in fewer load applications, assist in characterizing the full test section.

Measurements of transverse surface rut depth at each longitudinal reference point using the laser profilometer, which records data every 9 mm over a total transverse distance of 2.3 m [7.5 ft], permit determination of:

- the location and magnitude of the maximum rut
- the average rut which occurred throughout the test section, and
- the rate of permanent deformation, or rut rate.

Permanent deformations occurring in the layers during the course of loading are measured using the MDDs at the two locations shown in Figure 2.3. The surface deflection measured at MDD4 provides a check on the RSD deflection measured at this point.

All pavement temperature measurements using the thermocouples (locations shown in Figures 2.2 and 2.3) were obtained at one-hour intervals during HVS operation. Air temperatures near the test section were recorded at the same intervals and at the time of data collection.

Visual observation of surface distress was primarily directed to the identification and demarcation of surface cracks as well as measurements of their lengths.

It should be noted that at the conclusion of testing of the overlaid section 500RF a trench will be dug to allow visual inspection and measurement of all the layers and to obtain material for laboratory testing. This will provide essential data and clarify any inconsistencies generated during the test.

2.3 ENVIRONMENTAL CONDITIONS

Temperature has an important influence on the fatigue performance of a pavement. Accordingly, it was desired that the pavement surface temperature not exceed about 24°C (75°F)

to minimize rutting in the AC, and not go below about 16°C (61°F) in order to accelerate fatigue damage.

Building 280 at the RFS is a warehouse type of structure. On occasion, heat trapped inside the building raised the temperature above that observed outside. On hot days the outside temperatures were amplified and extended in the afternoon; however, during the morning hours lower temperatures were not increased by direct sunlight, delaying the warming of the test section. To maintain a fairly constant temperature, fans and heat lamps were used in an attempt to cool and warm the section as necessary to maintain a fairly constant temperature of about 20°C (67°F). Recognizing that improved temperature control for subsequent tests was extremely desirable, a refrigeration unit and temperature control cabin, or "cold box," were installed on the HVS after the test on Section 500RF had been completed.

Except for direct rainfall onto the surface, since the test sections are within Building 280, the pavement test sections at the RFS are subjected to water conditions much like actual roads. Water can accumulate underneath the pavement due to lateral movement of water from outside the building and fluctuations in the water table. Initially, during the rainy season of 1994-95 and before construction of the first test pavements, excessive water penetrated into the building from the west side. To mitigate the influence of this water on the test pavements a drainage system was installed around the outside of the building. The drainage system built into the test pavements is described in detail in Reference (*2*).

CHAPTER 3

DATA SUMMARY: TEMPERATURES, PERMANENT DEFORMATIONS, ELASTIC DEFLECTIONS, CRACKING

This chapter provides a summary of the data obtained as well as a brief discussion of the results. Interpretation of the data in terms of pavement performance is discussed in Chapter 4.

3.1 TEMPERATURES

Temperatures were recorded at several locations as noted in Chapter 2. The air temperatures for the entire testing period (3 May 1995 to 8 November 1995) ranged from 13°C to 36°C.

Temperature data obtained at different depths in the pavement are important for analysis of the performance of the HVS test sections, and its translation to field conditions. The relation between air temperatures and pavement temperatures also can be used to calibrate pavement temperature prediction models so that in-situ performance around the state can be properly evaluated.

The temperature at a depth of 50 mm (2 in.) is critical for evaluation of permanent deformation performance, as this is approximately the depth at which critical shear stresses occur under typical in-situ loading (*5*). The temperature on the underside of the asphalt concrete is important for the evaluation of fatigue cracking performance (*6*) since this is where the maximum value of tensile strain is assumed to occur. Temperature gradients throughout the

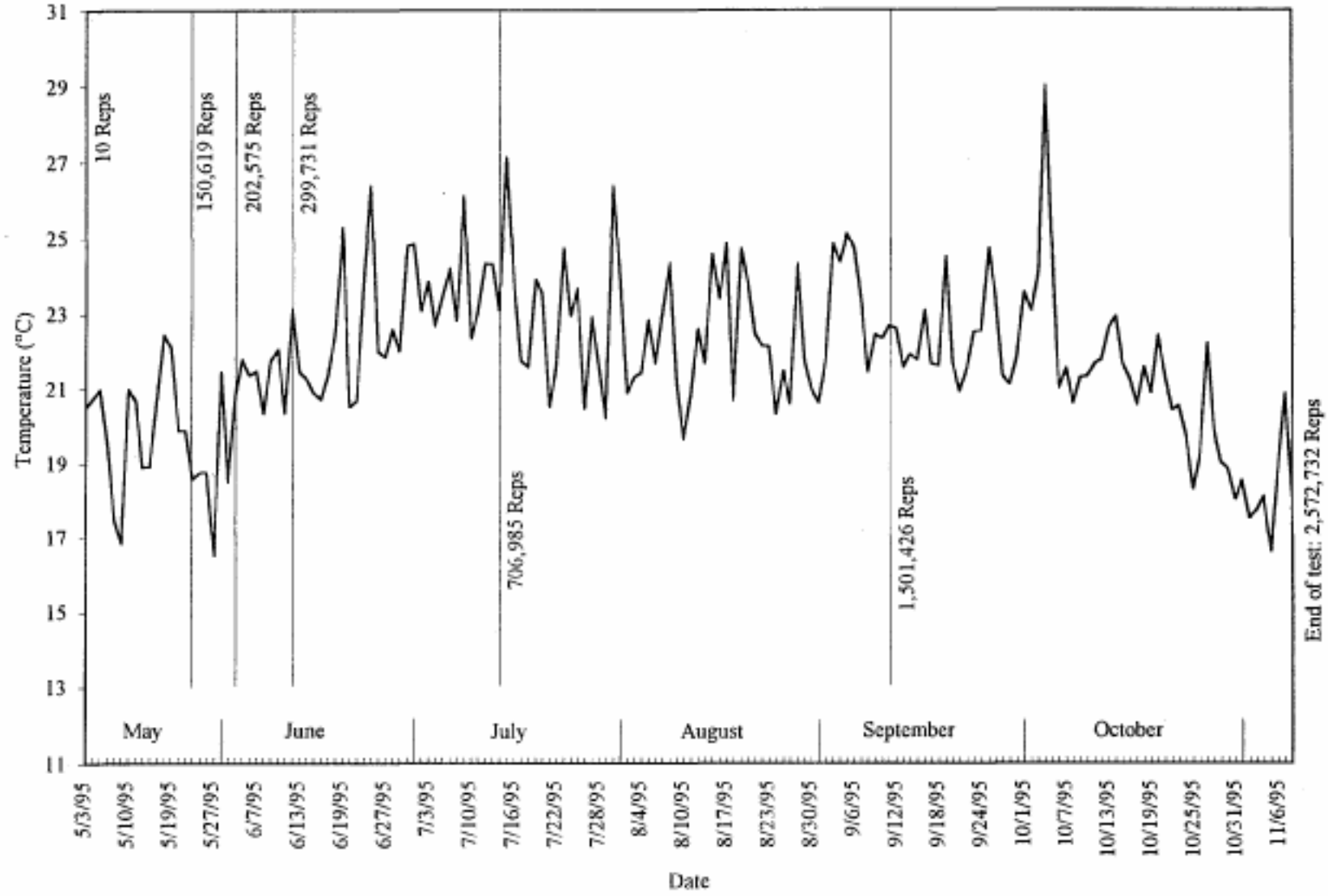

Figure 3.1 Daily Average Air Temperature for the Entire Testing Period of Section 500RF

asphalt concrete are also required for the evaluation of temperature effects on pavement performance (*7*).

3.1.1 Air

The average daily air temperature data are graphically presented in Figure 3.1. The daily averages are calculated from the hourly temperatures taken during HVS operation. The average air temperature varied from 16.5°C (recorded on 27 May 1995) to 29°C (recorded on 4 October 1995). From the figure, it is evident that air temperatures during the testing period experienced weekly variations. For instance, the average air temperature for 15 July 1995 was 27.1°C, but 7 days later the average air temperature was 21.5°C. However, the air temperature for the majority of test 500RF varied between 20°C and 25°C.

Overall, there was a warming trend from May through the end of June and slight cooling in the month of July. The average air temperature leveled off and remained fairly constant for the months of August and September and eventually dropped during October and November as seen in Figure 3.1.

In addition to the daily average, air temperature data were divided into four 6-hour intervals to illustrate temperature variation during the day. In the first interval, all the temperatures collected at the end of hour 0100 to the end of hour 0600 were averaged. The other periods, 0700 to 1200 hours, 1300 to 1800 hours, and finally 1900 to 2400 hours, were averaged in a similar manner. The average temperatures for each of the intervals for the entire test period are presented in Table 3.1. The lowest air temperatures occurred during 0100 hours to 0600 hours (19.3°C average) and the highest during 1300 hours to 1800 hours (25.1°C average).

Table 3.1 Average Temperature (Deg C) of 6-Hour Intervals for Air, Surface, and In-Depth Levels

	Air	Surface	50 mm*	70 mm	137 mm	175 mm
Hours 0100-0600	19.3	23.8	24.2	24.3	24.6	24.6
Hours 0700-1200	21.3	23.4	23.5	23.6	23.8	24.0
Hours 1300-1800	25.1	25.3	25.2	25.0	24.7	24.7
Hours 1900-2400	21.3	24.7	24.9	25.0	25.0	24.9
Maximum** Difference	5.8	1.9	1.7	1.4	1.2	0.9

*temperatures at this depth are interpolated
**difference between minimum and maximum 6-hour interval averages

The “maximum difference” data in Table 3.1 show that pavement temperatures did not fluctuate as much as air temperatures throughout each day. The maximum variation was 1.9°C for the surface level while the air temperature experienced a maximum variation of 5.8°C. The morning intervals (0100 hours to 1200 hours) experienced lower temperatures, averaging 23.6°C, than the evening intervals (1300 hours to 2400 hours), which averaged 25.0°C. Table 3.1 also shows that the warming of the pavement surface lagged behind the rise in air temperature. Air temperatures start to increase after the morning (0100-0600 hours), while surface temperatures continue to decrease during that same period. Eventually, the surface temperatures increase after 0700-1200 hours.

3.1.2 Surface

Daily averages of the surface temperature are shown in Figure 3.2. These temperatures have a more pronounced warming and cooling trend than do the daily average air temperatures, and the surface temperatures were greater on average than were air temperatures. There was again a warming period from May to the middle of July and cooling thereafter until the end of August. Surface temperatures experienced a slight warming trend in the month of September unlike the daily average air temperature which remained fairly constant.

Table 3.2 presents the average temperatures for four periods during the test, which had trends of warming, slight cooling, constant, and cooling temperatures, respectively from the beginning to the end of the test. It can be seen that regardless of the trend in temperature, the average temperature at the surface is higher than the average air temperature.

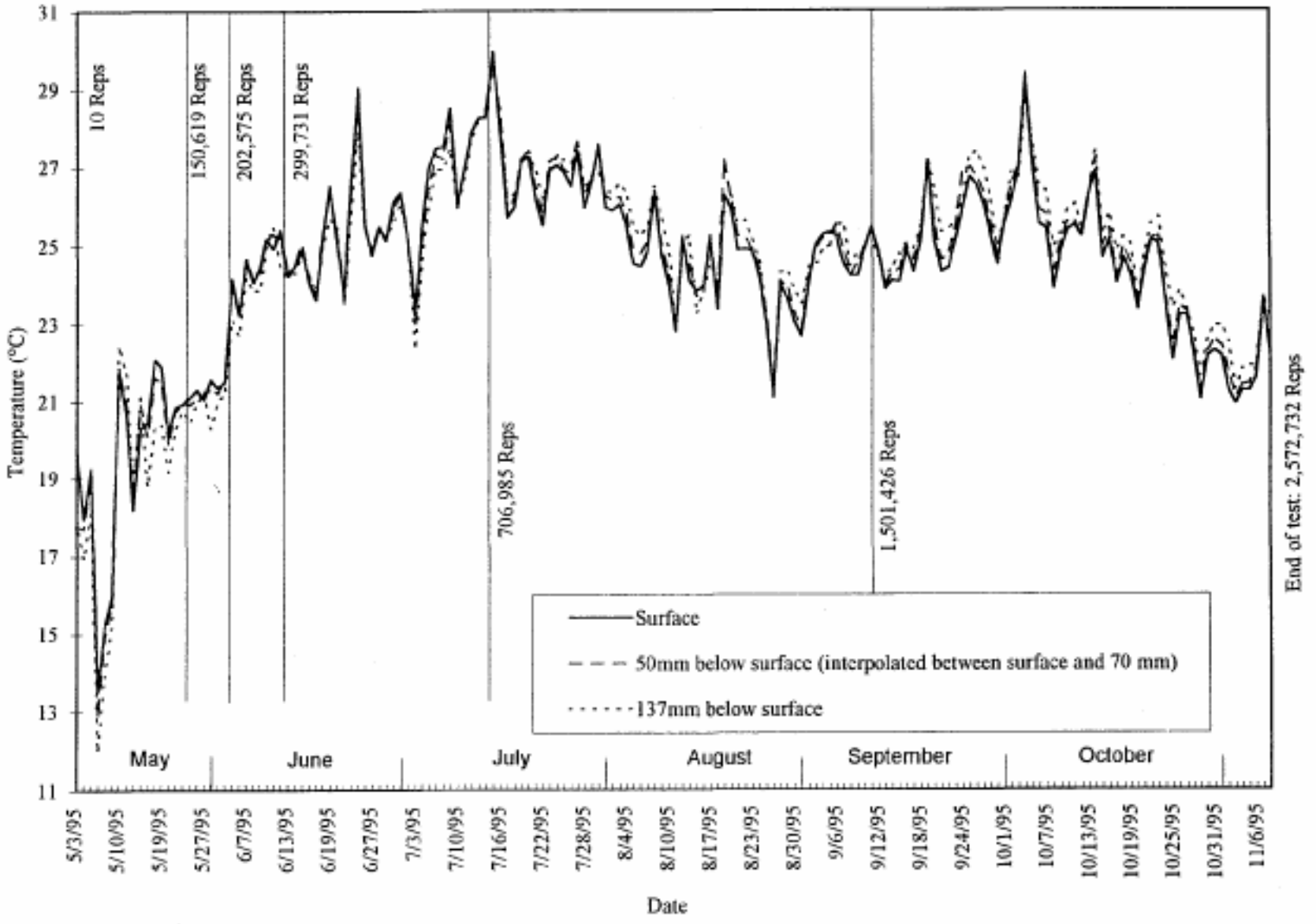

Figure 3.2 Daily Average Temperature at Surface, 50 mm, and 137 mm Below Surface for the Entire Testing Period

Table 3.2 Average Daily Temperature and Temperature Gradient for all Levels at Different Temperature Trends (N.B. negative number indicates temperature decreases with depth)

Trends, Dates, and Repetitions	Warming 5/3/95 to 7/15/95 10 to 718,434		Slight Cooling 7/16/95 to 7/29/95 734,803 to 917,042		Constant 7/31/95 to 10/4/95 917,042 to 1,892,082		Cooling 10/5/95 to 11/8/95 1,911,813 to 2,572,732	
Level	Avg Temp (°C)	Temp Gradient (°C/mm)	Avg Temp (°C)	Temp Gradient (°C/mm)	Avg Temp (°C)	Temp Gradient (°C/mm)	Avg Temp (°C)	Temp Gradient (°C/mm)
Air	21.7	-	22.4	-	22.6	-	20.3	-
Surface	23.6	-	26.6	-	24.9	-	23.7	-
50 mm*	23.5	-0.0021	26.8	0.0042	25.1	0.0042	23.9	0.0044
70 mm	23.5	-0.0002	26.9	0.0042	25.1	0.0010	24.0	0.0033
137 mm	23.1	-0.0049	27.0	0.0007	25.3	0.0018	24.3	0.0045
175 mm	23.0	-0.0020	26.9	-0.0018	25.2	-0.0026	24.3	0.0006

*data at this level are interpolated

3.1.3 50 mm Depth

For the mix evaluation procedure to assess permanent deformation response, the temperature occurring in the pavement at depth of 50 mm is used (*6*). For section 500RF, thermocouples were not installed at 50 mm; thus interpolation was required between 0 mm and 70 mm to determine temperatures at this level. Figure 3.2 and Tables 3.1 and 3.2 show that the daily average temperature for the 50 mm depth is similar to that of the daily average surface temperature. The variation among the 6-hour intervals is much like the surface temperature data, as summarized in Table 3.1.

3.1.4 70 mm Depth

Temperatures at this level are similar to temperatures at the 50 mm depth. It will be noted in Table 3.1 that as the depth increases, the difference in temperature between different periods of the day decreases.

3.1.5 137 mm Depth

Temperatures 137 mm below the surface are important since this depth is near the lower lift of AC. Average temperatures 137 mm below the surface divided into 6-hour intervals are more uniform throughout the day than at lesser depths (Table 3.1).

3.1.6 175 mm Depth

Temperatures 175 mm below the pavement surface located in the ATPB, show trends similar to those at shallower depths in the AC (Tables 3.1 & 3.2).

3.1.7 Temperature Gradient

Temperature gradients (°C/mm) within the asphalt layer are summarized in Table 3.2. A negative number indicates that temperatures decreases with depth. The data of Table 3.2 are shown graphically in Figure 3.3. In general, it can be observed that the variation in average temperature with depth is small, the maximum difference between the top and bottom sensors being of the order of 0.6°C.

3.2 RAINFALL AND WATER CONTENTS OF UNTREATED MATERIALS

Prior to construction of the test sections there were large amounts of rain during the period November 1994 through March 1995, as shown in Figure 3.4 which shows the monthly rainfall from July 1994 to April 1996 as recorded by the National Weather Service at Richmond, California (near the Richmond Field Station). Construction of the test sections started at the end March of 1995, when there was little or no rainfall, and finished near the end of April.

During the trafficking of section 500RF, in the period 3 May 1995 to 8 November 1995, there was little rainfall. Figure 3.4 shows that there were very small amounts during June, October, and November of 1995. Water contents of the unbound materials measured prior to construction, during construction, and after testing of section 500RF show some decrease in water content, Table 3.3. These reductions in water content for the three untreated layers between construction and the end of testing are likely the result of the lack of rain as shown in Figure 3.4.

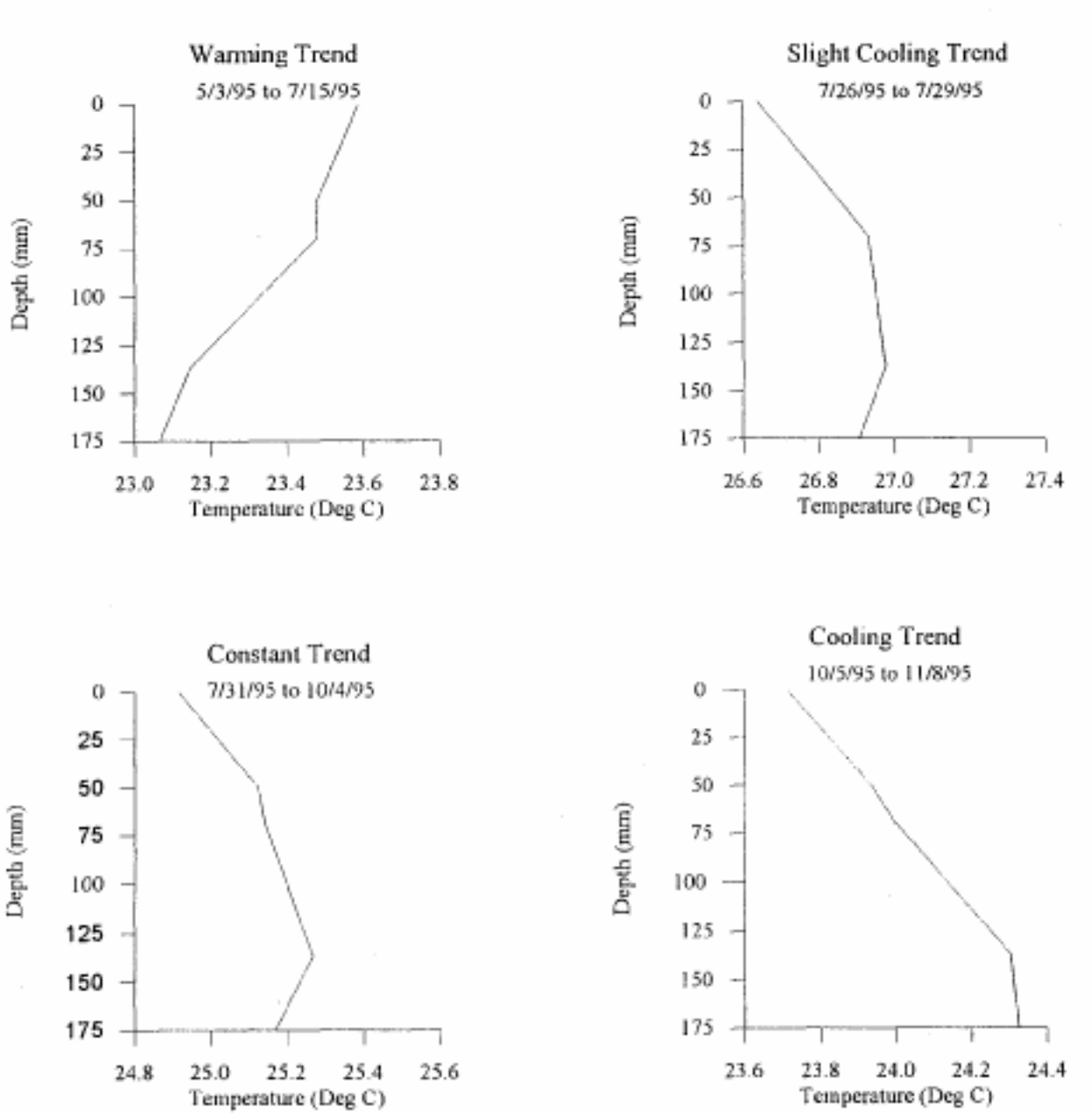

Figure 3.3 Average Temperatures at Surface and In-Depth Levels for Four Trends

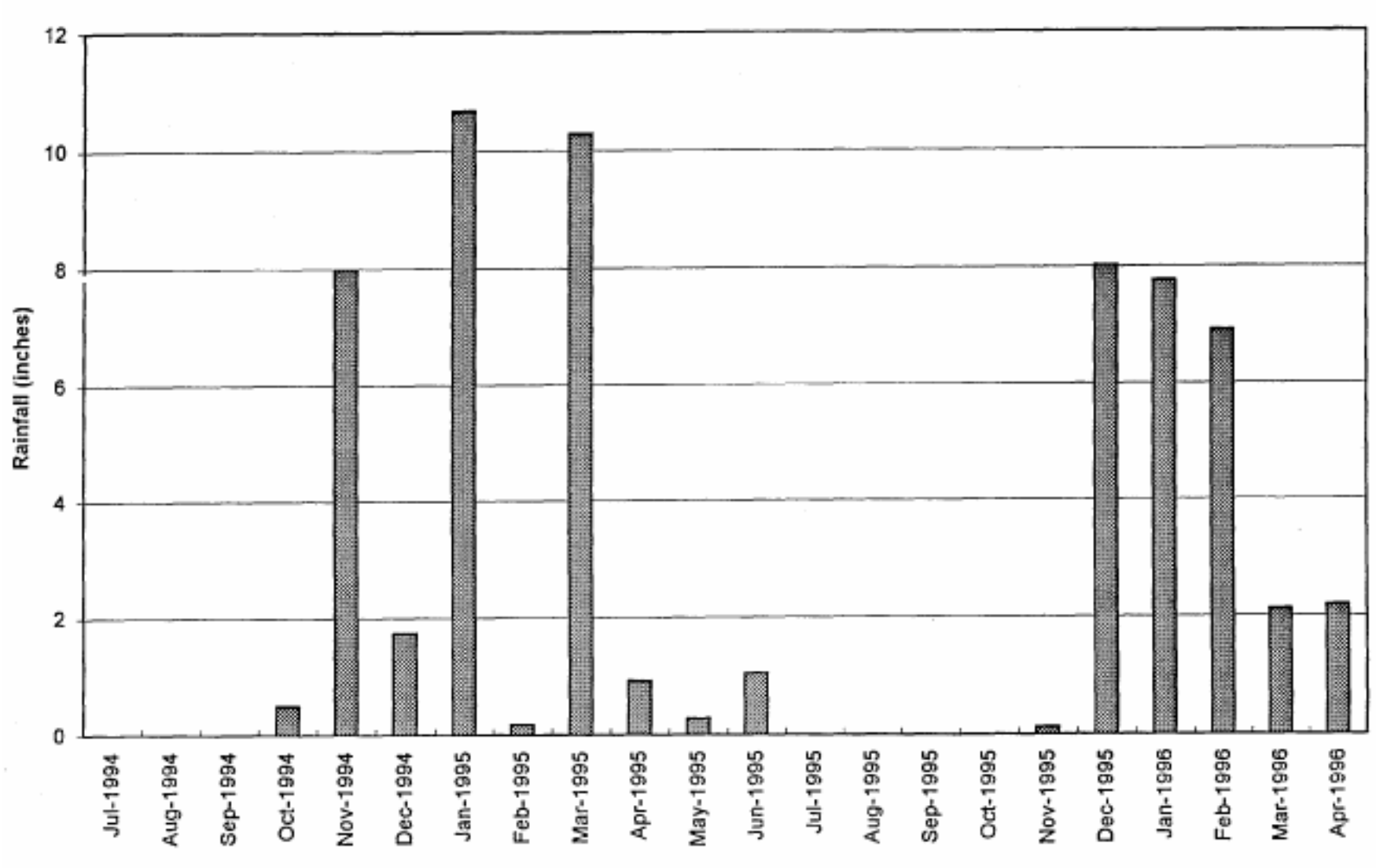

Figure 3.4 Monthly Rainfall Data in Richmond from the National Weather Service

Table 3.3 Water Contents (Percent) of Untreated Pavement Layers in HVS Pavement Test Sections

	Date Sample	2 March 1995[1]		30 March 1995[2]	4 April 1995[2]	8 Dec 1995[3]
Layer	Agency	UCB	CCCo*	CCCo*	CCCo*	CCCo*
AB	Max	-	-	-	6.0	4.9
	Min				5.0	4.4
	Ave				5.7	4.7
ASB	Max	7.3	7.9	7.5	-	6.2
	Min	4.6	7.3	5.4		5.7
	Ave	5.6	7.6	6.9		6.0
SG	Max	22.8	15.7	-	-	16.6
	Min	16.2	15.7			13.7
	Ave	18.7	15.7			15.3

* Contra Costa County
[1] Borehole Samples Before Construction
[2] During Construction
[3] Transition Area Samples Taken After Test 500RF

3.3 PERMANENT DEFORMATION

The permanent deformation response of the pavement is monitored using the laser profilometer for surface rutting and the MDDs for both the permanent deformation at the surface and various depths within the pavement. The following two sections discuss the surface and in-depth rutting respectively.

3.3.1 Permanent Surface Deformation

From the laser profilometer data, maximum, minimum, average, and average maximum ruts are determined for each set of readings. Figure 3.5 shows the development of permanent deformation with load repetitions for section 500RF. Three sets of data are commonly presented: 1) average rut; 2) average rut without MDDs; and 3) average maximum rut. The average rut is the average of profilometer readings from all points measured in the section excluding the one meter turnaround sections at each end. The average maximum rut is the maximum of the 256 data readings per measuring point averaged throughout the 13 (numbers 2 to 14) data collection reference points. Due to pavement variability and the traffic loading distribution across the test pad, a significant difference between the average rut and the average maximum rut exists as shown in Figure 3.5.

At points 4 and 12, where MDD modules were installed, brass topcaps cover the MDD hole; these rigid caps can resist the rutting action experienced by the surrounding pavement and may thus protrude above the rutted pavement surface. Accordingly, the reported average rut may contain some error and the true average rut (excluding the effects of the MDD topcaps) may be higher than that calculated. To compensate for this potential error, a third line can be plotted representing the average rut through all the points excluding the observed

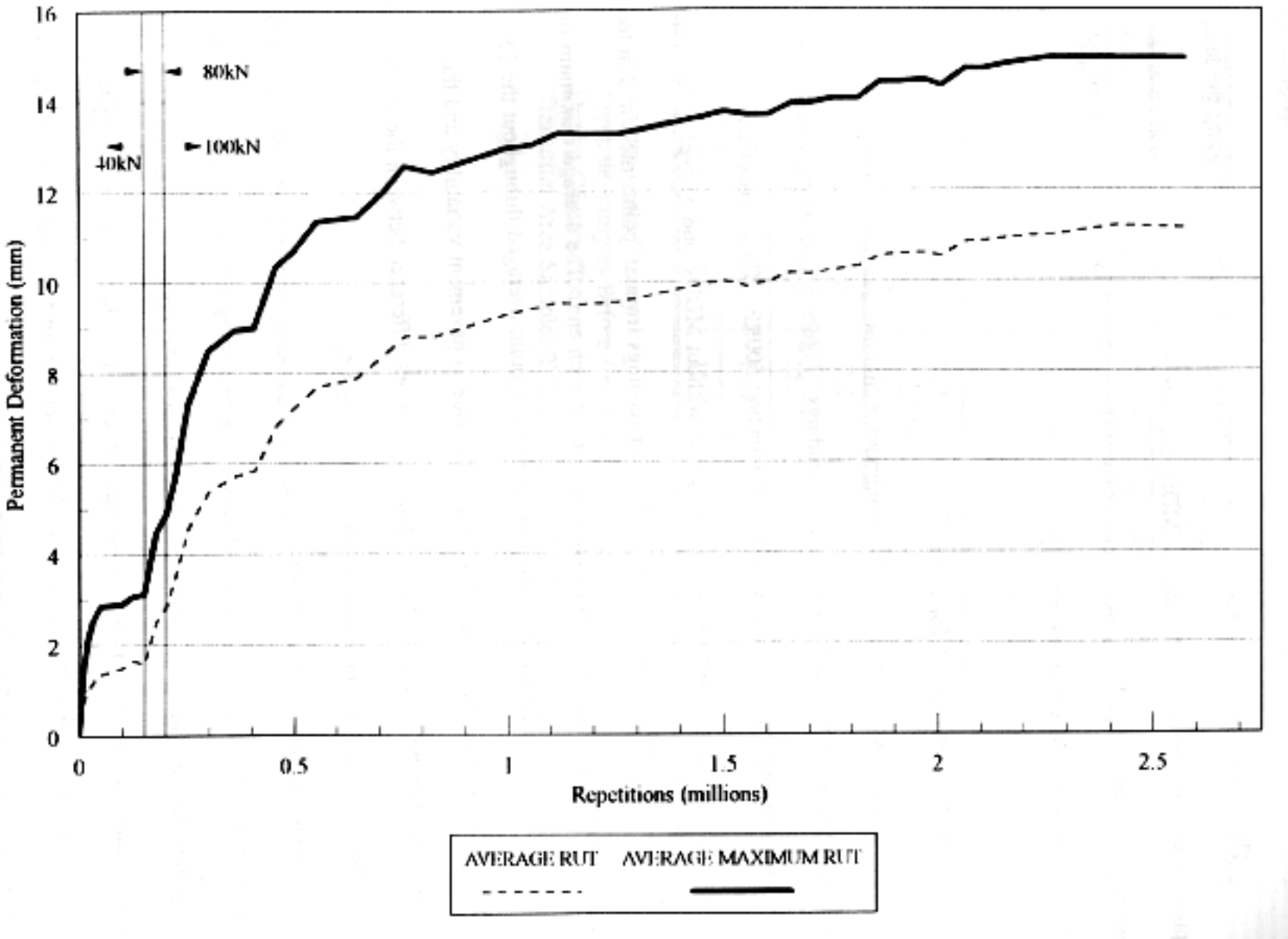

Figure 3.5 Permanent Deformation from Laser Profilometer

readings at MDD locations. The line is termed the "average rut without MDDs." The effects of the MDD topcaps was negligible for test 500RF, and, in fact, superimposed the "average maximum rut" line. Therefore, to eliminate ambiguity, the term was deleted from the legend.

3.3.1.1 Rut Depth Development. While Figure 3.5 presents an indication of the overall development of rutting with load repetitions determined from the laser profilometer measurements, the resulting data also provide the opportunity to examine the changes in elevation of the entire test section surface with load repetitions. Results of these analyses are presented in Figures 3.6 through 3.10. Figure 3.6 illustrates the pavement surface at 10,000 repetitions with a minimal amount of rutting. Figures 3.7 and 3.8 show the surface at 50,000 and 150,000 repetitions respectively. By comparing Figures 3.7 and 3.8 with 3.6 it will be noted that the rutting increased in the interval 10,000 to 50,000 repetitions but changed little from 50,000 to 150,000 repetitions with the rut depth not exceeding 5 mm.

At 150,000 repetitions the load was increased to 80 kN and a rapid increase in rutting per load repetition was observed (Figure 3.5). The load was further increased to 100 kN at 200,000 repetitions and the rut depth per load repetition increased significantly. By 700,000 repetitions, parts of the test section exhibited ruts in excess of 15 mm, Figure 3.9. It should be noted that these more deeply rutted areas occurred near the MDD installations and would be, at least partially due to localized weaker areas resulting from the MDD installations. At the conclusion of trafficking (2.57×10^6 repetitions), the average rut was just over 11 mm and the average maximum rut had reached 15 mm. Within the 6 m evaluated portion of the test section, the maximum rut was at point 4, near the MDD location.

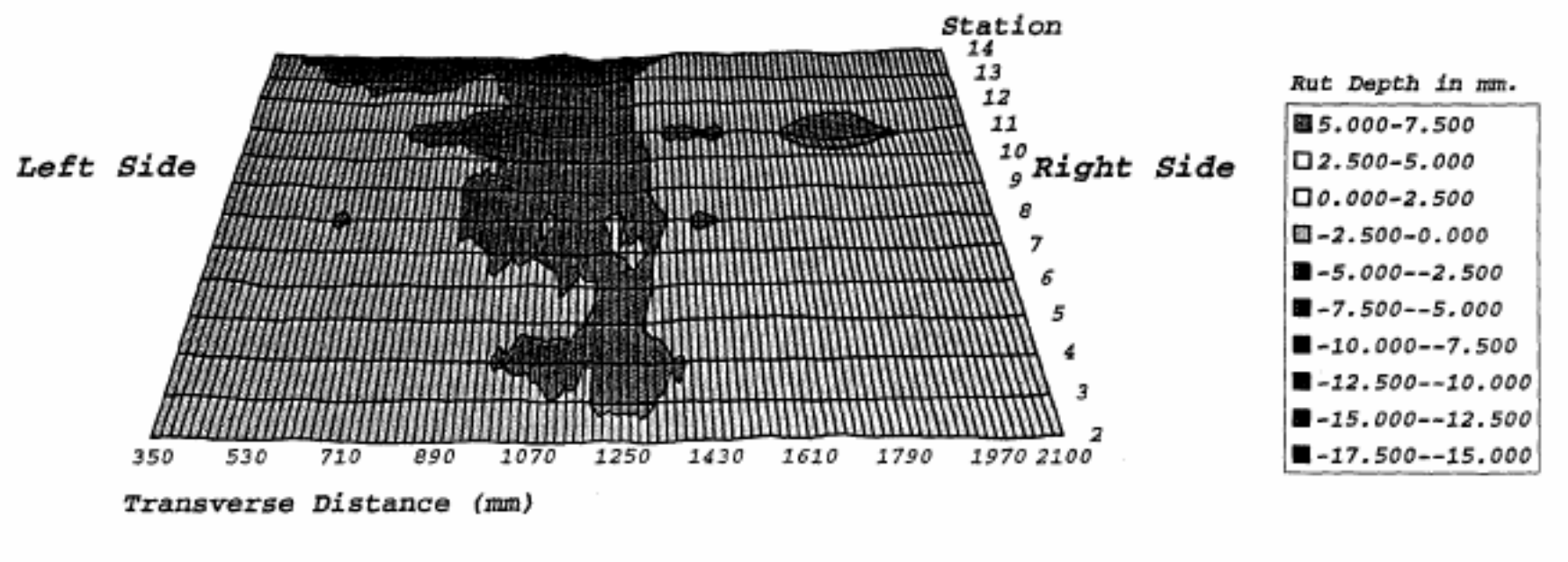

Figure 3.6 Deformed Test Section Surface at 10,000 Repetitions

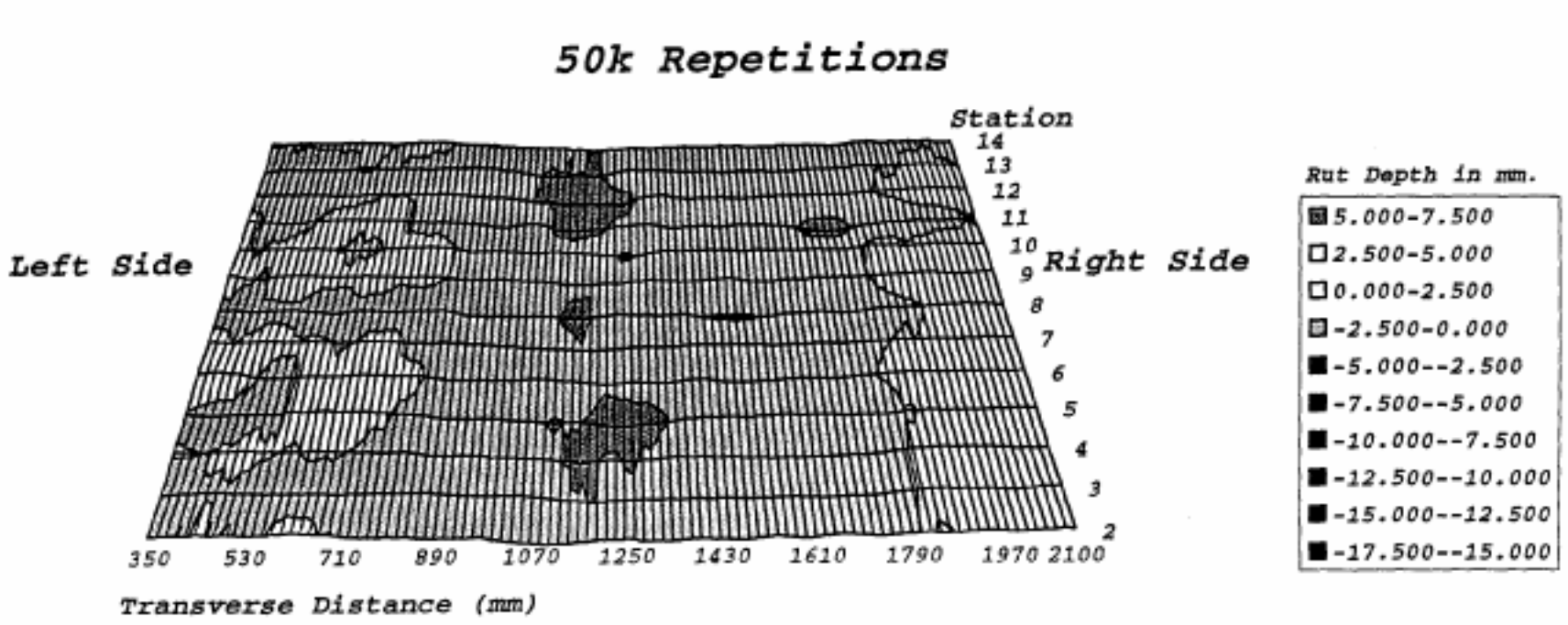

Figure 3.7 Deformed Test Section Surface at 50,000 Repetitions

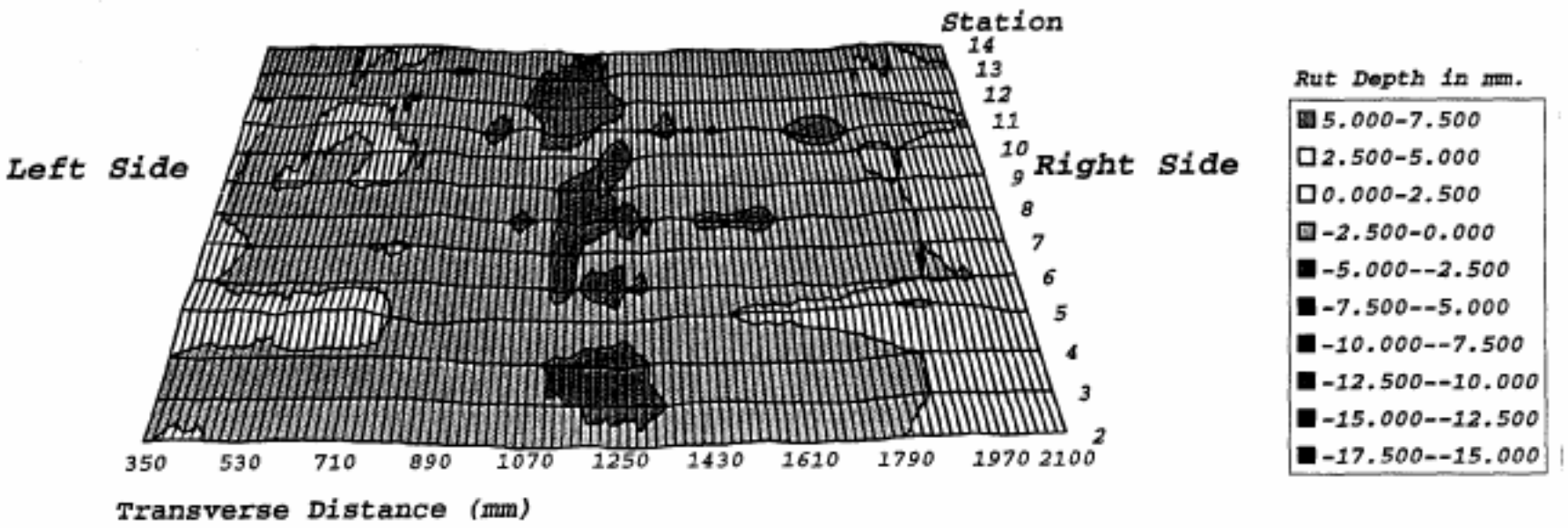

Figure 3.8 Deformed Test Section Surface at 150,000 Repetitions

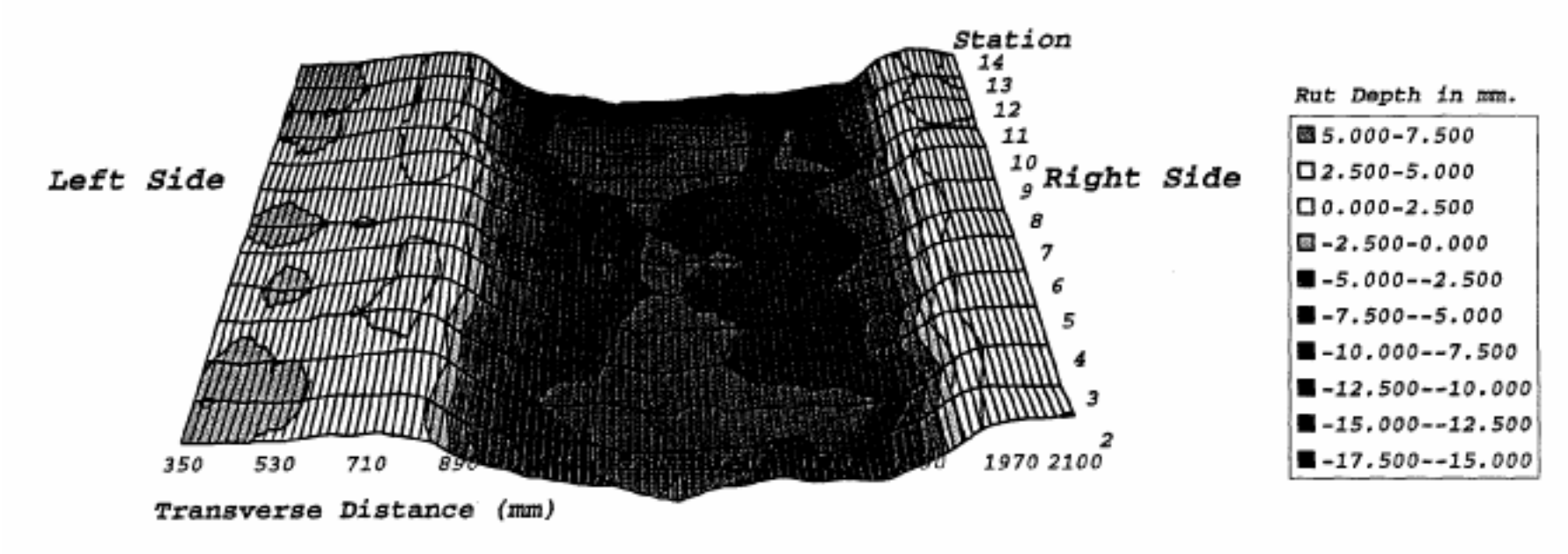

Figure 3.9 Deformed Test Section Surface at 700,000 Repetitions

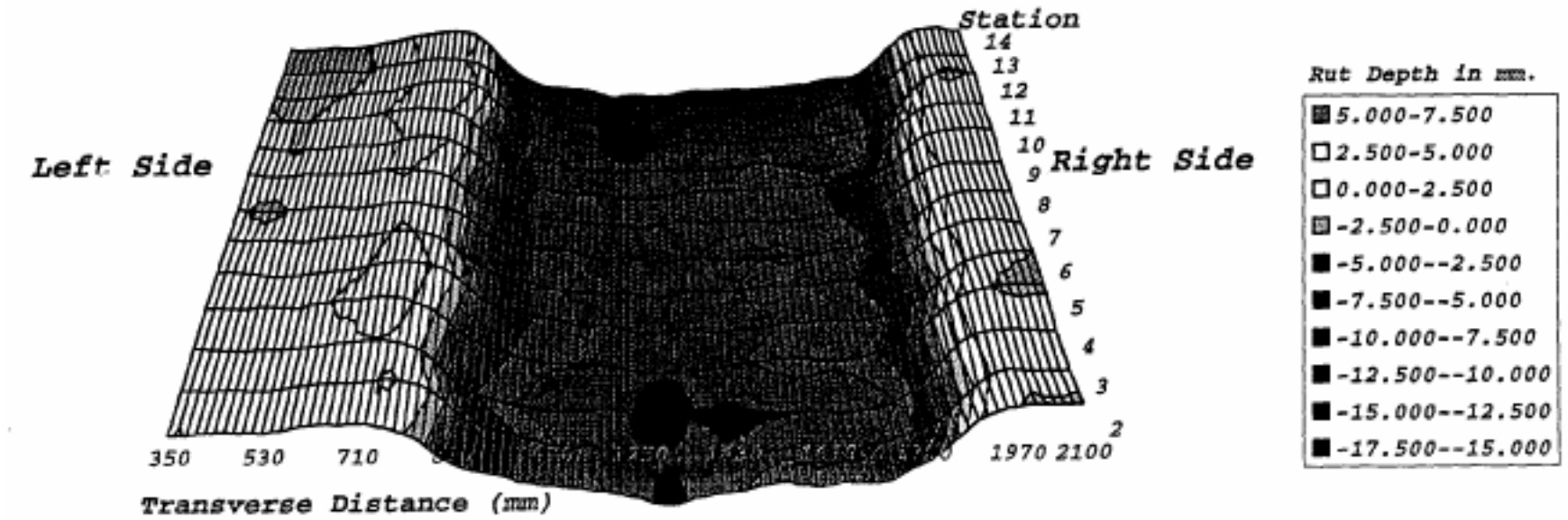

Figure 3.10 Deformed Test Section Surface at 2,500,000 Repetitions

At 299,731 repetitions over half of the total permanent deformation had developed and at 759,754 repetitions, approximately 75 percent of the total permanent deformation had occurred. For the final one million repetitions, the rut depth increased by only approximately one mm. Essentially, 95 percent of the rutting developed during the first 60 percent of trafficking.

At the conclusion of the test, rut depth measurements were taken both with the laser profilometer and with a straight edge at all measuring points. The data for Point 15 are presented in Figure 3.11 which represents the location of maximum rutting with a value of 19 mm. It will be noted that there is excellent correspondence between the two measurement methods. In the case of the laser profilometer measurements the small irregularities are due to changes in surface texture of the pavement.

3.3.1.2 Rate of Rutting. From examination of Figure 3.5 it is apparent that there are variations in the rate of development of rutting throughout the test. To characterize stages in rut development during the life of the pavement, the data presented in Figure 3.5 were visually divided into phases which were determined from changes in the loading and the visually apparent changes in the rate of permanent deformation. The phases are summarized in Table 3.4 with calculated rutting rate expressed in millimeters of rut per million load applications (mm/MiLA). Three stages of significant rut development are apparent with rates greater than 24 mm/MiLA: zero to 50,000 repetitions; 150,000 to 200,000 repetitions; and 200,000 to 300,000 repetitions.

The first significant stage, zero to 50,000 repetitions, is an embedding phase in which the asphalt pavement undergoes post-construction compaction as the result of the 40 kN

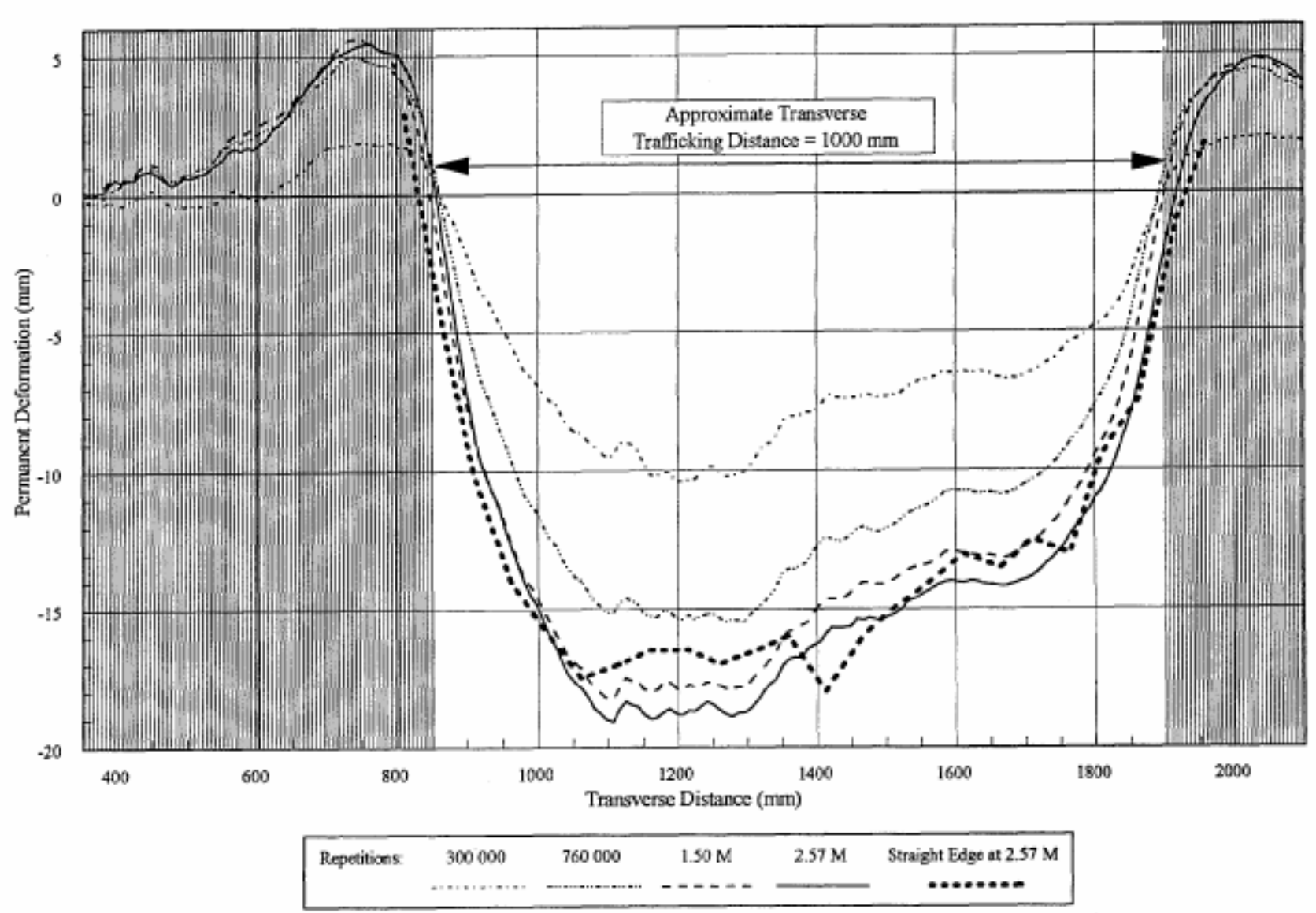

Figure 3.11 Profilometer Cross Section and Final Straight Edge Measurement

traffic loading. Likely contributing to this rate is a 9°C increase in the daily average temperature 50 mm below the surface during this period, Figure 3.2. From Figure 3.5, the embedding phase appears completed at approximately 50,000 40 kN load repetitions. The test plan required that the 40 kN load be maintained to 150,000 repetitions to ensure that this initial embedding phase was complete so that the pavement would be able to withstand the higher wheel loads (80 and 100 kN) without excessive rutting in the asphalt concrete.

Each time the load is increased a new embedding phase is observed; the 150,000 to 200,000 repetitions stage represents the embedding phase resulting from the 40 kN to 80 kN increase in load; and the embedding phase when the load was increased at 200,000 to 100 kN repetitions lasted to approximately 300,000 repetitions.

Based on prior experience with HVS testing, the rutting rate between 300,000 and 700,000 repetitions, 7.3 mm/MiLA, is larger then the usual one to three mm/MiLA observed during relatively stable conditions after the embedding phase. This rutting rate is a secondary embedding probably related to increasing temperature rather than change in load and has been termed a transition phase herein. It should be noted that temperatures within the asphalt concrete were increasing during this period, reaching a peak of 30°C just beyond 700,000 repetitions (Figure 3.2). While temperatures of this order of magnitude are not considered high from a rutting stand point, it was shown in Reference (*2*) that in combination with the 100 kN load they could have some influence on the rutting rate observed.

After about 700,000 repetitions, the rutting rate under the 100 kN load again reached essentially a steady-state condition ranging from 1.1 to 2.1 mm/MiLA. During this period the average temperature was decreasing slightly (about a 1°C drop).

In general, there is a reasonable correlation between the rutting rates and the applied loads. During phases III and IV (Table 3.4) the increased loads are likely responsible for the relatively large rutting rates.

3.3.2 In-Depth Permanent Deformation

With the aid of the MDD modules it was possible to measure the accumulation of vertical permanent deformation in the various layers situated between the modules during the course of the HVS test. Unfortunately, the permanent deformation (PD) data for the first 250,000 load repetitions in test 500RF are not available because of problems initially incurred with the data acquisition system. Thus, as seen in Figure 3.12, the layer deformations from 250,000 repetitions until the end of the test (2.57 million reps) have been plotted. The net result is that direct comparisons between the surface permanent deformation values measured by the laser profilometer (Figure 3.5) and the permanent deformation values measured from the MDD4 surface module (Figure 3.12) are not available from the beginning of the test. Instead, the comparison initiates at 250,000 repetitions and continues throughout the remainder of the test (Figure 3.13.). This graph exhibits the strong correlation between the two devices given the different measuring techniques.

From the data presented in Figure 3.12 it is possible to estimate the deformation occurring in each layer. Table 3.5 contains the results of this analyses, ignoring any deformation that occurred prior to 250,000 repetitions.

3.3.2.1 Asphalt Concrete Layer. From Table 3.5 it can be seen that the AC layer contributed more than 50 percent of the observed vertical permanent deformation.

Table 3.4 Rutting Rates During HVS Loading on Section 500RF

Phase	Repetitions ($\times 10^3$)	Load (kN)	Condition	Ave-rage Rut (mm)	Average Maximum Rut (mm)	Rut Rate (mm/MiLA)*	Average Surface Temp (°C)
I	0 – 50	40	Embedding	1.4	2.8	27.0	17.6
II	50 - 150	40	Steady-State	1.6	3.1	2.3	20.6
III	150 - 200	80	Embedding	2.9	4.9	24.6	21.3
IV	200 - 300	100	Embedding	5.4	8.5	26.0	24.5
V	300 - 700	100	Transition	8.3	12.0	7.3	25.9
VI	700 - 1500	100	Steady-State	10.0	13.7	2.1	25.2
VII	1500 - 2570	100	Steady-State	11.2	14.9	1.1	24.2

*MiLA=Million Load Application; rut rate based on average rut depths.

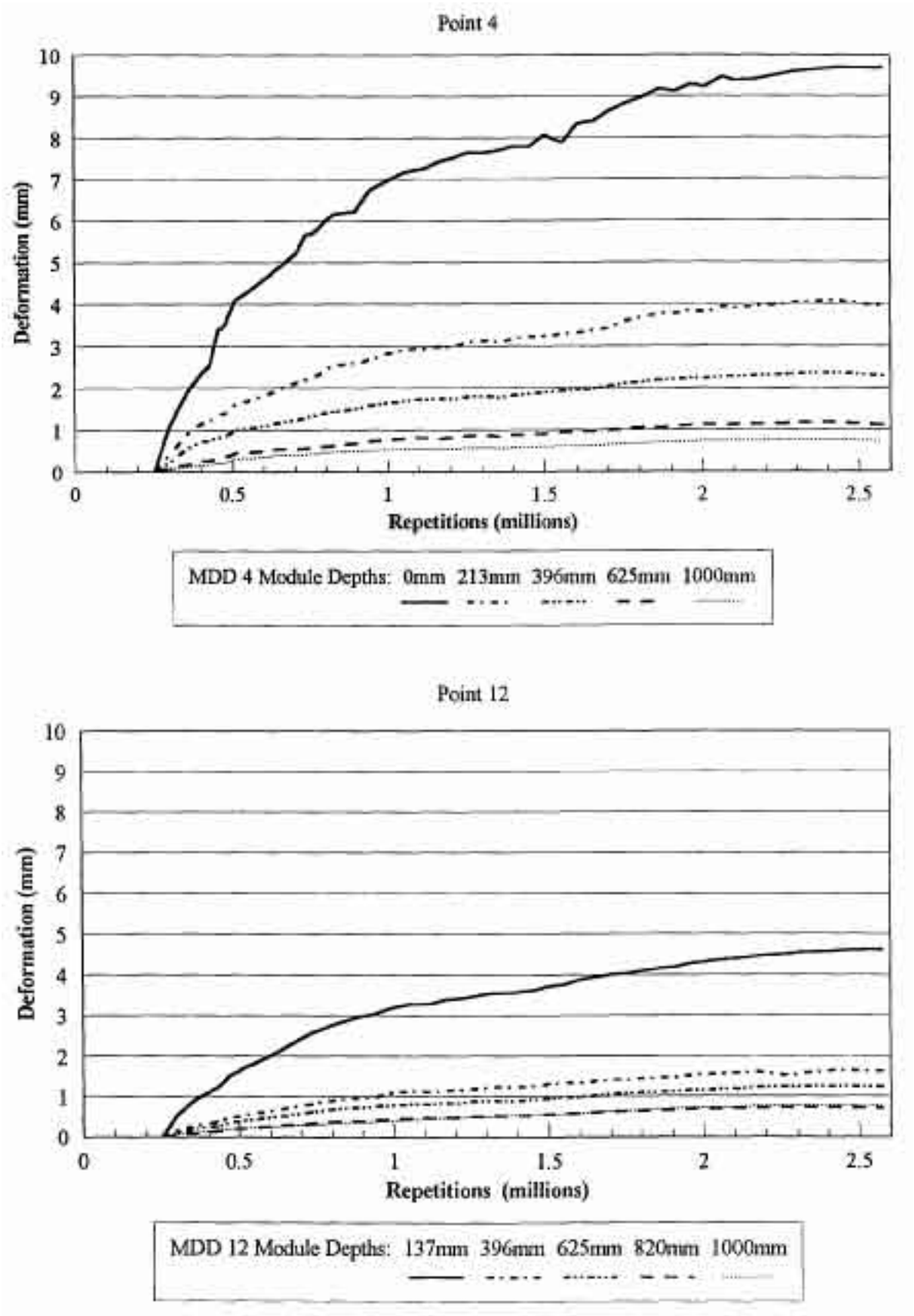

Figure 3.12 Permanent Deformation of Various Layers

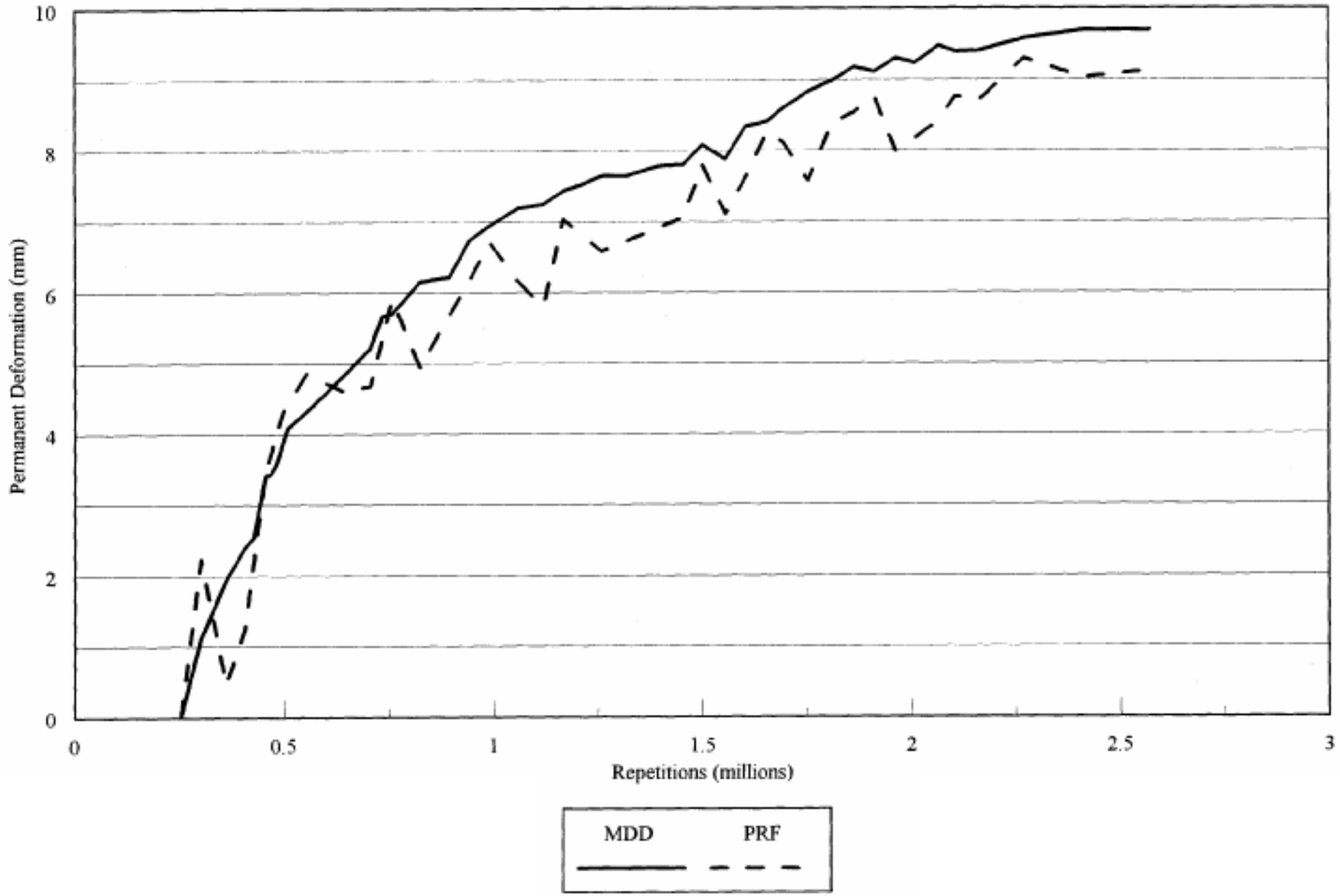

Figure 3.13 Permanent Deformation Comparison of MDD4 and the Laser Profilometer

Table 3.5 Permanent Deformation as Measured by MDD Modules (Repetitions 250,000 to 2.57 Million)

Layer	Thickness (mm)	Vertical Permanent Deformation (mm)	Percentage of Total Deformation
Asphalt Concrete	137	5.1	52
ATPB	76	0.7	7
Aggregate Base	183	1.6	17
Aggregate Subbase	229	1.2	12
Subgrade	semi infinite	1.1	12
Total		9.7	100

From an examination of Figures 3.6 through 3.11 it would appear that the permanent deformation taking place in the AC is the result of both volume decrease (densification) and shear deformations (as evidenced by the increased elevation of the pavement adjacent to the loaded system).

To ascertain the contribution of volume decrease to the rutting in the asphalt concrete, cores were extracted so that their air void contents and heights could be measured. These cores were obtained from outside the trafficked area at points 10 and 16 and stations 1+82 and 1+24 from inside the test section at points 0, 13, and 15. Results of the air void determinations and height measurements are presented in Table 3.6 for the specific core locations.

From the information presented in this table it can be seen that the majority of the densification during loading occurred in the top lift. The relatively few cores indicate that up to 11 mm of rut depth can be attributed to the top AC lift, compared to 5 mm of permanent deformation measured by the MDD. At the most about 1.2 mm of the rut depth can be attributed to volume decrease (i.e. the 1.6 percent reduction in air void content in the 73 mm top lift noted in Table 3.6). Thus the additional permanent deformation is likely due to shear deformations

occurring in the top lift (Figure 3.11). Results of the simple shear tests on the AC reported in Reference (*2*) would appear to support this statement.

Table 3.6 Air Void Contents and Core Thicknesses in the Asphalt Concrete Layer

		Top Lift		Bottom Lift	
	Core Location	% Air Voids	Core height (mm)	% Air Voids	Core height (mm)
Outside Trafficked Area	10	7.6	74	4.5	75
	16	8.1	71	4.3	82
	Sta 1+24	7.6	69**	C	C
	Sta 1+82	7.8	68**	C	C
	Average	7.8	73	4.4	78
Inside Trafficked Area (after completion of trafficking)	0*	7.5	59	3.4	81
	13	5.4	63	4.6	76
	15*	5.7	62	3.1	78
	Average	6.2	61	3.7	78

* In turn-around area at ends of trafficked section.
** Not included in determination of average height.

The repetitive simple shear tests at constant height (RSST-CH) were performed on cores from the test pavement and on specimens made from field mix prepared by rolling wheel compaction. Results of the simple shear tests (obtained by UC Berkeley and Caltrans) on these specimens all indicated less resistance to permanent deformation of the less well compacted (higher air void content) mix in the top lift.

Finite element simulations have indicated that under 40 kN and larger loads the location of the maximum shear stresses occurs about 50 mm below the area where the tire sidewalls contact the pavement surface (*6*). While the critical shear stresses occur above the interface between the top and bottom AC lifts in the Section 500RF pavement, it is likely that the lower lift was also subjected to comparatively large shear stresses. Determination of the relative rutting must await the trenching study after completion of the Goal 3 overlay testing. If those measurements indicate that most of the rutting occurred in the top lift, after accounting for densification, they will definitely confirm the RSST-CH results.

It must be emphasized, however, that the percentage air-voids is not the only factor which controls the resistance to permanent deformation in asphalt concrete; gradation and quality of aggregate, type and quantity of asphalt also play an important role. However, the positive effects of properly compacted mixes are illustrated by these results. By ensuring good compaction of asphalt concrete during construction, improved rutting performance can be obtained.

It should be noted that when the cores were removed, it was observed that there was no bond between the two lifts as is discussed in more detail in Section 3.5.2 herein. This supports the observation contained in the Interim Report which indicated the likelihood of a lack of bonding between the two lifts of asphalt concrete when cores and slabs were taken from the newly constructed pavement. The effect of the lack of bonding on the magnitude and location of maximum shear stresses can be seen in Figures 3.14 and 3.15 for the unbonded and bonded cases, respectively. The analyses for both cases were performed by Symplectic Engineering Corporation (*8*) using the Finite Element Program (FEAP), with viscoelastic elements used for the AC and elastic elements used for other layers of the

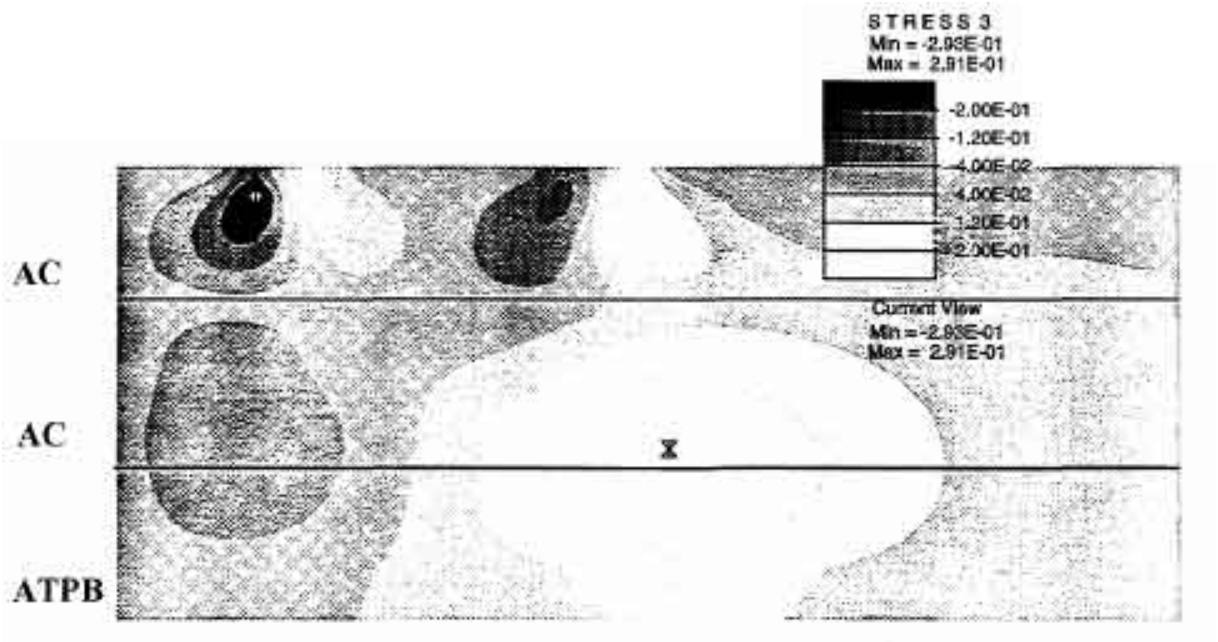

Figure 3.14 Finite Element Calculation of Shear Stresses (MPa) Under HVS Loading for No Bonding Case (Close-up of AC Layers Under Tire)

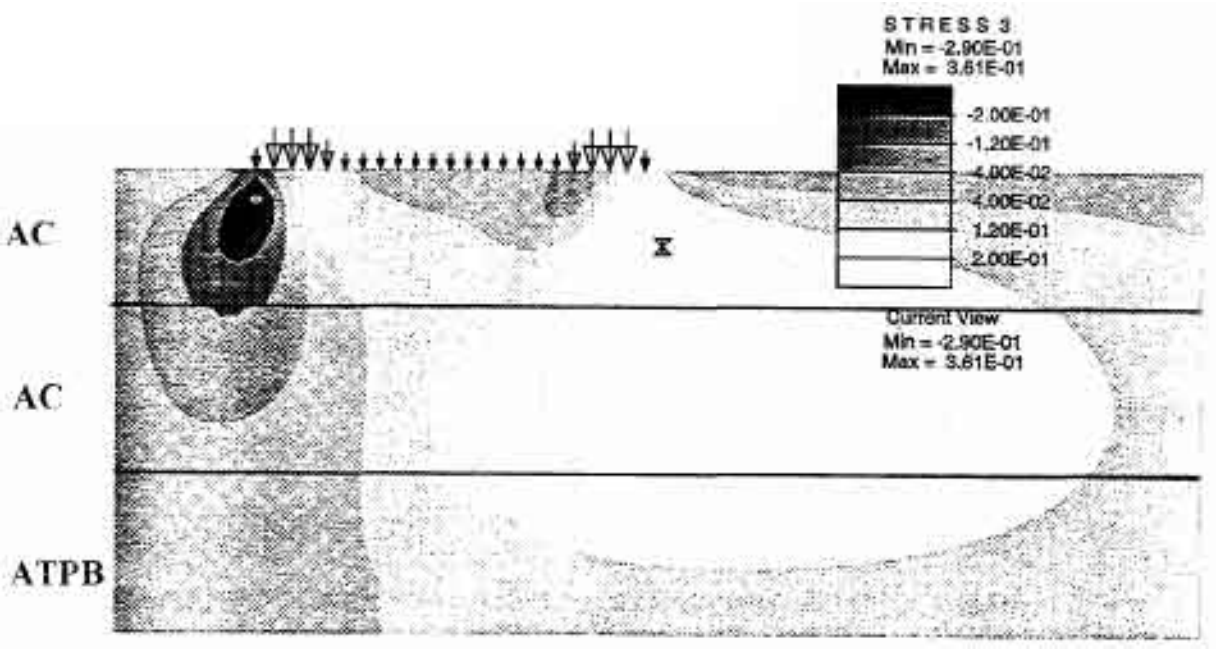

Figure 3.15 Finite Element Calculation of Shear Stresses (MPa) Under HVS Loading for Fully Bonded Case (Close-up of AC Layers Under Tire)

pavement. The resultant shear stresses under one of the tires shown in Figures 3.14 and 3.15 are for 100 kN load and a loading time of 0.3 seconds, as applied by the HVS.

The analyses indicate that the bonded case results in a larger maximum shear stress than does the unbonded case, 0.361 MPa (52.4 psi) versus 0.293 MPa (42.5 psi). The locations of the critical shear stresses also change. For the bonded case the maximum shear stresses occur within the top AC lift, with the largest stress at the center of the lift near the outside edge of the tire. For the unbonded case, one area of large shear stresses occurs under the inside edge of the tire at the center of the top lift. The other areas of equally large shear stresses occurred below the outside edge of the tire at the interface between the bottom AC lift and the ATPB, and in the center of the top AC lift.

The finite element simulations suggest that the level of bonding between the AC lifts influenced the magnitude of the maximum shear stress, with about a 20 percent increase in shear stress for the bonded case. The locations of large shear stresses occurred at the edges of the tires in the center of the top AC lift for both cases, however distribution of the shear stresses near the outside edge of the tire was somewhat different for the two cases.

3.3.2.2 Asphalt Treated Permeable Base. Permanent deformation in the ATPB was determined by subtracting the permanent deformation measurement for MDD4 at 213 mm from the measurement for MDD12 at 137 mm. The estimation that 7 percent of the total deformation calculated occurred in the ATPB (Table 3.5) is therefore based on the assumption that the deformation trend which occurred at MDD4 was repeated at MDD12. To verify the results reported in Table 3.5, a trench will be dug after completion of the entire series of HVS tests.

Under the conditions of this test, the ATPB layer has performed very well, with only a minimal amount of permanent deformation occurring in this layer. Three 150 mm diameter cores were taken at points 10, 13 and 15 after the test had ended; these cores revealed that the ATPB layer was still intact. From the cores it was not possible, however, to directly measure the actual deformation which had taken place in the ATPB layer. It must be remembered, moreover, that this test was performed with the ATPB layer in the dry state and that a proper investigation of the structural strength of this type of material should include its performance under the influence of water. *To investigate the structural behavior of the ATPB layer properly, HVS testing should also be performed with the material exposed to water and it is hoped that this can be accomplished eventually with these test pavements.*

3.3.2.3 Unbound Layers. The remaining permanent deformation, 41 percent, occurred in the unbound layers, i.e., the base, subbase, and subgrade, with only minimal deformation occurring at the subgrade level at the end of the test. (As seen from Table 3.5, about 72 percent of the 41 percent occurred in the base and subbase layers). These results suggest that an adequate pavement thickness has been provided above the subgrade by the Caltrans design procedure to minimize subgrade effects on rutting at the pavement surface even for the 100 kN loads applied.

3.4 ELASTIC (RECOVERABLE) DEFLECTIONS

Elastic (recoverable) deflections provide an indication of the overall stiffness of the pavement structure and, therefore, a measure of load carrying capability. As the stiffness of a structure decreases, its ability to support load decreases due to damage in the pavement materials with the result that for a given load, deflection increases. In this program elastic deflections are

measured with two instruments, the MDD and the RSD. The RSD measures surface deflections whereas the MDD measures the surface deflections at MDD 4 and the in-depth deflections at both MDD locations. [Section 500RF was the first HVS test at the Richmond Field Station and during this test a number of unforeseen problems with the data acquisition system occurred as noted earlier. Electrical and electronic problems (such as surges in the power supply at the HVS test site, cables and connectors which were not properly shielded from outside electrical and magnetic fields and electronic hardware incompatibility) lead to various spikes and outliers in the electronically collected data. To capture the behavior of pavement layers under the influence of HVS loading, close screening of all data collected is necessary and the exclusion of data points should be discouraged. The data which is presented in the graphs in the following sections clearly show these inconsistencies. Although difficult, it was nevertheless possible to detect and analyze certain behavioral patterns which are discussed in the following sections. Since the completion of test 500RF most of the data acquisition problems have been eliminated, leading to much higher quality results, as reflected in the results of the remaining test sections (501RF, 502CT, and 503RF), which will be presented in future reports].

3.4.1 Surface Deflections

In this section, surface deflections as measured by the RSD and at MDD4 will be summarized. Since the temperature varied somewhat during the test, a small analytical study was also completed to ascertain the influence of temperature on the deflections measured by the RSD. The results of that study are included in this section as well.

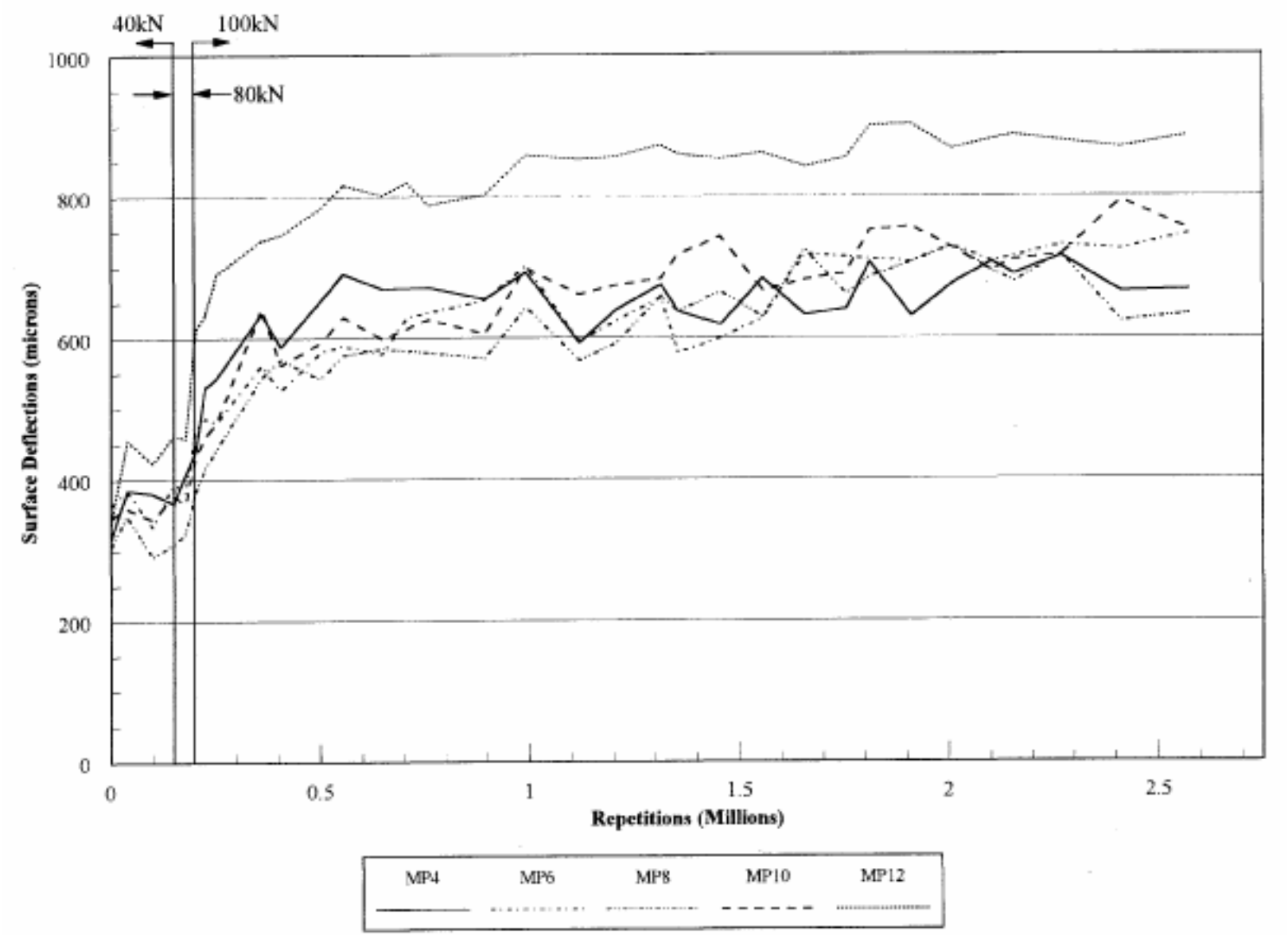

Figure 3.16 Road Surface Deflections, 40 kN Test Load

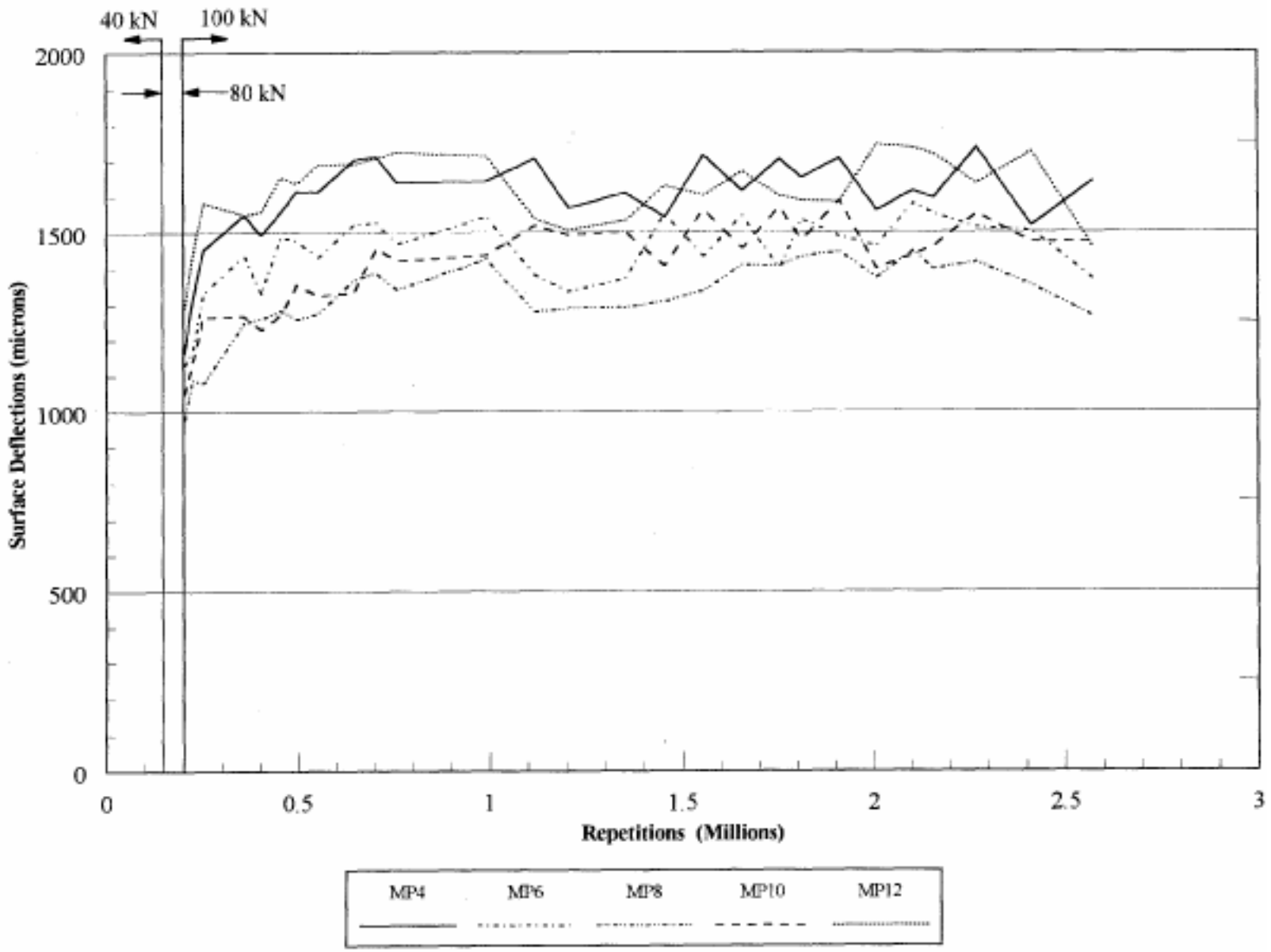

Figure 3.17 Road Surface Deflections, 100 kN Test Load

3.4.1.1 RSD Surface Deflection Results. Figures 3.16 and 3.17 show the individual RSD deflections for centerline measuring points 4, 6, 8, 10, and 12. These deflections are all within a narrow band (Figures 3.16 and 3.17) which means that the section had uniform structural behavior. The variation between the centerline deflections at points 4, 6, 8, and 10 is approximately 20 percent throughout the whole testing period. Under the 40 kN load the deflections at point 12 are somewhat higher than the deflections at points 4 to 10, but follow the same upward trend observed at points 4 to 10 (Figure 3.16). The average 40 kN deflection at the end of the test (2.57×10^6 repetitions) for points 4 to 10 is 699 μm, and for point 12 is 880 μm.

A summary of the average of all 40 kN RSD deflection data measured on the test section before HVS loading commenced and after 2.57×10^6 load applications is contained in Table 3.7.

Table 3.7 Average of 40 kN RSD Deflections

	Before HVS testing	After 2.57×10^6 HVS Load applications
Average Deflection (microns)	320	703
Standard deviation	38	84

Deflection data for the 100 kN test load are shown in Figure 3.17. The average deflection for all points (4 to 12) under this load at the end of HVS testing is 1441 μm. It will be noted that the localized weak area (near point 12) was not observed under the 100 kN load. This effect is probably due to the magnitude of deflection caused by the 100 kN test load in comparison with the deflections caused by the 40 kN test load.

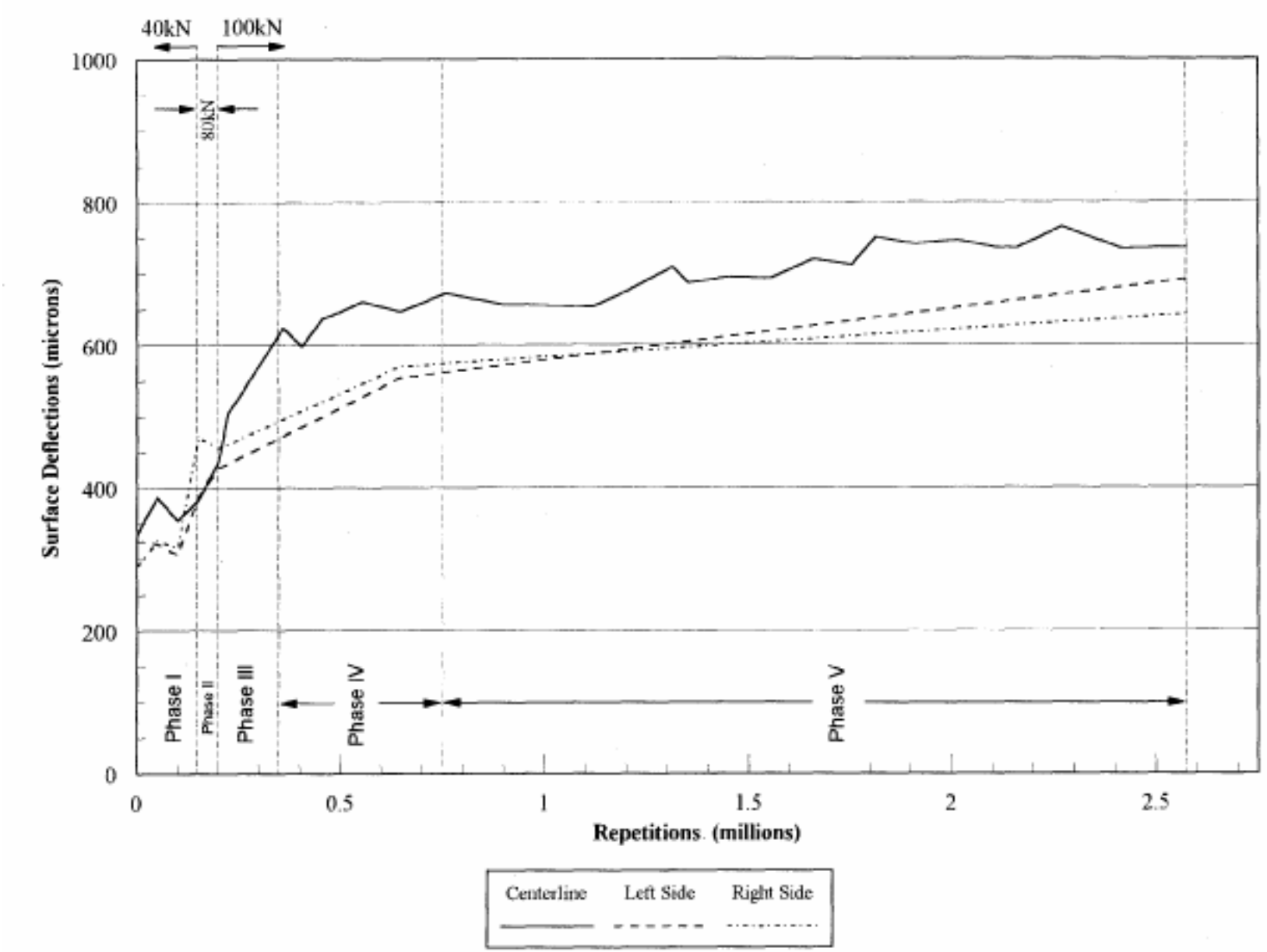

Figure 3.18 Average Road Surface Deflections, 40 kN Test Load

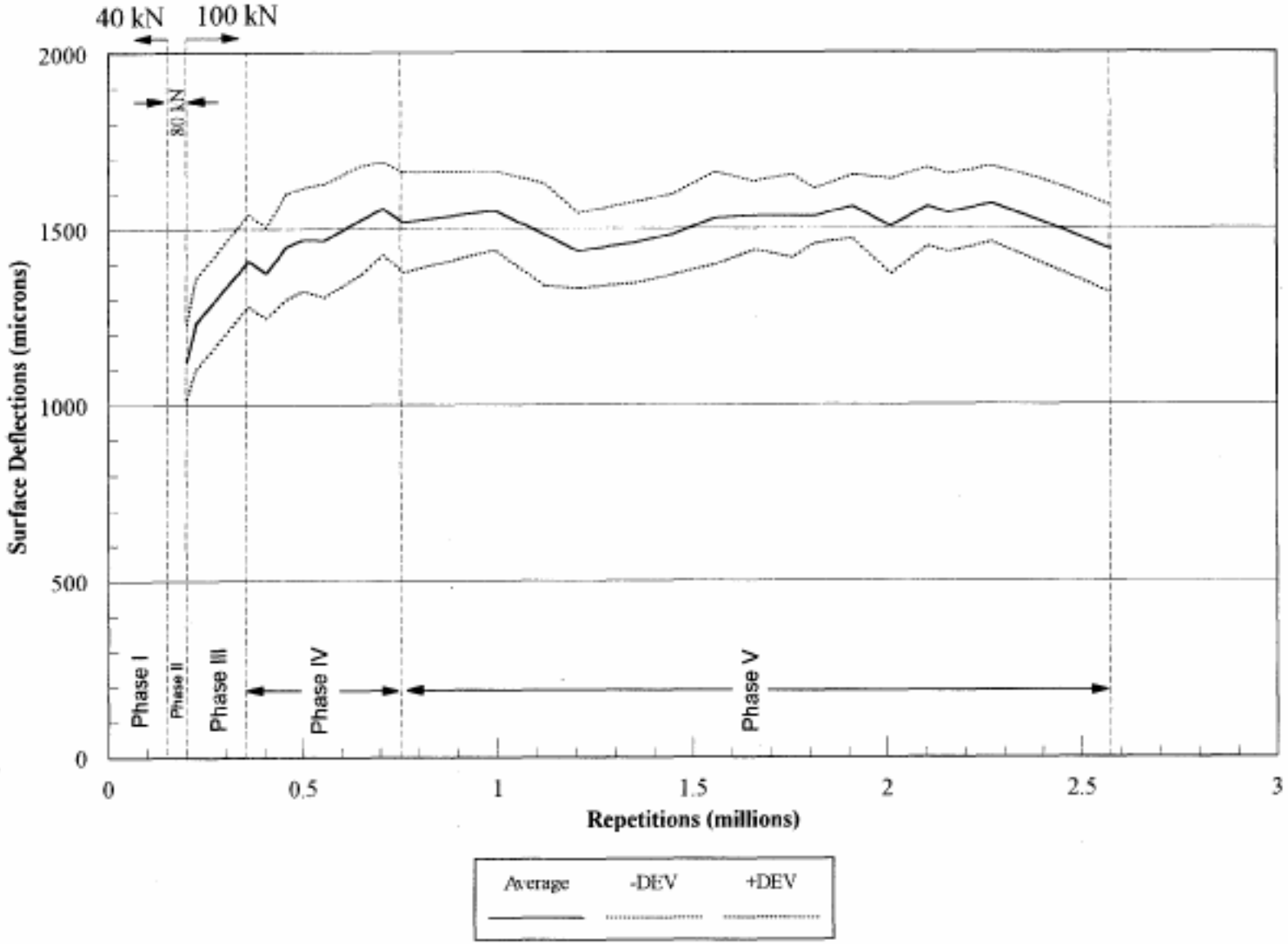

Figure 3.19 Average Road Surface Deflections, 100 kN Test Load

Figures 3.18 and 3.19 show the average RSD deflections under the 40 kN and 100 kN loads, respectively. Periods with similar trends in the rate of increase in elastic deflection are indicated on Figures 3.18 and 3.19 by Roman numerals. The temperatures shown on all the RSD figures are air temperatures at the time of deflection measurement, and indicate small variations in measurement temperature (a deflection measurement correction factor to account for measurement temperature is presented in Section 3.4.1.3 herein).

Deflections in periods I, II, III occurred as the load was increased from 40 to 80 to 100 kN, respectively, and indicate increased damage rates as loading was increased. Deflections in Period IV (350,000 to 750,000 repetitions) do not increase with load repetitions as much in Period III (200,000 to 350,000 repetitions) despite equivalent 100 kN loads. The rate of deflection increase appears to slow substantially again under continued 100 kN loading in Phase V (750,000 to 2,570,000 repetitions). As is discussed in Section 3.5.1 herein, cracking appeared at the surface of the pavement at about the end of Period IV, and substantial cracking was visible at the surface at the beginning of Period V.

3.4.1.2 MDD Surface Deflection Results. Figures 3.20 and 3.21 summarize the surface deflections measured at MDD point 4 using the 40 kN and 100 kN loads respectively. Also shown in these figures are the results the RSD deflections measured at these points at the same time. Excellent agreement between the measurements by the two devices is illustrated. These data emphasize the usefulness of the RSD data in defining the uniformity or lack thereof in the performance throughout the 1 by 8 m test sections, and as an independent check of MDD measurements.

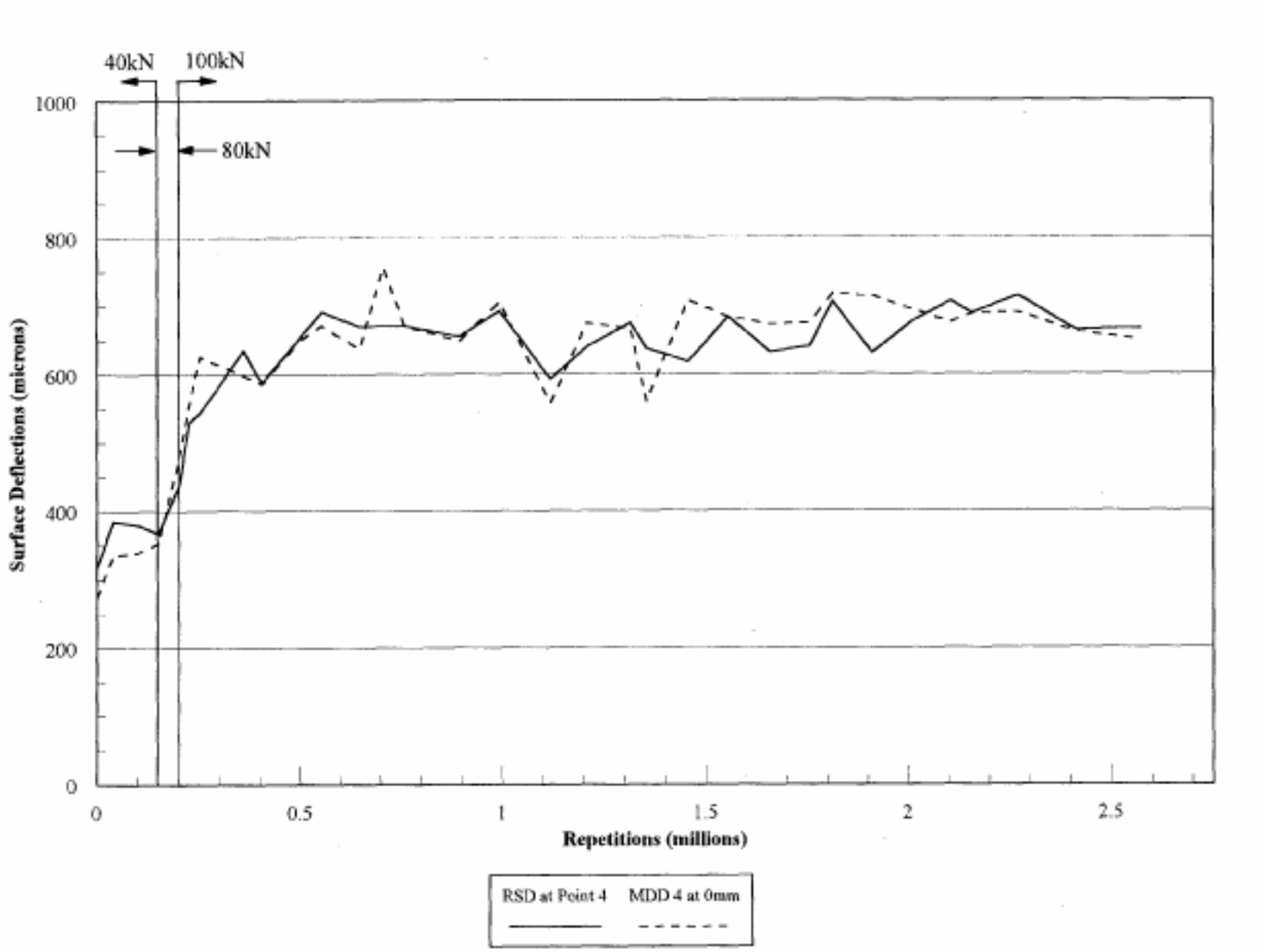

Figure 3.20 Comparison of Elastic Deflections Determined by the RSD and by the MDD at Point 4 with a 40 kN Load

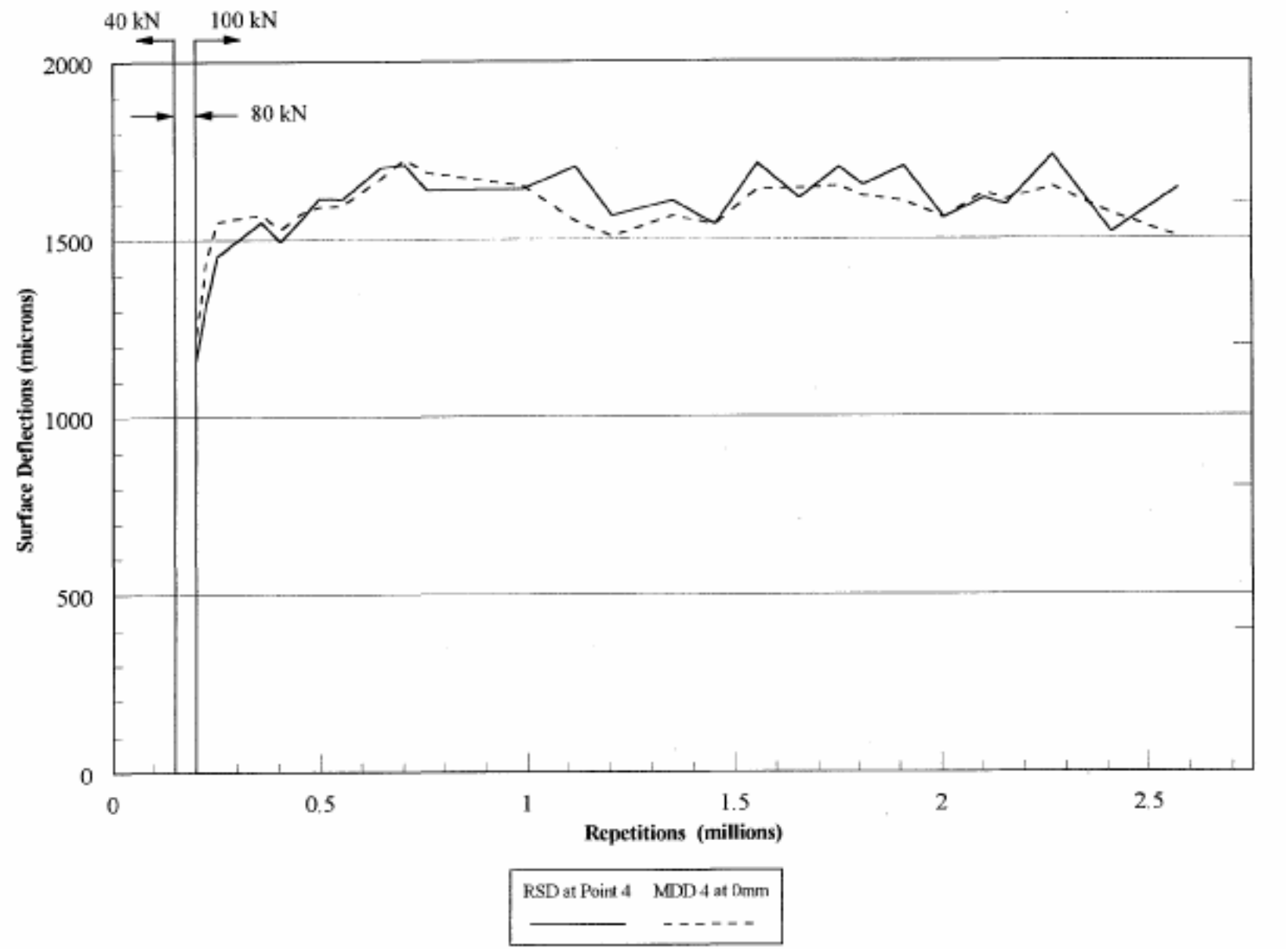

Figure 3.21 Comparison of Elastic Deflections Determined by the RSD and by the MDD at Point 4 with a 100 kN Load

3.4.1.3 Deflection Corrections for Temperature. Measured elastic deflections are influenced by the temperature of the pavement. Therefore, to relate deflections measured at different temperatures it is necessary to normalize the deflections to a standard temperature. In this analysis, a temperature of 20°C has been selected. To determine conversion factors for the measured deflections and to evaluate the extent to which temperature influenced these deflections, an analytical study was made of the deflection response of the pavement structure as affected by temperature.

The pavement was modeled considering the interface between the AC lifts to be frictionless and using the material characteristics given in Table 3.8.

A relationship between AC stiffness and temperature was determined using available laboratory data (*2*). With the AC stiffness vs. temperature relationship, analyses were performed on the pavement structure of Table 3.8 using the layered elastic analysis program CIRCLY to determine the surface deflection between the tires of the dual tire configuration of the HVS for the range of temperatures occurring during testing of Section 500RF. A regression equation was then developed from the CIRCLY results to predict deflection using

Table 3.8 Pavement Structure Model and Material Characteristics Used to Calculate Temperature Conversions

Pavement layer	Thickness (mm)	Poisson's ratio	Stiffness (MPa)
AC top lift	74	0.35	varies with temperature
AC bottom lift	76	0.35	varies with temperature
ATPB	76	0.4	690
Aggregate base/subbase	310	0.35	242
Subgrade	4	0.45	69

the stiffnesses of the two lifts. This regression equation (with a R^2=0.996) is composed of 5 terms: stiffness of top lift; square of the stiffness of top lift; stiffness of bottom lift; square of stiffness of bottom lift; and the product of the stiffness of top and bottom lifts.

Pavement temperature data collected at the times of deflection measurement were used to calculate AC stiffnesses using the AC stiffnesses vs. temperature relationship. When temperature data corresponding to the times of deflection measurement were not available, temperatures were estimated using data for the same hour from other days. The temperatures used to determine the AC stiffnesses from the stiffness vs. temperature relation were those occurring at the middle of each lift.

With the calculated AC stiffnesses for the specific hours at which deflections were measured, deflections were then determined using the AC stiffness vs. deflection regression equation. A deflection of the pavement structure at 20°C was also computed using the regression equation. The ratio of the computed deflection at 20°C to the computed deflection at the actual pavement temperature in each AC lift provided the conversion factor to normalize deflections to 20°C.

Measured and corrected deflections to 20°C for the RSD data at 11 selected data acquisition intervals are plotted in Figure 3.22 for deflections resulting from a 40 kN and 100 kN wheel load, respectively. The conversion factors ranged between 0.919 and 1.054 for the 40 kN deflections and 0.907 and 1.000 for the 100 kN deflections. The corrected deflections result in a more consistent relationship between deflection and repetitions and reduce some of the scatter. However, the differences between the converted deflections and measured deflections are not of significant magnitude to justify calculating and applying a conversion to all the measured surface deflections.

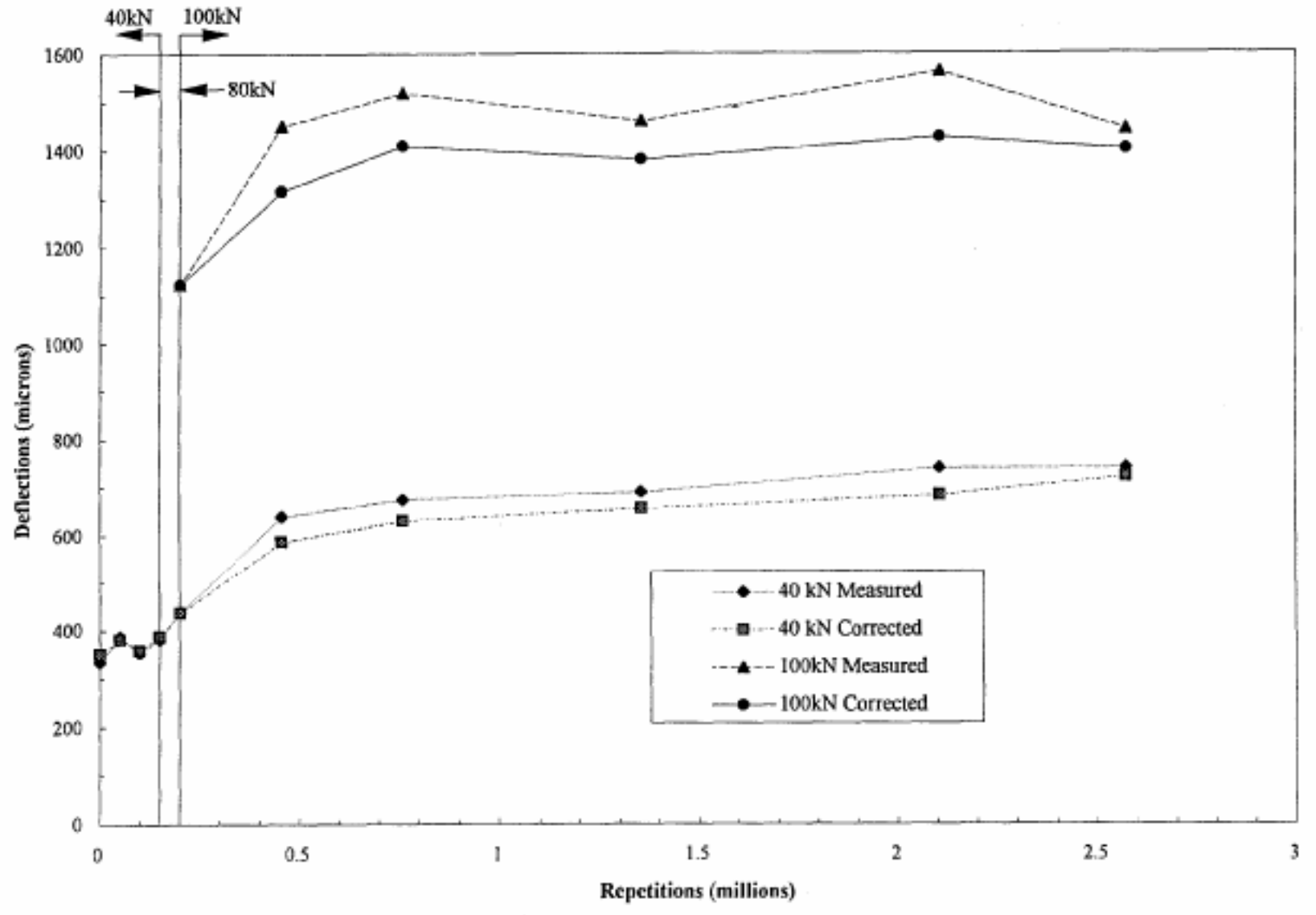

Figure 3.22 40 kN and 100 kN RSD Deflections Corrected to 20°C Deflections

3.4.2 In-Depth Elastic Deformations

Figures 3.23 and 3.24 summarize the deflections measured at various numbers of load applications at both MDD4 and MDD12. The deflections are reported separately for the measurements under the 40 kN and 100 kN loads.

Averages of all 40 kN and 100 kN MDD elastic deflection data measured on section 500RF before HVS loading commenced and after 2.57 million load applications are summarized in Table 3.9 for 40 kN and Table 3.10 for 100 kN test loads, respectively. These tables include the measurements recorded by both MDDs (MDD4 and MDD12). The 100 kN test load deflections were measured only after the HVS had reached 200 000 load repetitions at which point the traffic load was increased to 100 kN (Table 2.1). The data contained in these tables represent the average of 3 deflection measurements per measuring point.

From Tables 3.9 and 3.10 it is possible to determine the proportion of total surface deflection that under the test load is contributed by each layer. Results of this analysis are presented in Tables 3.11 and 3.12 for 40 kN and 100 kN test loads, respectively.

From Table 3.11 it can be seen that the percentage deflection which originated from the AC and ATPB layers changed from 14 percent to 19 percent under the 40 kN load. This would suggest the damage which took place in the AC layer (as manifested by surface cracking) could be responsible for this increase in elastic deflection. Unfortunately, due to the physical limitations of the MDD modules it was not possible to isolate the deflection in the AC layer from that of the ATPB. However, the deflection measured across the ATPB layer in conjunction with the AB layer (measured with MDD12) remained relatively constant (from 27 percent to 28 percent) during the test.

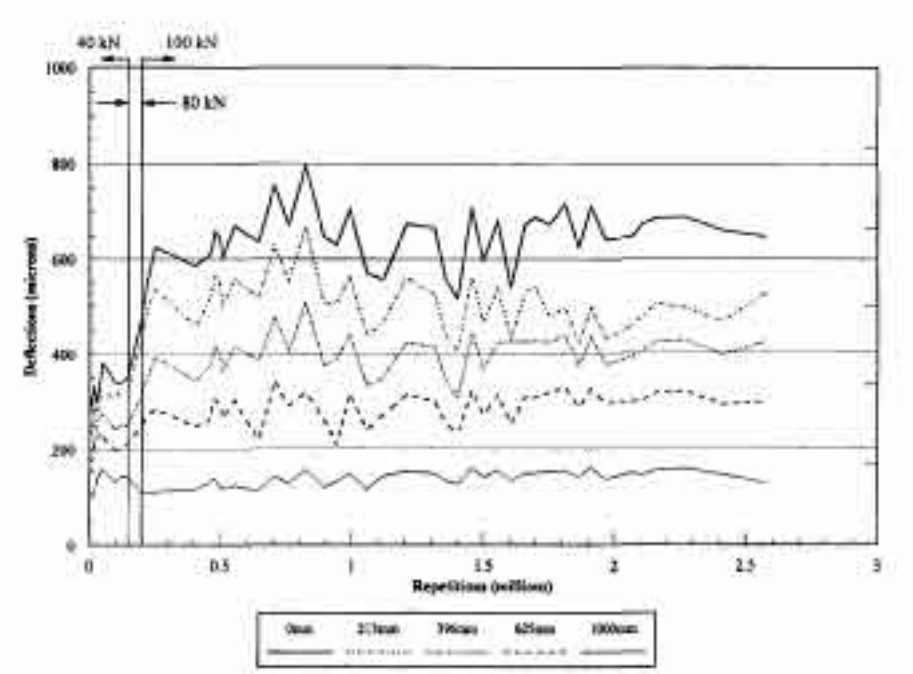

a. MDD4

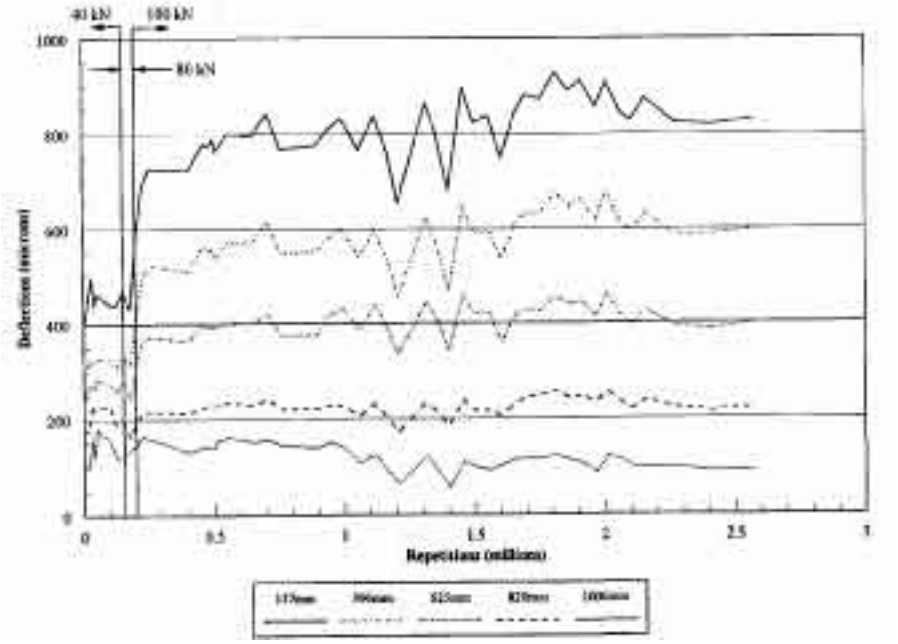

b. MDD12

Figure 3.23 Measured MDD Deflections vs. Load Repetitions at Various Depths Below Pavement Surface, 40 kN Test Load

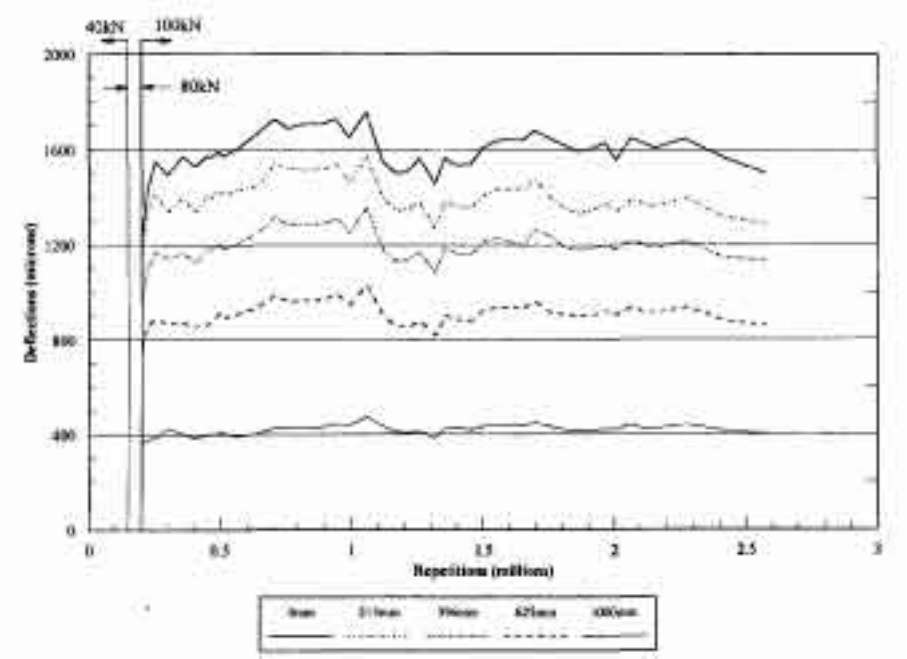

a. MDD4

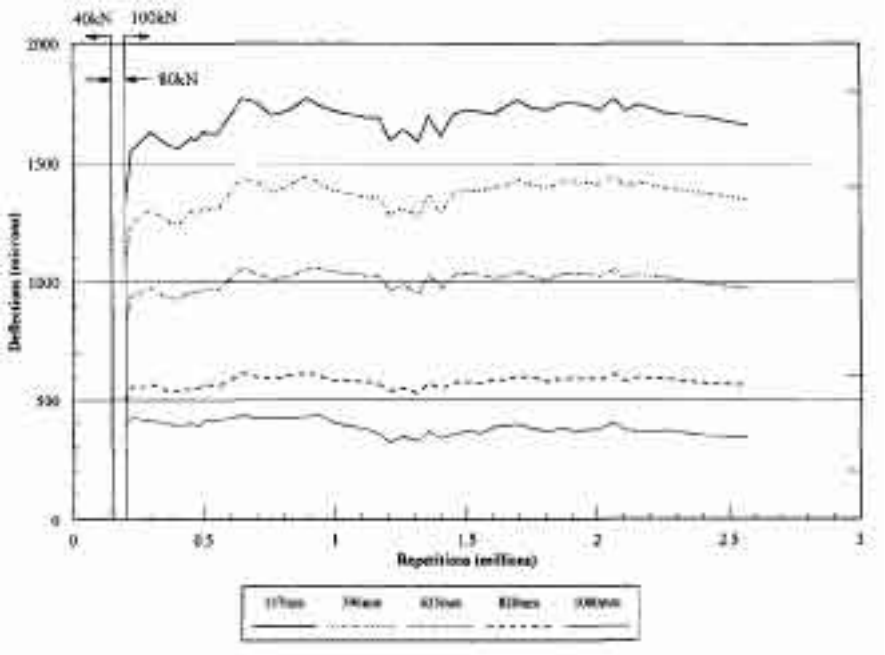

b. MDD12

Figure 3.24 Measured MDD Deflections vs. Load Repetitions at Various Depths Below Pavement Surface, 100 kN Test Load

Table 3.9 Summary of 40kN MDD Elastic Deflections

Level (mm)	Pavement Layer	Elastic in-depth Deflections (microns): Test Load = 40kN			
		MDD 4		MDD 12	
		Before HVS loading	After 2.57 M load applications	Before HVS loading	After 2.57 M load applications
0	AC	274	650	*	*
137	ATPB	*	*	391	829
213	AB	235	527	*	*
396	ASB	183	425	286	599
625	SG	149	300	243	399
820	SG	*	*	176	223
1000	SG	106	128	103	92

* MDD modules were not placed at these locations (see Figure 2.2)

Table 3.10 Summary of 100kN MDD Elastic Deflections

Level (mm)	Layer	Elastic in-depth Deflections (microns): Test Load = 100kN			
		MDD 4		MDD 12	
		After 200k load repetitions	After 2.57 M load repetitions	After 200k load repetitions	After 2.57 M load repetitions
0	AC	1 232	1 504	*	*
137	ATPB	*	*	1 329	1 659
213	AB	1 162	1 291	*	*
396	ASB	965	1 135	1 071	1 346
625	SG	768	859	832	973
820	SG	*	*	499	564
1000	SG	360	402	391	340

* MDD modules were not placed at these locations (see Figure 2.2)

Table 3.11 Percentage Elastic Deflection Per Layer, 40 kN Test Load

Pavement Layer	Percentage of total elastic deflection			
	MDD 4		MDD 12	
	Before HVS loading	After 2.57 M load applications	Before HVS loading	After 2.57 M load applications
AC+ ATPB	14	19	*	*
ATPB +AB	*	*	27	28
AB	19	16	*	*
ASB	12	19	11	24
SG	54	46	43	32

* MDD modules were not placed at these locations (see Figure 2.2)
Note: Calculated from Table 3.9

In the aggregate base the percentage deflection dropped from 19 to 16 percent during the course of the test which suggests that some stiffening likely occurred in this layer. At the same time, the percentage of total deflection occurring in the aggregate subbase increased from 12 percent to 19 percent at MDD4 and from 11 percent to 24 percent, at MDD12, which possibly indicates a weakening of that layer.

The percentage of total deflection occurring in the subgrade decreased from 54 percent to 46 percent at MDD4 and from 43 percent to 32 percent at MDD12. This change likely was due to some reduction in the water content of the subgrade. Before test 500RF commenced, heavy rainfall was recorded at the Richmond Field Station (see Figure 3.4) but no further precipitation took place during the summer months, and it is therefore quite possible that some drying of the subgrade occurred.

Table 3.12 presents similar results as in Table 3.11, but with the 100 kN test load. Because the trafficking load was increased to 100 kN only after 200,000 load applications, no 100 kN deflection data are available prior to 200,000 repetitions. Table 3.12 presents the

percentage relative deflections as measured by MDD4 and MDD12 between 200,000 and 2.57×10^6 load applications. The trends are the same as in Table 3.11.

3.5 VISUAL INSPECTIONS

Since fatigue distress in an asphalt pavement manifests itself in the form of surface cracks, crack monitoring was an essential part of data collection for test section 500RF. Crack data were collected by both visual inspection and direct measurement of crack length

Table 3.12 Percentage Elastic Deflection Per Layer, 100 kN Test Load

Pavement Layer	Percentage elastic deflection			
	MDD 4		MDD 12	
	After 200k load applications	After 2.57 M load applications	After 200k load applications	After 2.57 M load applications
AC/ATPB	6	14	*	*
ATPB/AB	*	*	19	19
AB	16	10	*	*
ASB	16	18	18	22
SG	62	57	54	45

* MDD modules were not placed at these locations (see Figure 2.2)
Note: Calculated from Table 3.10

and supported by photographic documentation. This section discusses the methodology used for determining surface cracking (both extent and severity) and the results of several cores taken from the section at the end of HVS testing.

3.5.1 Visual Inspection of Cracks

The first surface cracks were observed at approximately 650,000 repetitions and regular inspection of crack development was made from that point through the end of the test. To obtain crack length data, the pavement was illuminated with high-power lights followed by the marking of the cracks with spray paint in order to make them easily visible. A small chain was then laid out on each crack along its course and then stretched out and measured with a ruler. The observed average crack length obtained by this method as a function of load repetitions is shown in Figure 3.25.

Operator error is possible with this method of crack detection and the fluctuations evident in Figure 3.25 are due to the subjective nature of the crack observation procedure. The observed cracks were hairline cracks and at times difficult to detect visually. It is presumed therefore that operator error will result in fewer cracks being detected than actually exist. It was also assumed that cracks, once they appeared, did not cease to exist even if they were not detected by visual inspection and so a curve was fit to the crack length data with emphasis on peaks in the data as seen in Figure 3.25.

The lack of expansion, spalling, and other deterioration of the hair line cracks observed on the pavement surface can likely be attributed to two factors: 1) lack of rainfall and mineral particles on the surface of the test pavement, and 2) lack of cracking in bottom lift of AC. The first is discussed in the next paragraph while the second is discussed in Section 3.5.2 and Chapter 4.

In the field, crack formation is coupled with the effects of weather, mineral particles and other minute debris and high-speed traffic, all of which serve together to accelerate deterioration of the crack interfaces, making the cracks readily visible from a “windshield survey.” In contrast,

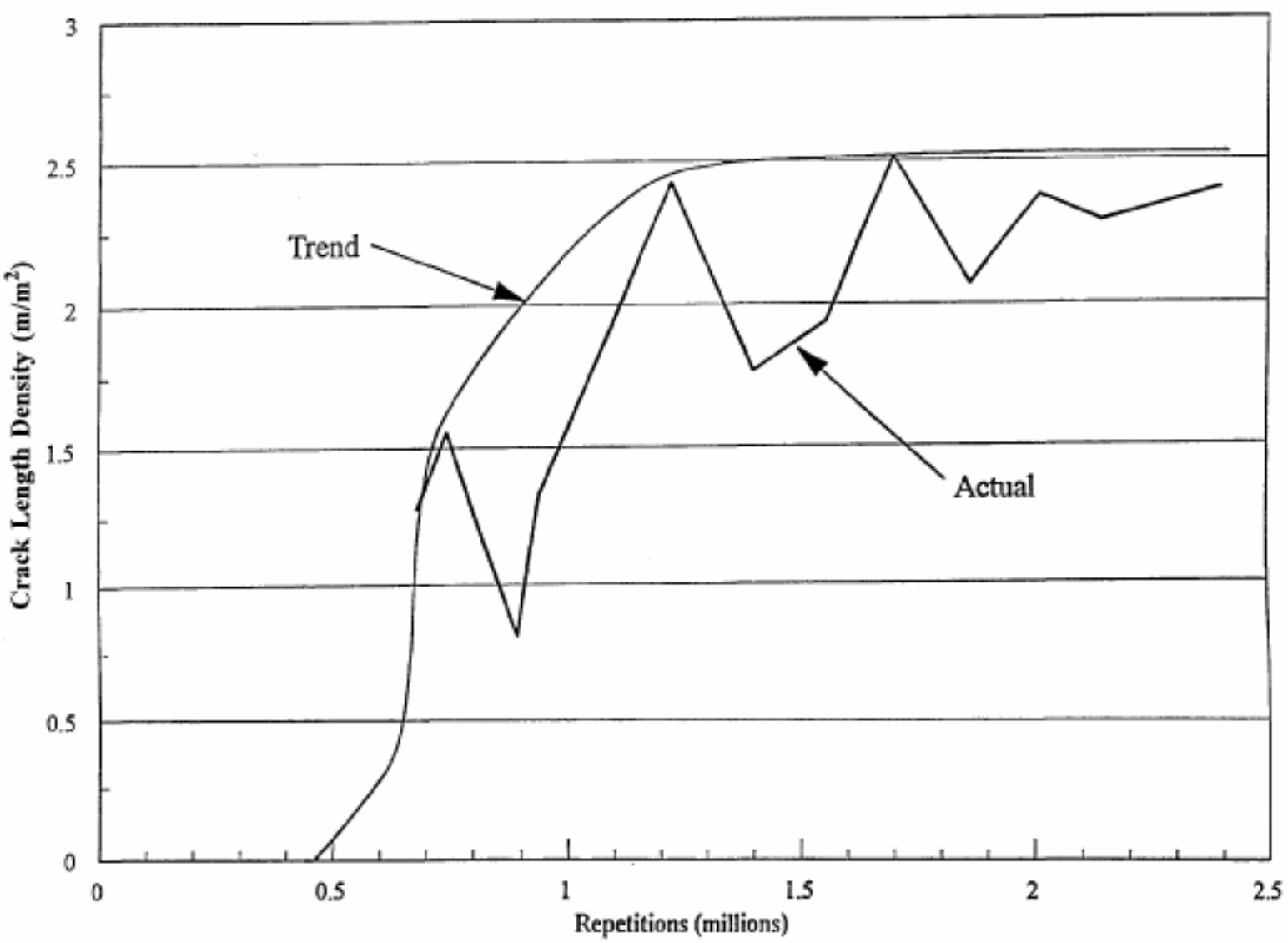

Figure 3.25 Crack Length Density Versus Load Repetitions

the hairline cracks observed on the trafficked HVS section do not experience rain on the surface which would enter cracks and possibly damage the material in the crack interface. If they did, it is likely that their visual nature would more closely correspond to that observed in the field. They also do not have mineral particles and other debris being washed or blown into the cracks, which may contribute to deterioration in the cracks when coupled with trafficking and thermal changes.

In spite of the obvious fluctuations shown in the figure, the expected increase in crack growth with respect to repetitions is evident. From approximately 600,000 to 1.2 million repetitions (Figure 3.25), observed crack length density increased from 0 to 2.0 m per m^2. After this period of rapid crack growth, the rate of crack propagation decreased significantly.

Because of the concerns expressed above, a new method for crack detection was explored during the course of the test to remove some of the subjective variation in crack detection. This new method was employed for the last crack inspection on Section 500RF and subsequent inspections on other HVS test pavements.

In this new procedure, photographs were made at regular intervals to record crack progression during the test. As mentioned previously, spray paint was used to mark the cracks and ensure that cracking patterns show up on film. This system involved identifying cracks as before, using bright lights and visual inspection; however, cracks were traced with a "lumber crayon"—a brightly colored waxy chalk—which allows for finer detail and closer adherence to the crack pattern than spray paint. A medium-format camera with a 60 mm by 70 mm negative was then used to photograph the marked cracks in approximately one meter squares. The resulting photos were then scanned into a computer, realigned to remove any camera perspective,

and then combined to obtain a two-dimensional schematic representation of crack growth as shown in Figures 3.26 and 3.27 at 700,000 and 2.5 million repetitions, respectively.

The surface cracking shown in Figure 3.27 clearly illustrates the areas which experienced the greatest amount of fatigue distress. These areas are located between points 5 and 8, and points 11 and 14. One of the first cracks to appear intersects the MDD12 topcap. Cracks originating at the MDD locations are expected since the installation process induces local disturbances in the pavement and the hole becomes an area of stress concentration. In addition, the highly cracked area between points 11 and 14, including MDD12, corresponds to a weaker spot in the pavement (at least as reflected in the RSD data obtained with the 40 kN load [Figure 3.16]).

3.5.2 Cores Taken From Section 500RF

In the Interim Report (*2*) it had been noted, from inspection of some cores taken after construction for mix evaluation, that there appeared to be little or no bond between the two asphalt concrete lifts. No tack coat was placed between the lifts because it was not required by Caltrans specifications, and would not have been used in typical Caltrans practice. It is likely, however, that a tack coat would have contributed to an improved bond between the lifts.

After completion of the test, a few cores were taken from observed crack locations to determine whether both AC lifts were cracked. As can be seen in the line drawings from photos in Figures 3.28 and 3.29, it was evident that the cracks went completely through the top lift and there was no evidence of cracking in the bottom AC lift. More cores will be necessary to fully assess the cracking condition of the pavement. Further investigative coring is not possible, however, until Goal 3 testing is completed.

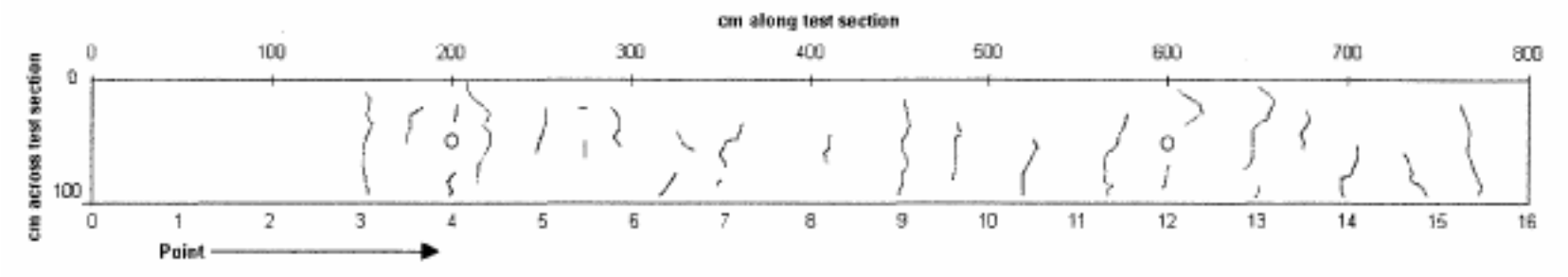

Figure 3.26 Crack Schematic at 750,000 Repetitions

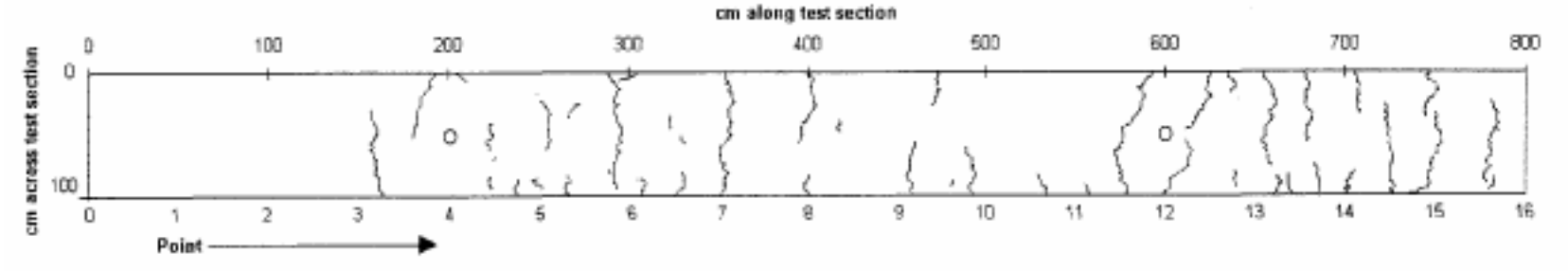

Figure 3.27 Crack Schematic at 2.5 Million Repetitions

As will be seen in Chapter 4, the absence of a tack coat and resultant weak bond between the two asphalt concrete lifts resulted in the critical horizontal tensile strain occurring at the bottom of the top AC lift. As a result, it is likely that crack formation started in this location rather than on the underside of the lower AC layer.

Another factor which can influence fatigue performance of asphalt concrete is the degree of compaction. In this instance, the top AC lift exhibited an average air void content after construction of about 6.5 percent while that of the lower lift was about 3.9 percent (*2*). Predictions based on laboratory fatigue test results suggest a decrease of 35 percent in fatigue life for an increase in void content in this range for this mix, assuming a uniform air-void content in both lifts and a uniform temperature distribution (*2*).

Based on these observations it is apparent that the fatigue life could have been longer if cracking had not initiated in the top lift, because the top lift had lower fatigue resistance than the bottom lift, and because the distance that cracks had to propagate to reach the surface is one-half of the distance had the cracks started on the underside of the lower lift.

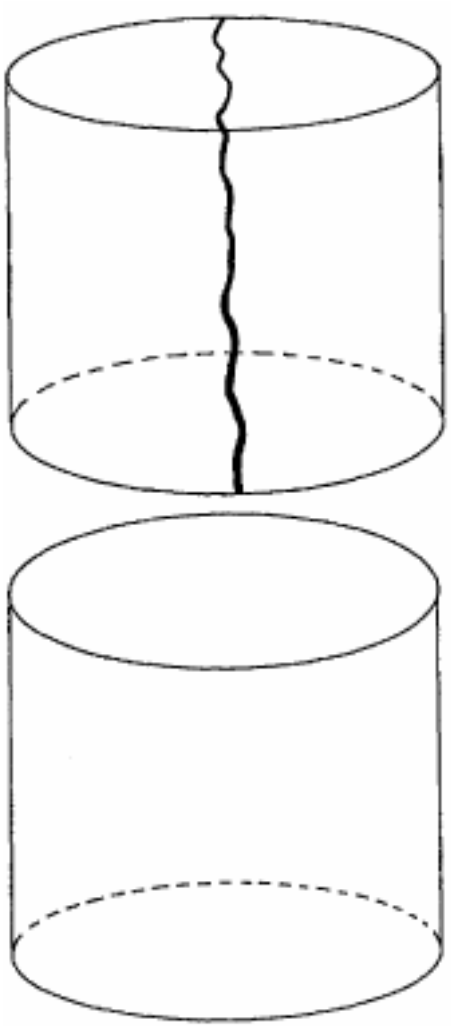

Figure 3.28 Line Drawings from Photographs of Core 1 from Cracked Section 500RF

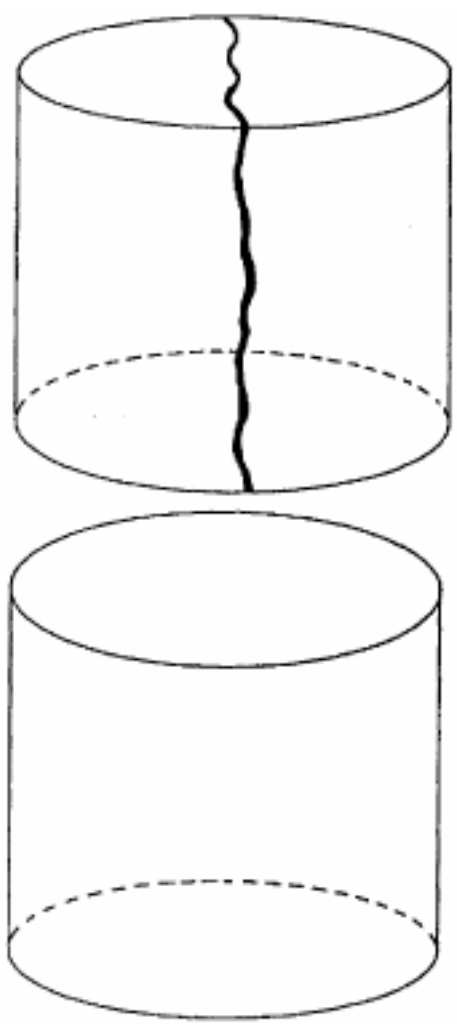

Figure 3.29 Line Drawings from Photographs of Core 2 from Cracked Section 500RF

CHAPTER 4

SECTION 500RF PERFORMANCE EVALUATION

At the conclusion of HVS loading, Section 500RF had been subjected to 150,000 applications of 40 kN loading, 50,000 applications of 80 kN loading, and 2,370,000 applications of 100 kN loading. Using an exponent of 4.2 in calculating load equivalency factors according to Caltrans procedures[2], Section 500RF experienced approximately 112,000,000 ESALs during its useful life, much greater than its design life of approximately 1,000,000 ESALs. It is the primary purpose of this chapter to investigate this large difference between the Caltrans design loading and the test measurement.

The Caltrans flexible pavement design procedure is a largely empirical one that does not identify and distinguish among various modes of pavement distress and does not enable detailed examination of many of the factors that can affect pavement performance. As a result, its use in reconciling the difference between the 1,000,000 Caltrans design ESALs and the 112,000,000 measured HVS ESALs is very limited. Fortunately, a mix analysis and design system, having the necessary attributes for this task and calibrated to current California design practice, is available for assessing fatigue behavior. Its use is particularly relevant in this case because the predominant distress mode in Section 500RF was judged to be surface cracking due to fatigue. When the HVS test was terminated, surface cracking, averaging 2.5 m in length for each square meter of area, was visible throughout the test section. The fatigue analysis and design system is

---

[2]Load equivalency factor = (wheel load in kN/40)4.2.

the primary tool used herein for evaluating factors responsible for the large difference between design and measured HVS loadings.

In addition to fatigue cracking, surface rutting was also observed in Section 500RF. The average rut depth at the surface was approximately 11 mm. The MDD measurements indicated that the asphalt concrete surface layers contributed approximately 52 percent to this average followed by 30 percent for the aggregate base and subbase, 11 percent for the subgrade, and 7 percent for the asphalt treated permeable base. Despite the fact that techniques are not readily available that would permit as detailed an examination of rutting as is possible for fatigue, a cursory examination of subgrade rutting is made herein based on the Asphalt Institute's subgrade strain criterion.

4.1 FATIGUE ANALYSIS AND DESIGN SYSTEM

The fatigue analysis and design system used herein was developed as a part of the Strategic Highway Research Program Project A-003A (*6*) as a performance based procedure for designing asphalt mixes to resist fatigue cracking. Recently upgraded (*14*), the system considers not only fundamental mix properties but also the level of design traffic, the temperature environment at the site, the pavement structural section, laboratory testing and construction variabilities, and the acceptable level of risk. Although it was not developed as a structural design tool, it has the necessary capabilities for assessing the impact of the structural section on pavement performance in fatigue.

4.1.1 System Description

For purposes of this study, the fatigue analysis and design system is used primarily to estimate the number of ESALs that can be sustained either in a design setting or in the HVS enclosure at the Richmond Field Station. The estimation is based on the following equation:

$$ESALs = \frac{N \bullet SF}{TCF \bullet M}$$

in which ESALs = the number of equivalent, 80 kN single axle loads that can be sustained in situ before failure, N = the number of laboratory load repetitions to failure under the anticipated in situ strain level, SF = a shift factor necessary to reconcile the difference between fatigue in situ and that in the laboratory, TCF = a temperature conversion factor which converts loading effects under the expected range of temperatures in the in situ temperature environment to those under the single temperature typically used in laboratory testing for conventional asphalts (20°C), and M = a reliability multiplier based on the level of acceptable risk and variabilities associated both with computing N and with estimating actual traffic loading.

The estimate of N is based on laboratory testing which measures the stiffness and fatigue life of the asphalt mixture and on elastic multilayer analysis which determines the critical strain (ε) expected at the underside of the asphalt layer in situ under the standard 80 kN axle load. N is simply the laboratory fatigue life that would result from the repetitive application of the strain expected in situ. The computer code, CIRCLY (*13*), was used for the elastic multilayer analyses reported herein.

The critical strain is also used in determining the shift factor, SF, as follows:

$$SF = 3.1833 \bullet 10^{5} \ \varepsilon^{1.3759} \quad for \quad \varepsilon \geq 0.000040$$

The shift factor accounts for differences between laboratory and field conditions, including, but not limited to traffic wander, crack propagation, and rest periods. The shift factor

relation is based on calibration of laboratory results against the Caltrans pavement thickness design procedure *(14)*.

The temperature conversion factor, TCF, has been previously determined for three representative California environments including those in coastal, desert, and mountain regions. For this study, in situ performance simulations were based on the TCF for a coastal environment as follows:

$$TCF = 1.754 \ \ln(d) - 2.891$$

in which d = the asphalt concrete thickness in centimeters. A separate analysis, reported later in this chapter, was performed to ascertain the impact of temperatures in the testing enclosure at the HVS site on pavement performance. This analysis found that the HVS temperature environment was more severe than that anticipated in situ and that HVS ESALs to failure predicted from simulation using the UCB-ISAP system would total only about 84.2 percent of the number of simulated HVS ESALs to failure for the coastal environment. Subsequent calculations used this percentage in estimating the ESALs to failure under HVS loading.

The reliability multiplier, M, is calculated as follows:

$$M = e^{z \sqrt{var(\ln N) + var(\ln ESALs)}}$$

in which e = the base of natural or Naperian logarithms, Z = a factor depending solely on the design reliability, var(ln N) = the variance of the logarithm of the laboratory fatigue life estimated at the in situ strain level, and var(ln ESALs) = the variance of the estimate of the logarithm of the design ESALs (i.e., the variance associated with uncertainty in the traffic estimate). Z is related to design reliability as follows:

Design reliability (percent)	Z	Design reliability (percent)	Z
98	2.05	80	0.841
95	1.64	60	0.253
90	1.28	50	0.000

The variance in the logarithm of the laboratory fatigue life, var(ln N), is currently calculated using a Monte Carlo simulation procedure. This procedure accounts for the inherent variability in fatigue measurements; the nature of the laboratory testing program (principally the number of test specimens and the strain levels); the extent of extrapolation necessary for estimating fatigue life at the design, in situ strain level; mix variability due to construction (namely asphalt and air-void contents); and structural variability due to construction (namely thickness of the asphalt concrete surface and the equivalent stiffness or modulus of supporting layers). The calculations of design ESALs reported herein use construction variances thought to be typical of prevailing California construction practice (*14*). A var(ln ESALs) of 0.3 has also been used in these calculations. Figure 4.1 contains a flow diagram of the ESALs determination embodied in this methodology.

4.1.2 Important Differences Between Pavement Design and HVS Testing

Summarized in this section are some of the important factors that help to explain the large difference between the Caltrans design estimate of approximately 1,000,000 ESALs and the HVS measurement of approximately 112,000,000 ESALs. Recognized and emphasized at the outset is the unknown error that results from assuming that the Caltrans design estimate is

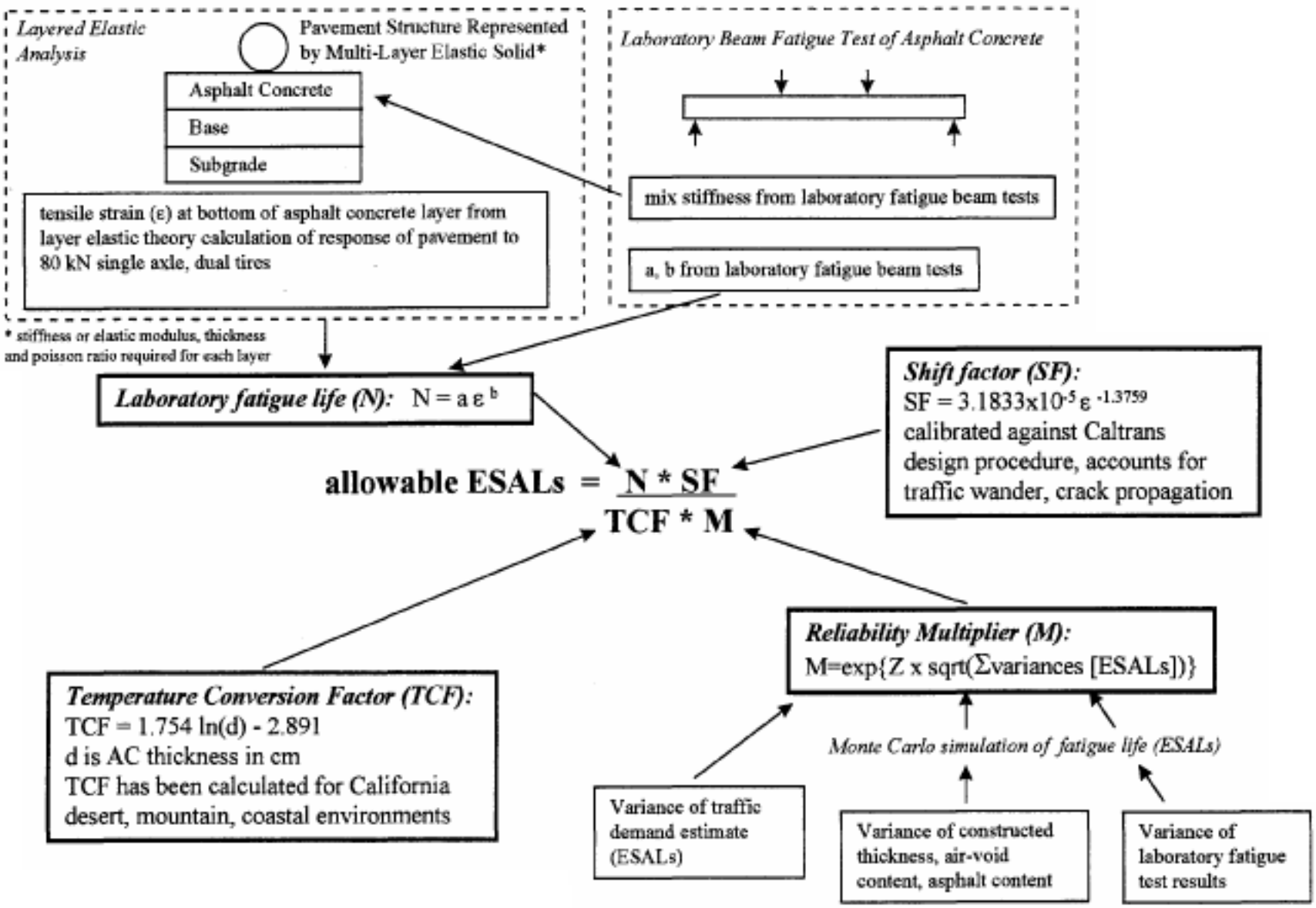

Figure 4.1 Methodology Followed in the Fatigue Analysis System to Determine ESALs.

dictated primarily by the prevention of premature fatigue cracking and not other distress modes.

The most fundamental difference between a pavement design estimate and the corresponding test measurement is that design must accommodate a range of mixtures of varying performance characteristics and must incorporate a safety factor to prevent premature failure as a result of testing, construction, and traffic variabilities. A direct measurement in the HVS test, on the other hand, reflects the performance characteristics of a specific mix, it is independent of laboratory testing and traffic variabilities, and, because the test section is limited to a small area, 1 by 8 m in dimension, the influence of construction variabilities is minimal. The design estimate is always expected to be much smaller in magnitude than the test measurement with the difference between the two increasing as the design reliability increases. The fatigue design and analysis system has the capacity to distinguish between design estimates and test measurements and to assess the impact of reliability on design estimates. No reliability factor is associated with simulations of HVS test ESALs for the reasons described above.

The next type of difference between design and testing relates primarily to pavement structural effects. In the current case, four notable differences distinguished Section 500RF from its design scenario including a top asphalt concrete lift thickness of 73 mm instead of 61 mm, a combined thickness of aggregate base and subbase of 310 mm instead of 411 mm, a distinct difference in the air voids within the two asphalt concrete lifts instead of uniform air voids, and a largely unbonded interface between the lifts instead of a fully bonded one (*2*).

Important differences are also found between the standard mix used for calibrating the fatigue analysis and design system and that used in HVS Section 500RF. Asphalt and air-void contents for the standard mix were set at 5 and 8 percent, respectively representing the approximate asphalt content found from the Hveem mix design procedure and relative

compaction of about 97.3 percent. The asphalt content in Section 500RF averaged 4.8 percent, the asphalt content determined by the Hveem procedure. The air-void contents averaged 7.8 percent in the upper lift and 4.4 percent in the lower lift corresponding to about 96.0 percent and 99.6 percent relative compaction for the section 500RF (HVS) mix, respectively. Besides construction, there were other differences between the standard mix and the mix used in the HVS test section as well.

The aggregates for the two mixes came from different sources and did not have the exactly same gradations, although both constructed gradations met Caltrans standard specifications for 19 mm coarse Type A mixes. The asphalt binders in both mixes were identified as being from California Valley sources and exhibited strikingly similar rheological and aging behavior in laboratory testing performed at TransLab (*15*). However, the binders were manufactured 6 years apart and not necessarily at the same refinery or using duplicate processes. The HVS mix laboratory test results are for beams cut from the HVS test pavement soon after construction, while the standard mix laboratory test results are from laboratory mixed and compacted specimens. Specimen compaction is not a likely source of significant differences because comparison of HVS mix laboratory test results from site and laboratory rolling wheel compaction indicated very little difference in stiffness and fatigue properties (*2*). Large differences in mix properties caused by laboratory mixing and short-term oven aging (STOA) versus plant mixing are also considered unlikely at this time although they have only been evaluated in terms of mix and binder stiffness and not in terms of fatigue properties. More data will be obtained from future CAL/APT test pavements to compare differences in fatigue properties between lab- and plant-mixed, laboratory compacted specimens.

As described elsewhere (*9*), laboratory testing of the standard mix yielded the following calibrations:

$$\ln N = -22.0012 - 0.164566 + AV + 0.575199\,AC - 3.71763\ \ln \varepsilon$$

and

$$\ln S = 10.282 - 0.076AV - 0.172\ \ AC$$

in which N = laboratory fatigue life in controlled-strain flexure, AV = air-void content in percent, AC = asphalt content in percent, ε = flexural strain, and S = laboratory flexural stiffness in mPa. The HVS mix (*2*) yielded the following calibrations for an asphalt content averaging 4.8 percent:

$$\ln N = -21.9252 - 0.106663AV - 4.14248\ \ln \varepsilon$$

and

$$\ln S = 9.5603 - 0.084914\ AV$$

As above S = laboratory stiffness in MPa. Based on these calibrations, the laboratory fatigue life of the HVS mix is two to eight times that of the standard mix, and its stiffness is 1 to 8 percent greater. The HVS mix is therefore expected to perform much better than the standard mix.

Potential factors contributing to the large difference in fatigue behavior between the two mixes presented herein do not provide a clear understanding of its cause. The similarity of the mix stiffnesses provides further evidence that it is likely that the binders come from a similar source. The difference in fatigue behavior provides a strong example of the benefit of laboratory fatigue testing to assess mix performance. It also emphasizes that factors in addition to asphalt type, air-void content and asphalt content, can affect fatigue performance. *Laboratory fatigue testing to assess fatigue performance is particularly important when selecting mixes for high-cost jobs and other important projects and when considering new or unique mixes.*

Finally environmental differences also distinguish HVS conditions from design conditions. One of these has already been mentioned, namely, temperature. As explained later, detailed analysis has shown that pavement performance is better under natural conditions than in the protected environment of the HVS enclosure. Specifically, the protected environment may limit the number of ESALs to only about 84.2 percent of that capable of being supported by a pavement similar to Section 500RF under the natural temperatures expected in California coastal areas during the period of the 500 RF test, i.e., May to November. The second major environmental difference is due to the effects of moisture. The protected HVS environment limits the amount of moisture in the pavement and practically eliminates cyclic wetting and drying. The net effect is expected to be beneficial. Moisture effects are simulated in this analysis by assuming that effective moduli of all supporting layers (ATPB, AB, ASB, and subgrade) under natural conditions are 80 percent of those in Section 500RF. It must be emphasized that the 80 percent is an assumed quantity used for illustration purposes only. It is not a result of detailed, scientific inquiry.

Quantification of the effects of these differences, using the fatigue analysis and design system, is the objective of the next section of the report.

4.1.3 General Performance Analysis

For this analysis, the computer code, CIRCLY, was used in computing critical strain levels. The applied load consisted of a 40 kN (9,000-pound) wheel load distributed on dual tires (30.5 cm [12 inches] center-to-center) with a contact pressure of 690 kPa (100 psi). A distinction was made between Section 500RF *design conditions* and the as-built and as-tested *HVS*

conditions with respect to layer thicknesses and environmental influences. Quantitatively the differences are as follows:

	Design conditions	HVS conditions
Thickness of upper asphalt concrete lift (mm)	61	73
Combined thickness of aggregate base and subbase (mm)	411	310
Moduli of all supporting layers (ATPB, AB, ASB, and subgrade)	80% of HVS moduli	

Further distinction was made between a *standard mix* and the *HVS mix*. The standard mix was that used in calibrating the fatigue analysis and design system. Components included a Watsonville granite and an AR-4000, apparently from California valley sources. Asphalt and air-void contents were assumed to be 5 and 8 percent, respectively. The HVS test utilized a different aggregate but the grading was similar to that of the standard mix. The asphalt was an AR-4000 from California Valley sources, and the asphalt content of the mix was 4.8 percent. Air voids averaged 7.8 percent in the upper lift and 4.4 percent in the lower lift.

The temperature environment was essentially ignored for the analyses, with a constant temperature of 20°C assumed for both design conditions and HVS conditions. This assumption results in a TCF of 1.00 because the laboratory test temperature is 20°C. A preliminary comparison of the temperature environments at the HVS site and for the California coastal environment is included later in this chapter.

Five different cases, defined as follows, were analyzed:

Case	Description	Critical strain location
1	Design conditions with standard mix (8% AV and 5% AC); full friction interface	Bottom of lower lift
2	HVS conditions with standard mix (8% AV and 5% AC); full friction interface	Bottom of lower lift
3	HVS conditions with standard mix (4.4% AV bottom lift, 7.8% AV top lift and 5% AC); full friction interface	Bottom of lower lift
4	HVS conditions with HVS mix (4.4% AV bottom lift, 7.8% AV top lift and 4.8% AC); full friction interface	Bottom of lower lift
5	HVS conditions with HVS mix (4.4% AV bottom lift, 7.8% AV top lift and 4.8% AC); frictionless interface	Bottom of upper lift

Elastic parameters used in the CIRCLY computations are identified in Table 4.1.

Table 4.1 Elastic Parameters for CIRCLY Analyses

Layer	Case				
	1	2	3	4	5
Modulus (MPa)					
Upper AC lift	6,729	6,729	6,829	7,317	7,317
Lower AC lift	6,729	6,729	8,839	9,766	9,766
ATPB	827	1,034	1,034	1,034	1,034
AB	240	300	300	300	300
ASB	120	150	150	150	150
Subgrade	55	69	69	69	69
Poisson's ratio					
Upper AC lift	0.35	0.35	0.35	0.35	0.35
Lower AC lift	0.35	0.35	0.35	0.35	0.35
ATPB	0.40	0.40	0.40	0.40	0.40
AB	0.35	0.35	0.35	0.35	0.35
ASB	0.35	0.35	0.35	0.35	0.35
Subgrade	0.45	0.45	0.45	0.45	0.45
Thickness (mm)					
Upper AC lift	61	74	74	74	74
Lower AC lift	76	76	76	76	76
ATPB	76	76	76	76	76
AB	182	182	182	182	182
ASB	229	137	137	137	137
Subgrade	Semi-infinite	Semi-infinite	Semi-infinite	Semi-infinite	Semi-infinite

The first matter to be addressed includes both the effect of reliability on estimates of design ESALs as well as the fundamental difference between design ESALs whether from the Caltrans or UCB-ISAP procedures, and HVS ESALs whether measured under HVS loading or simulated using the UCB-ISAP system. In computing HVS ESALs, variances of the several parameters (asphalt content, air-void content, asphalt concrete thickness, foundation support, and traffic) were assumed to be negligible. Computations using the UCB-ISAP system for Case 1 conditions yield the following ESAL estimates:

Simulated HVS ESALs	UCB-ISAP Design ESALs for reliabilities of:			
	80%	90%	95%	98%
8,056,000	3,393,000	2,161,000	1,493,000	979,000

This tabulation shows quite clearly the influence of reliability on design ESALs. It is interesting that the fatigue analysis and design system estimated 2,161,000 design ESALs at 90-percent reliability, about twice the Caltrans design estimate of approximately 1,000,000 ESALs. The fatigue analysis and design system estimated 979,000 ESALs at 98 percent reliability, very nearly the same as the Caltrans design estimate. As expected, the 8,056,000 simulated HVS ESALs is considerably greater than any of the design ESALs: for a design reliability level of 90 percent, the computed ratio of simulated HVS ESALs to UCB-ISAP design ESALs is approximately 3.7.

Next, in order to demonstrate the significant difference between as-built and as-tested HVS conditions and assumed Caltrans design conditions, the simulated HVS ESALs estimate for Case 2 was compared with that for Case 1. Results are as follows:

Simulated HVS ESALs for:	
HVS conditions with standard mix (8% AV and 5% AC): full friction interface	Design conditions with standard mix (8% AV and 5% AC): full friction interface
18,133,000	8,056,000

The ratio of HVS ESALs for HVS conditions to that for design conditions is approximately 2.3. The enhanced simulated performance for the HVS environment stems from a combination of thickness differences and environmental effects including those of both temperature and moisture.

To demonstrate the effect of the excellent mix compaction achieved in the construction of Section 500RF, particularly of the lower lift, the simulated HVS ESALs estimate for Case 3 was compared with that for Case 2. Results are as follows:

Simulated HVS ESALs for:	
HVS conditions with standard mix (4.4% AV bottom lift, 7.8% AV top lift and 5% AC): full friction interface	HVS conditions with standard mix (8% AV and 5% AC): full friction interface
52,951,000	18,133,000

The very significant effect of air-void content is illustrated by a ratio of approximately 2.9 in the HVS ESALs estimate for a 4.4-percent bottom lift and 7.8-percent top lift compared to that for an 8-percent mix in both lifts. This finding emphasizes the importance of good construction practice and the potential impact of greater compaction than current Caltrans specifications typically require. An even larger improvement in simulated fatigue life than that shown here would have been observed if the 4.4-percent air-void content had been obtained in both lifts. These corroborate similar findings for a variety of typical Caltrans pavement structures reported previously (*9*).

To demonstrate the effect of the superior fatigue performance of the HVS mix compared to the standard mix, the simulated HVS ESALs estimate for Case 4 was compared with that for Case 3. Results are as follows:

Simulated HVS ESALs for:	
HVS conditions with HVS mix (4.4% AV bottom lift, 7.8% AV top lift and 4.8% AC): full friction interface	HVS conditions with standard mix (4.4% AV bottom lift, 7.8% AV top lift and 5% AC): full friction interface
292,237,000	52,951,000

The ratio of Simulated HVS ESALs for these two conditions is approximately 5.5. This large difference is not clearly attributable to any one particular component of the two mixes, and is likely due to a combination of potential differences in components including aggregate type, asphalt production and aggregate gradation.

It should be noted that the Simulated HVS ESALs for Case 4 (292,237,000) exceeds the measured number of 112,000,000 HVS ESALs (assuming a 4.2 exponent for load equivalency) by a rather significant amount. A part of this difference may well be due to imprecision of the fatigue analysis and design system, to inappropriate assumptions made for this analysis, and/or to important factors not yet identified and accounted for.

One such factor relates to the lack of bonding at the interface between upper and lower asphalt concrete lifts. CIRCLY allows an examination of the interface condition but, unfortunately, only at the two extremes, full-friction and frictionless interfaces. The interface condition of Section 500RF is likely somewhere between these two extremes: the interface is rough (but unbonded) and the weight of the upper layer combined with vertical compressive stress beneath the load should allow some of the horizontal interface movement to be transmitted from one lift to the other. Even though partial friction conditions can not be modeled with

available techniques, the notable effect of interface condition can be demonstrated by comparing the HVS ESALs estimate for Case 5 with that for Case 4. Results are as follows:

Simulated HVS ESALs for:	
HVS conditions with HVS mix (7.2% AV top lift, 3.2% AV bottom lift and 4.8% AC): frictionless interface	HVS conditions with HVS mix (7.2% AV top lift, 3.2% AV bottom lift and 4.8% AC): full friction interface
6,744,000	292,237,000

This remarkably large effect is due to two factors, one of which is the nature of friction at the interface between lifts. The other results from a shift in the critical strain location from the bottom of the lower lift for the full friction interface to the bottom of the upper lift for the frictionless interface. In the upper lift the air-void content is much greater, and load repetitions necessary to propagate cracks to the top surface are expected to be smaller because of the reduced thickness through which the cracks must penetrate. The combined effect of a larger air-voids content and a reduced overlying thickness is a significant decrease in simulated fatigue life.

Although this analysis is not definitive because the interface condition can not be accurately modeled, the estimate of 292,237,000 ESALs seems to be realistically in line with the measurement of 112,000,000 ESALs under HVS loading following qualitative evaluation of interface conditions discussed in Chapter 3. The simulation results indicating that cracking would occur in the upper lift before it occurred in the lower lift for the frictionless interface condition corroborate the cracking observations from Section 55RF cores.

Certainly the analysis reported herein is of significant help in reconciling the difference between the Caltrans design estimate of 1,000,000 ESALs and the HVS test measurement of 112,000,000 ESALs. In addition it has highlighted factors such as mix, air-void content and interface condition that can have a significant impact on pavement performance.

4.1.4 Specific Effects of HVS Temperatures

Of interest in the analysis and interpretation of HVS test results is the influence of the temperature environment on fatigue performance and the impact of the relatively controlled environment of the HVS Test Sections at RFS on pavement life as compared to other environments in California and to the assumption of a constant 20°C environment assumed for the General Performance Analysis (4.1.3 of this chapter). To assess this temperature influence, a number of simulations were performed using four temperature environments which included the pavement temperatures measured in section 500RF and pavement temperatures simulated by a software program CMS4 (*10*) for three typical California temperature environments; coastal, mountain and desert. The period of analysis for section 500RF included June 2, 1995 when the 100 kN load trafficking began, through November 8, 1995, the end of the test. For the three California environments the same dates were used in the analysis but the data was obtained from 1988, an arbitrarily chosen year for which the necessary weather data were readily available.

Because of limited laboratory mix fatigue data at multiple temperatures at the time of the analysis and to simplify the analysis procedure, AC stiffness and fatigue life relationships developed earlier were employed (Figures 4.2 and 4.3). The simulations assumed that the critical strain location was at the bottom of the bottom AC lift at the centerline of the dual-tire assembly. Full friction was assumed between the AC lifts and between all other layers. ELSYM5 was used to determine the critical tensile strains under dual tires having a

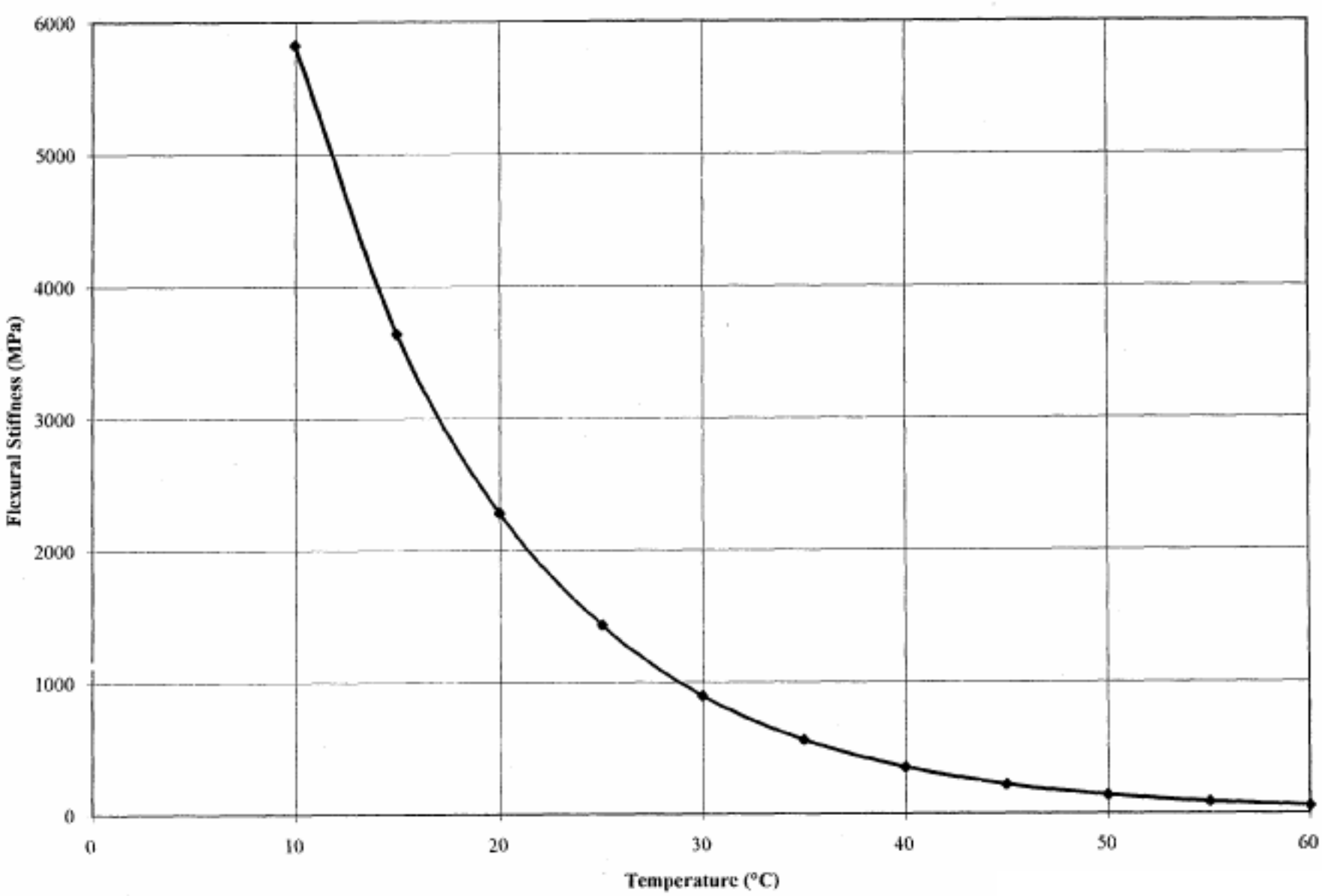

Figure 4.2 Asphalt Concrete Stiffness and Temperature Relationship (*7*)

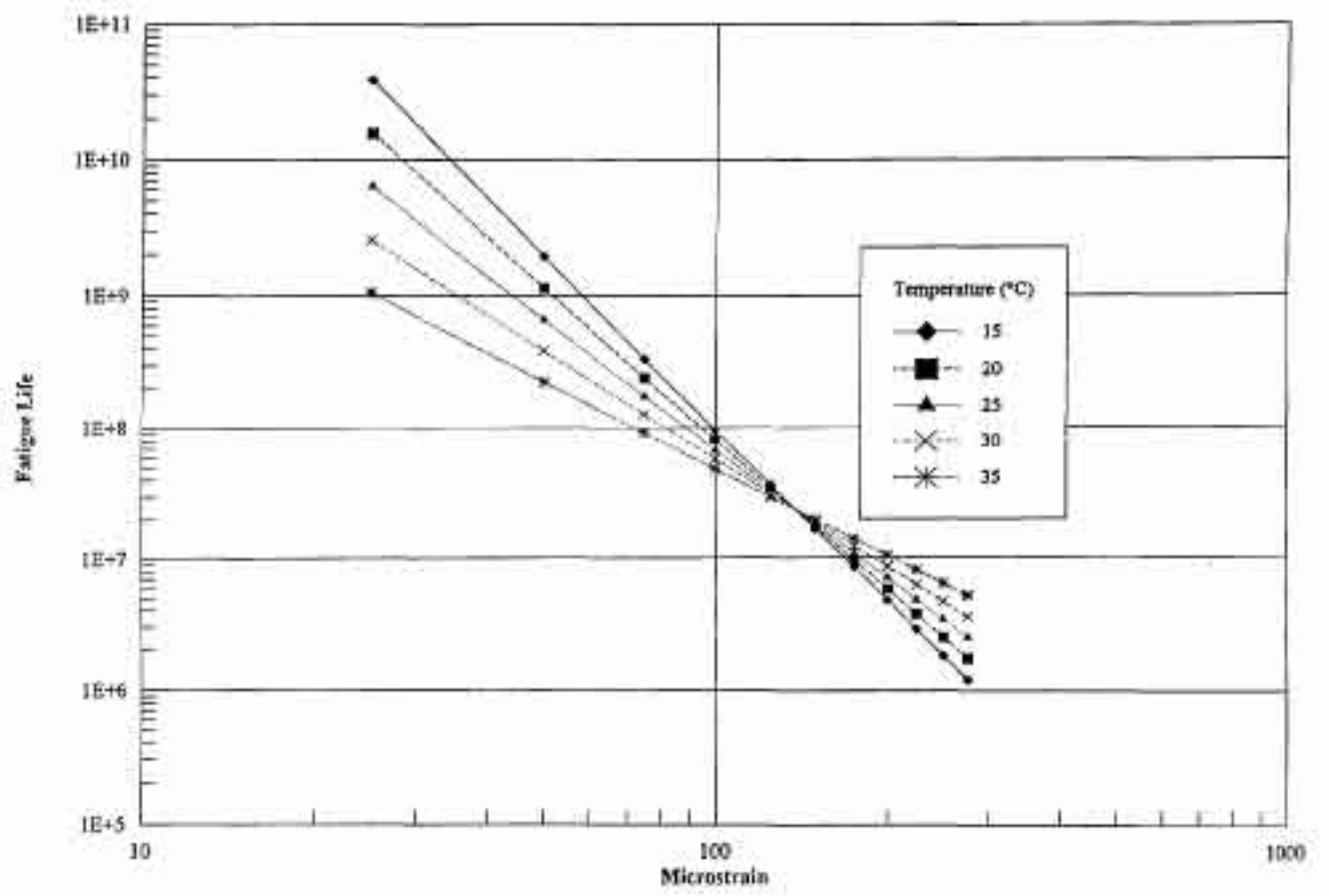

Figure 4.3 Fatigue Life and Strain Relationship (*7*)

combined load of 100 kN with center-to-center spacing of 366 mm and tire pressures of 690 kPa. The pavement structure that was evaluated is shown in Table 4.2 with the relevant material characteristics.

Table 4.2 Pavement Structure and Material Characteristics for Investigation of Temperature Environment Effects

Pavement Layer	Thickness (mm)	Poisson's ratio	Stiffness (MPa)
AC Top lift	74	0.35	varies with temperature
AC Bottom lift	76	0.35	varies with temperature
ATPB	76	0.4	1200
Aggregate base/subbase	310	0.35	242
Subgrade	4	0.45	69

The simulated fatigue damage was accumulated on an hourly basis. For each hour, the average temperatures in the top and bottom lifts were first tabulated. Because of occasional missing temperature data for the HVS pavement, interpolation was sometimes necessary to assure that each hour was represented in the analysis. AC layer stiffnesses, determined from these temperatures and the AC stiffness-temperature relationship, were used to compute the critical tensile strain at the bottom of the bottom lift. Next, the combination of bottom-lift temperature and maximum tensile strain determined the fatigue life. The product of the reciprocal of fatigue life and the number of load repetitions represented the relative amount of damage accumulated during the hour. Simple summation produced the total damage accumulated during the simulation period. The accumulated fatigue damage totals as a fraction of total fatigue life are as follows:

HVS	0.183
Coastal	0.154
Mountain	0.131
Desert	0.067

Very little significance should be attached to the magnitude of these estimates because the mix used in the HVS sections differs from the hypothetical mix evaluated herein and because an appropriate shift factor was not applied. Nevertheless, the totals suggest that the most damaging environment with respect to fatigue distress is the enclosed environment at the RFS, followed by the coastal, mountain and desert environments. Similar investigations, but changing the material characteristics or loading conditions, were completed and also resulted in the rankings listed above.

The effect of pavement temperatures measured during HVS loading of Section 500RF was evaluated for the hypothetical mix rather than the standard mix in the 500RF structure. For Case 1 a Temperature Conversion Factor (TCF) was computed for the design pavement structure with the standard mix and the coastal environment. The TCF for that case was 1.702. Assuming that the hypothetical mix has temperature susceptibility similar to that of the standard mix, application of the 500RF TCF to Case 1 of the general performance analysis results in the following estimates:

Simulated HVS ESALs	UCB-ISAP Design ESALs for reliabilities of:			
	80%	90%	95%	98%
4,733,000	1,993,000	1,270,000	877,000	575,000

It can be seen that with this assumption the estimated fatigue life for the 90 percent reliability is remarkably close to the design estimate of 1,000,000 ESALs.

For each temperature environment, the most damaging temperatures for fatigue performance were in the approximate range of 25°C to 30°C (Figures 4.4a-d). The fact that a greater fraction of the hourly temperatures were in this critical range at the RFS site than at the other locations for the portion of the year analyzed helps to explain why simulated fatigue damage accumulated more rapidly at the RFS than at the other three locations. Other analyses are included in Appendix B.

In general the analyses show that the HVS test environment at RFS is likely to result in greater accumulation of fatigue distress than other environments in California. However, it should be emphasized that the analysis did not recognize the weak bond between the top and bottom lifts of the asphalt concrete, and considered a "hypothetical" mixture rather than the actual mixture used in test section 500RF.

4.2 SUBGRADE RUTTING

The Caltrans pavement design procedure is intended to prevent premature failure from subgrade rutting as well as fatigue cracking. The average rut depth at the surface of Section 500RF at the termination of HVS trafficking was approximately 11 mm. MDD measurements indicated that about 30 percent, or 3.3 mm, occurred in the base and subbase layers, and about 11 percent, or 1.2 mm, occurred in the subgrade. A comprehensive procedure for evaluating the potential for rutting in the underlying layers including reliability has not been developed as it has been for fatigue cracking. A cursory evaluation of the

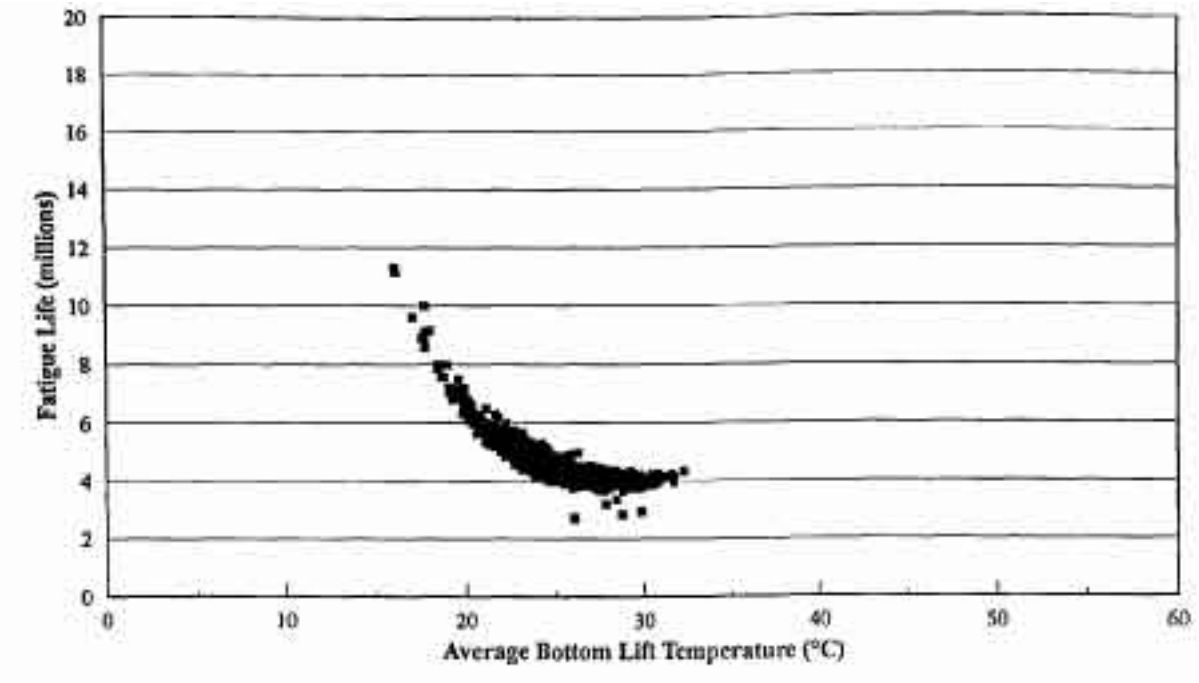

a. HVS test section at RFS

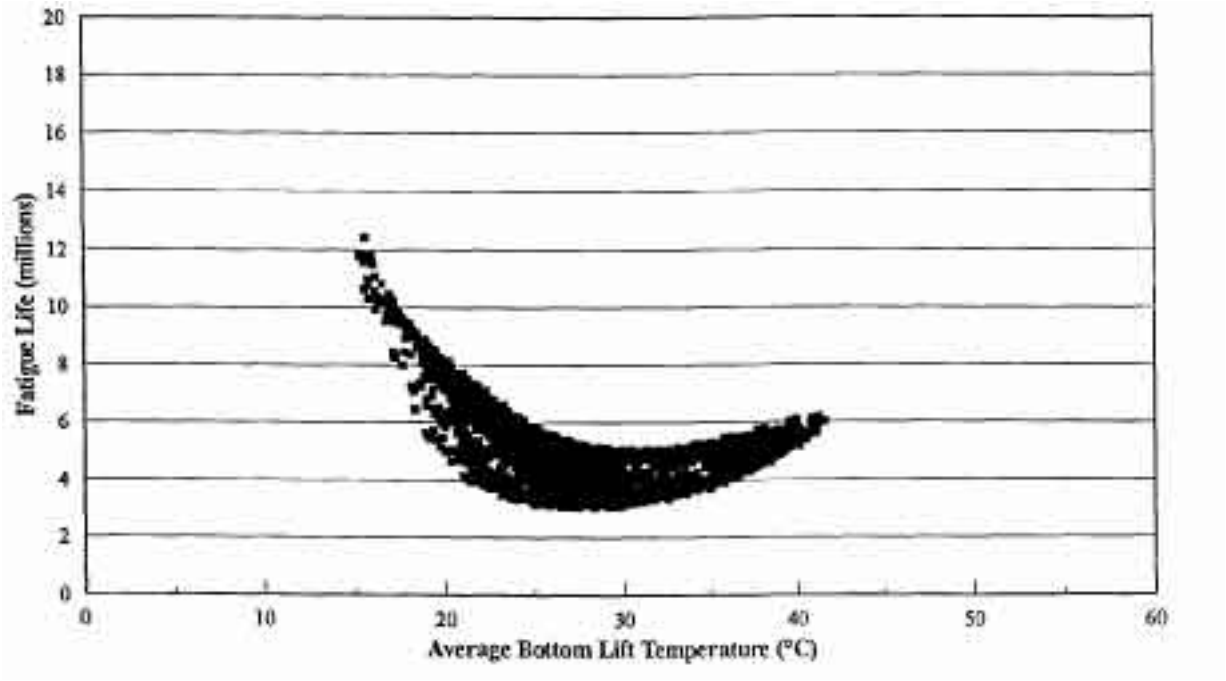

b. Coastal

Figure 4.4 Predicted Fatigue Life and Hourly Temperature of the Bottom Lift for Four California Environments

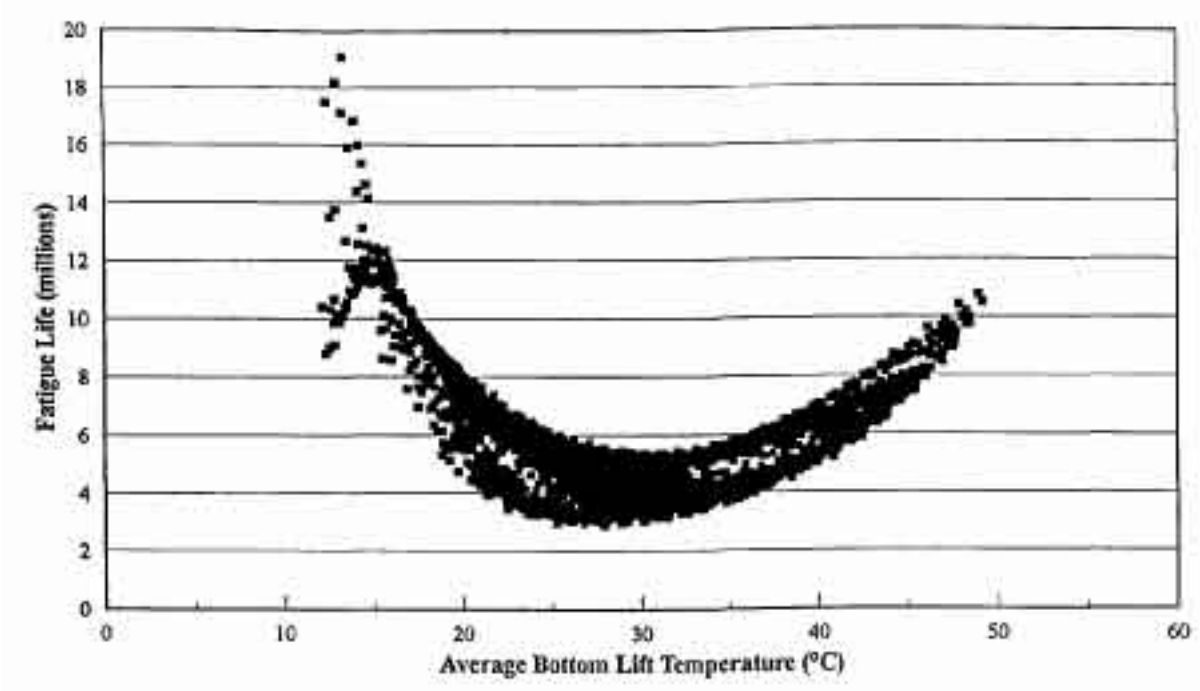

c. Mountain

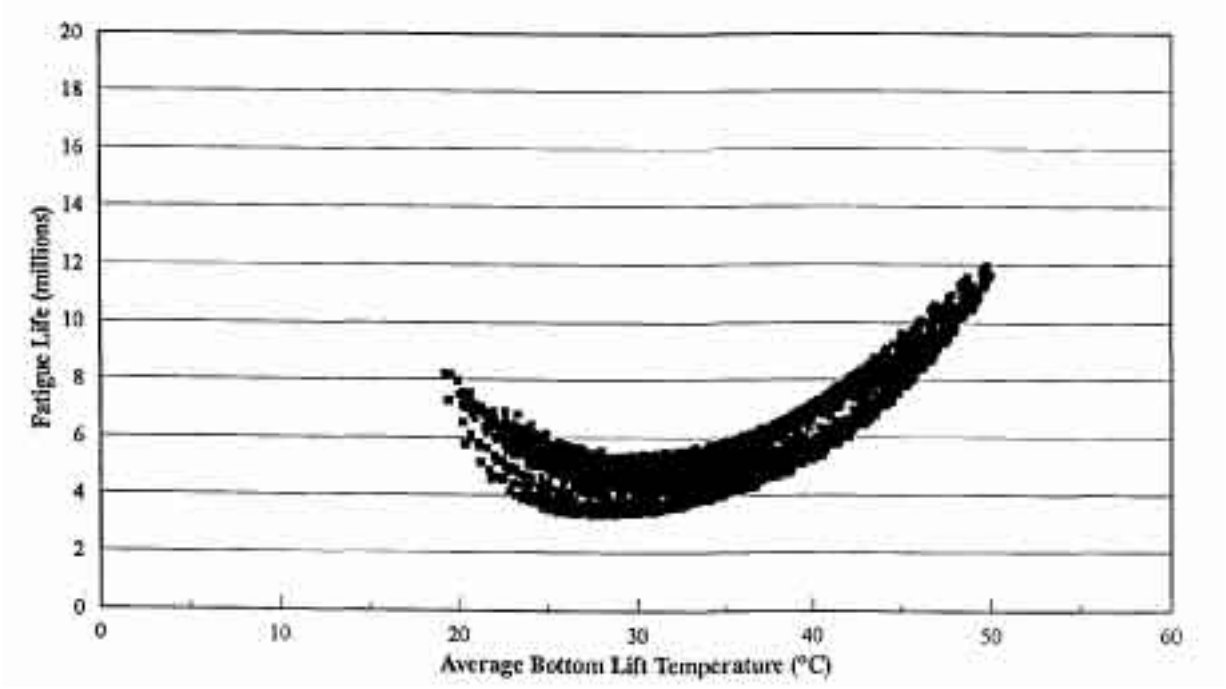

d. Desert

Figure 4.4 Predicted Fatigue Life and Hourly Temperature of the Bottom Lift for Four California Environments (cont.)

Section 500RF pavement with respect to rutting in the underlying layers was performed using criteria developed by the Asphalt Institute for vertical compressive strain at the top of the subgrade to minimize rutting. The subgrade rutting evaluation was performed for the five cases of mix type, site conditions and construction included in the fatigue evaluation.

4.2.1 Subgrade Rutting Criteria

The Asphalt Institute criterion for subgrade strain is:

$$N = 1.05\ (10^{-9})\ \varepsilon_c^{-4.484}$$

where N = number of load applications, and

ε_c = vertical compressive strain at subgrade surface.

The equation is based on that used by Santucci (*16*) and is based on analyses of pavements designed according to the Caltrans design procedure (*17*). The authors of the Asphalt Institute methodology state that

> *"if good compaction of the pavement components is obtained and the asphalt mix is well designed, rutting should not exceed about 12.7 mm (0.5 in.) at the surface for the design traffic, N."*

This statement implies some conservatism in the criterion; however it does not include an explicit factor of safety or reliability estimate.

The vertical strain at the top of the subgrade was calculated using the program CIRCLY, for the 40 kN (9,000 lb) dual tire wheel load (30.5 cm [12 in.] center-to-center) and 690 kPa (100 psi) contact pressure, and the pavement structures shown earlier. The difference in thermal environment between the design conditions and HVS conditions was not addressed in this study. The asphalt concrete and ATPB stiffnesses included in the subgrade strain computations are

those at 20°C, approximately the temperature maintained at the surface of the Section 500RF pavement. A temperature sensitivity study of the type used to estimate the effects on fatigue life of in-situ temperatures for typical California environments has not been performed for subgrade rutting.

4.2.2 Subgrade Rutting Performance Analysis

The permissible ESALs for the calculated subgrade strain for each of the five cases are compared with the simulated HVS ESALs to fatigue failure as follows:

Case	Permissible ESALs by Asphalt Institute Subgrade Strain Criteria	Simulated HVS ESALs to Fatigue Failure
Design conditions with standard mix (8% AV and 5% AC), full friction interface (Case 1)	18,770,000	8,056,000
HVS conditions with standard mix (8% AV and 5% AC), full friction interface (Case 2)	26,535,000	18,133,000
HVS conditions with standard mix (4.4% AV bottom lift, 7.8% AV top lift and 5% AC: full friction interface (Case 3)	30,050,000	52,951,000
HVS conditions with HVS mix (4.4% AV bottom lift, 7.8% AV top lift and 5% AC: full friction interface (Case 4)	33,279,000	292,237,000
HVS conditions with HVS mix (4.4% AV bottom lift, 7.8% AV top lift and 5% AC: frictionless interface (Case 5)	5,239,000	3,129,000

The permissible ESALs for subgrade rutting for Case 1 are more than 2.3 times greater than the simulated HVS ESALs to fatigue cracking for the same case. This indicates that fatigue cracking is probably the dominant failure mode for Section 500RF for the design conditions and

standard mix, which is the most critical case when a full friction interface between the asphalt concrete layers is assumed.

Comparison of the permissible ESALS for Cases 1 and 2 indicates that the HVS conditions were less critical than the design conditions with respect to subgrade rutting. The differences between the HVS and design conditions for the subgrade strain criteria evaluation consisted of the thicker asphalt concrete layer, thinner combined aggregate base and subbase layers, and increased ATPB, base, subbase and subgrade moduli of the HVS conditions. As for Case 1, fatigue appears to be the dominant failure mode for Case 2, since the permissible ESALs for subgrade strain are approximately 1.5 times greater than the simulated HVS ESALs to fatigue failure.

The beneficial effect of increased compaction of the asphalt concrete on subgrade rutting can be seen from comparison of the results for Case 3 versus Case 2. Reduction of the air-void content in the standard mix from 8 percent to the air-void contents obtained in the Section 500RF pavement increases the permissible ESALs for subgrade rutting by about 13 percent. The increase is the result of the greater protection provided to the subgrade by the increased stiffness of the asphalt concrete at the smaller air-void contents.

Comparison of Case 4 with Case 3 shows that substitution of the HVS mix for the standard mix results in a further increase in permissible ESALs for subgrade rutting, due to the larger stiffness of the HVS mix. Despite the increase in permissible ESALs for subgrade rutting, subgrade rutting becomes the presumed dominant failure mode for Case 4 due to the large difference in fatigue resistance between the HVS mix and the standard mix.

Simulation of a frictionless interface between the two asphalt concrete layers results in a significant reduction in the estimate of permissible ESALs for subgrade rutting, as can be seen

from comparison of Case 5 with Case 4. The permissible ESALs for the frictionless interface condition are about 6.4 times less than for the full friction condition. The difference is due to reduction of the ability of the pavement to distribute stresses within the asphalt concrete layer because of the frictionless interface, resulting in increased vertical compressive strain in all underlying layers. The actual interface condition lies in between the full friction and frictionless cases simulated, however, the estimates of permissible ESALs indicate that a reduction in the bonding between the asphalt concrete layers results in increased compressive strains and subgrade rutting in the underlying layers, as well as reduced asphalt concrete fatigue life.

All of the estimates of permissible ESALs for subgrade rutting are less than the 112,000,000 HVS ESALs applied to the section, which suggests that there is some conservatism in the Asphalt Institute criteria. The permissible ESALs estimated from the Asphalt Institute criteria should be considered design estimates which will be lower than measured performance, although the safety factor is unknown.

For all cases, except Cases 3 and 4, the simulated HVS ESALs to fatigue failure is less than the permissible ESALs for subgrade rutting based on the Asphalt Institute criteria, which strongly indicates that fatigue is the dominant distress mode for the Section 500RF pavement. This is validated by comparison of the 112,000,000 HVS ESALs applied to Section 500RF with the average rut depth in the combined base, subbase and subgrade layers of about 4.5 mm (0.17 in.), and the average maximum rut depth in the combined untreated layers of about 6.2 mm (0.24 in.). The majority of the rutting on Section 500RF occurred in the asphalt concrete and ATPB layers.

In addition, the results presented in this study provide a strong indication that the air-void content of the asphalt concrete surface and the interface condition between asphalt concrete layers can significantly impact subgrade rutting performance.

4.3 FINDINGS

In general, the analyses reported herein found a rather good correspondence between the Caltrans design estimate of approximately 1,000,000 ESALs and the HVS test measurement of approximately 112,000,000 ESALs. The major impediment to reconciling these two estimates seems to be the inability to accurately quantify effects of the layer interface condition. The following findings of this aspect of the study are considered to have been reasonably well demonstrated and to represent appropriate hypotheses for future inquiry and validation:

1. Based on the performance of Section 500RF under accelerated HVS loading, Caltrans flexible pavement designs for TI=9.0 pavements with ATPB layers that are relatively undamaged by water appear to be reasonably reliable, eliminating the risk of premature fatigue failure by providing reliability levels up to 90 percent or more. At the same time, some specific conditions have been identified in prior analysis where California pavement designs may be particularly susceptible to fatigue cracking (*9*).
2. Fatigue life measurements under full-scale accelerated loading are typically expected to exceed design estimates because design estimates must incorporate a safety factor to minimize the risk of premature failure while accommodating, at the same time, expected variabilities in testing, in construction, in traffic, and in mix design. For a design reliability level of 90 percent, the computed ratio using the fatigue analysis and design system of simulated HVS ESALs to design ESALs was approximately 3.7.

3. The mixture fatigue analysis and design system proved to be an effective tool for explaining fatigue performance of the HVS pavement. The relatively good agreement between the simulation estimate and actual HVS measurement suggests that the analysis and design system may eventually prove useful for structural design as well as for mixture design. The analysis suggests no need for recalibrating the analysis and design system based on the performance of this HVS test pavement.
4. According to the Asphalt Institute's subgrade strain criterion, severe subgrade rutting in the HVS pavement would not be expected. Testing of HVS Section 500RF generally confirmed the Asphalt Institute's criterion.
5. The analysis reported herein corroborates prior work showing the importance of good compaction of the asphalt concrete surface to superior fatigue performance. Good compaction of the mix also reduces the magnitude of subgrade rutting.
6. Loss of bonding at the interface between asphalt-concrete lifts can cause a significant degradation in fatigue life and an increase in subgrade rutting.
7. Different mixes, even with similar binders, can result in significantly different fatigue performance. The importance and effectiveness of laboratory fatigue testing and simulation to quantitatively estimate differences in fatigue performance in-situ was demonstrated by the analyses presented in this chapter.
8. The protected environment of HVS testing at the Richmond Field Station is different from that experienced in natural California settings. With regard to fatigue distress, the moisture environment is likely to be more benign in the testing enclosure at RFS while the temperature environment is slightly more severe than comparable, unprotected locations.

CHAPTER 5

SUMMARY AND CONCLUSIONS

5.1 SUMMARY

This report, the second in a series detailing the results of the CAL/APT program being performed jointly by UCB and Caltrans, describes the results of the first HVS test conducted by the UCB staff on the first of four pavement test sections, 500RF, an AC section containing an ATPB.[3] Also included are: initial analyses of the test section; analyses of the performance of the test section; comparison of its performance relative to the performance of comparable pavements in three climatic regions in California; evaluation of the effect of air-void content on its performance, and implications of these results relative to current Caltrans pavement construction requirements since the test pavements were constructed according to Caltrans specifications.

HVS trafficking of section 500RF commenced on 3 May 1995 and was completed on 8 November 1995. A total of 2.57×10^6 load repetitions were applied during this period consisting of 150,000 repetitions of a 40 kN (9000 lb) half axle load, 50,000 repetitions of an 80 kN (18,000 lb) load, and the remainder with a 100 kN (22,500 lb) load.

The first load associated (fatigue) cracks were observed at approximately 650,000 load repetitions. At 2.57×10^6 load repetitions cracking had reached a level which, according to

---

[3]It must be emphasized that the ATPB remained in a relatively dry state throughout the duration of the loading for this test program.

Caltrans pavement management criteria, resembled a newer pavement that had failed by alligator cracking. The average maximum vertical rut depth at the centerline of the test section at this point was 15 mm, considered failure due to rutting by Caltrans criteria. It was noted that the cracks were hairline (less than 1/32 inch) and pumping was not observed in contrast to typical field sections.

Thicknesses for the pavement sections were selected on the basis of a Traffic Index of 9 (800,000 to 1,200,000 ESALs) and a design "R" value for the subgrade of 10 (measured range, 4 to 30) (*2*). The number of ESALs actually carried according to the Caltrans conversion [(actual axle load/18000)$^{4.2]}$ is 112 million, which corresponds to a Traffic Index of 15.8.

When the construction of the test pavements had been completed (April 1995), cores and slabs of the asphalt concrete were taken from the pavement for testing. A weakness in the bond (and even a lack thereof) between the two asphalt concrete lifts was observed. At the conclusion of the loading on the test section, a number of cores were taken to check changes in densities of the lifts. When these cores were removed it was noted the two lifts were unbonded and that there was evidence of movement between the lifts resulting from the deflection of the pavement under load. Also, it was observed that the cracking observed at the surface existed only in the top lift; the lower lift was uncracked.

Measurements of densities on cores from the trafficked portion of the pavement indicated that traffic compaction was limited to the upper lift of the asphalt concrete. In this lift the air void content was reduced by about 1.6 percent (from about 7.8 percent to 6.2 percent).

5.2 CONCLUSIONS

From the results of tests on Section 500RF and associated analyses, the following conclusions appear warranted.

1. The HVS testing environment at the Richmond Field Station with respect to fatigue performance is more benign relative to moisture effects but provides a slightly more severe temperature environment than that which might be expected in natural California settings.
2. The importance of mix compaction on pavement performance has been conclusively demonstrated and the current Caltrans mix compaction specification has been shown to permit excessive air-void contents. Improved pavement performance that could result from "tightening" the specification has been demonstrated by the results obtained from Section 500RF. Such a change in the specification has the potential to result in large (and quantifiable) savings to the State.
3. The fatigue analysis and design system developed during the SHRP program and refined within the CAL/APT program has been used to explain the difference between the design estimate for Section 500RF of approximately 1×10^6 ESALs and the HVS measurement of approximately 112×10^6 ESALs. Although some of the discrepancy remains unaccounted for (possibly as a result of difficulties in modeling the bonding between the two lifts of asphalt concrete), the overall agreement helps to validate both the analysis and design system as a mechanism for structural design and the current Caltrans design methodology.
4. The weak bond between asphalt-concrete lifts in Section 500RF has been found to significantly degrade pavement performance. While the extent to which weak bonding may be prevalent in California pavements is unknown, the fact that the HVS test

pavement was constructed according to standard Caltrans procedures suggests possible problems within pavements in service. If additional investigations confirm such possible problems, remedial action such as the application of suitable tack coats will result in significant improvements in pavement performance.

5. The Asphalt Institute's subgrade strain criterion for controlling subgrade rutting has been confirmed by the 500RF test. While additional validation is necessary, this criterion enables a mechanistic/empirical analysis of subgrade rutting to supplement routine Caltrans design procedures in special investigations.

6. Results of the 500RF test suggest that the Caltrans structural design procedure is conservative, presumably because it must accommodate a wide variety of mixes, climates, construction practices, etc. The likely result in many instances is overdesign. The economic consequences of this overdesign can, conceptually at least, be evaluated by life-cycle cost models. The analysis and design system, being developed and refined is part within the CAL/APT program, will provide a basis for more accurate structural designs compatible with acceptable levels of reliability.

REFERENCES

1. California Department of Transportation, *CAL/APT Strategic Plan (July 1995-July 1997)*, adopted by the CAL/APT Steering Committee, May 18, 1995.

2. Harvey, J., et al., *Initial CAL/APT Program: Site Information, Test Pavements Construction, Pavement Materials Characteristics, Initial CAL/HVS Test Results, and Performance Estimates*, Report for the California Department of Transportation, Institute of Transportation Studies, University of California, Berkeley, June 1996.

3. California Department of Transportation, *Highway Design Manual*, Section 600, Sacramento, January, 1990.
   Also:
   California Department of Transportation, NEWCON90 Computer Program, Version April_30_91.1, Sacramento, 1991.

4. Transportek, CSIR, *Guideline to the Use and Operation of the Heavy Vehicle Simulator (HVS)*, March 1995.

5. Sousa, J.B., J. Deacon, S. Weissman, J. Harvey, C. Monismith, R. Leahy, G. Paulsen, and J. Coplantz (1994), *Permanent Deformation Response of Asphalt-Aggregate Mixes*, Strategic Highway Research Program Report No. A-414, National Research Council, Washington, D.C., 1994.

6. Tayebali, A.A., J.A. Deacon, J.S. Coplantz, J.T. Harvey, F.N. Finn, and C.L. Monismith, "Fatigue Response of Asphalt-Aggregate Mixes: Part I Test Method Selection; Part II Extended Test Program; Part III Mix Design and Analysis," Strategic Highway Research Program Report No. A-404, National Research Council, Washington, D.C., 1994.

7. Deacon, J., J. Coplantz, A. Tayebali, and C. Monismith, "Temperature Considerations in Asphalt-Aggregate Mixture Analysis and Design," Transportation Research Record 1454, Transportation Research Board, 1994, pp. 97-112.

8. Weissman, S.L., and J.L. Sackman, Heavy Vehicle Simulator: *Simulations of the Effects of Wheel Pressure on an Unbonded Layered Asphalt Concrete Pavement*, Symplectic Engineering Corporation, Albany, CA., August 1996.

9. Harvey, J., J. Deacon, B. Tsai, and C. Monismith, *Fatigue Performance of Asphalt Concrete Mixes and Its Relationship to Asphalt Concrete Pavement Performance in California,* RTA-65W485-2, Asphalt Research Program, CAL/APT Program, Institute of Transportation Studies, University of California, Berkeley, 1996.

10. Deacon, J.A., *Modification, Validation, and Calibration of Climatic-Materials-Structural Pavement Analysis Program*, Internal Report, UC Berkeley, September 23, 1995.

11. Harvey, J.T., and B. Tsai, *Asphalt Treated Permeable Base Performance: Comparison of Laboratory, APT, and Field Results* (draft pending).

12. American Association of State Highway and Transportation Officials, *DNPS86, AASHTO Design of New Pavement Structures Program Version 1*, September, 1986.

13. Wardle, L.J., *Program CIRCLY— A Computer Program for the Analysis of Multiple Complex Circular Loads on Layered Anisotropic Media: User's Manual*, Geomechanics Computer Program No. 2, CSIRO Division of Applied Geomechanics, Melbourne, Australia, 1976.

14. Harvey, J.T., J.A. Deacon, A.A. Tayebali, R.B. Leahy, and C.L. Monismith, "A Reliability-Based Mix Design and Analysis System for Mitigating Fatigue Distress," Paper prepared for 8th International Conference on Asphalt Pavements, Seattle, WA, August 1997.

15. Reese, R., Faxed results of comparison of Valley binders aging properties with CAL/APT goal 1 asphalt-concrete properties. Caltrans Engineering Service Center, Sacramento, October 6, 1985.

16. Santucci, L.E., "Thickness Design Procedure for Asphalt and Emulsified Asphalt Mixes," *Proceedings*, Fourth International Conference on the Structural Design of Asphalt Pavements, University of Michigan, August, 1977, pp. 424-456.

17. Shook, J.F., F.N. Finn, M.W. Witczak, and C.L. Monismith, "Thickness Design of Asphalt Pavements— The Asphalt Institute Method," *Proceedings*, Fifth International Conference on the Structural Design of Asphalt Pavements, University of Michigan, August, 1982, pp. 17-44.

APPENDIX A

HVS LOAD DISTRIBUTION

The HVS can simulate various traffic distributions varying from no wander (channelized traffic) to a uniform distribution. The wandering motion of the wheel on the 1 meter cross section of the test pad is controlled by two settings on the HVS. The first setting controls the lateral shift distance of the test carriage and the second controls the number of repetitions per lateral beam setting. For instance, it is possible to do 5 repetitions with the test carriage in a fixed position before it moves to the next lateral position. Different traffic distributions are therefore possible using both different configurations of lateral movement and different number of repetitions per lateral movement.

In ideal conditions the wandering width and traffic loading distribution should be determined from measurements on in-service real pavements and should then be simulated with the HVS using the appropriate settings. For the first series of tests at the Richmond Field Station it was decided to keep the number of repetitions per lateral movement at one and the lateral shift at 40 mm (~1.5 in). This setting, which is similar to the traditional HVS tests, produces a traffic pattern somewhat similar to a normal distribution. This traffic pattern has been presented in the report. in Chapter 2 as Figure 2.4.

Three plateaus are evident from Figure 2.4, one in the center of the section and one at either side of the center line area. These plateaus are caused by the effect which the dual tires have on the loading distribution and is a function of the distance between the two tires and is therefore not a function of the HVS settings. The dual tires are placed 366 mm apart, similar to the standard distance used in dual tire trucks, which causes the load distribution presented in Figure 2.4.

From this Figure it can be seen that the centerline area of the test section receives approximately 64 percent of the load applications applied to the 1 meter wide section, and the

left and right side measuring areas receive approximately 46 percent of the load applications. This means that the left and right side measuring areas experience approximately 30 percent less traffic than the center line area.

Care should be taken in the interpretation of these results. This traffic loading pattern has a definite influence on the permanent deformation pattern and plastic flow of surface material of the test pavement but its influence on elastic deflections should be handled with caution. Elastic deflections are influenced by many factors, such as material properties and temperature, and establishing a relationship between the traffic loading distribution and elastic deflections is complicated and is not included in this study.

APPENDIX B

EFFECT OF TEMPERATURE ENVIRONMENT ON FATIGUE IN HVS

From an examination of the results of the study reported in Chapter 4 some additional questions were raised. The strain computations that had been performed indicated the somewhat counter-intuitive result that critical. tensile strains increase with increases in top-lift stiffness (Figure B Moreover, the most damaging temperatures for the HVS pavement were found to be lower in magnitude than the range of 25°C to 35°C which has been identified in prior investigations (Figure B2).

To determine the extent to which these findings might result from the abnormally large loading of the HVS and the large ATPB modulus that had been used in the analysis, additional simulations were performed. The critical strain location was assumed to be the same but adjustments were made to the structure and loading as follows:

Top lift	74 mm	0.35	varies with temperature
Bottom lift	76 mm	0.35	varies with temperature
ATPB	76 mm	0.40	345 MPa
Aggregate base/subbase	310 mm	0.35	242 MPa
		0.45	69 MPa

Loading consisted of dual tires having a combined force of 40 kN with center-to-center spacing of 305 mm and contact pressure of 690

The revised simulations yielded a more expected relationship between tensile strain and AC moduli (Figure B3). Moreover, the range of damaging temperatures. was morenearly that which had been expected (Figure 4.4a. Chapter 4). Accumulated fatigue damage for the four temperature environments was as follows:

HVS	0.541
Coastal	0.510
Mountain	0.467
Desert	0.449

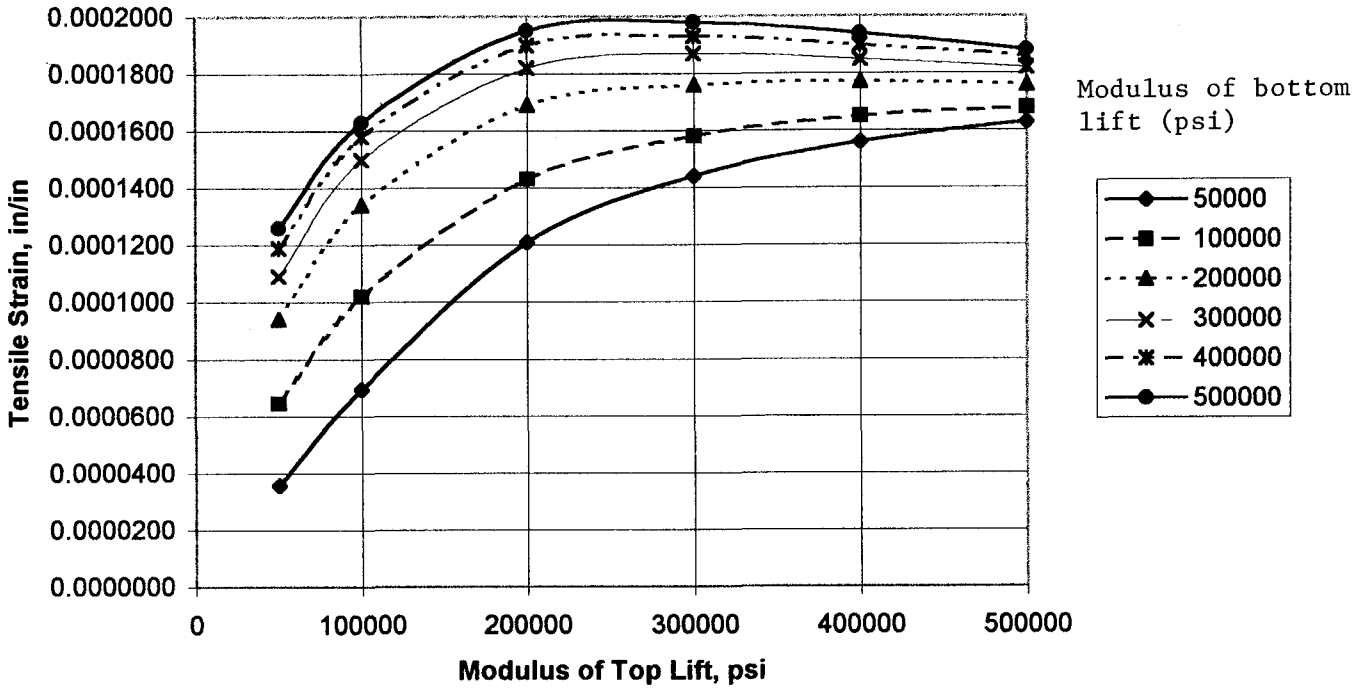

Figure B1 Tensile Strain as a Function of Modulus of Top Lift for Various Stiffnesses of the Bottom Lift (E for ATPB-1200 MPa, 40 kN Load on Dual Tires)

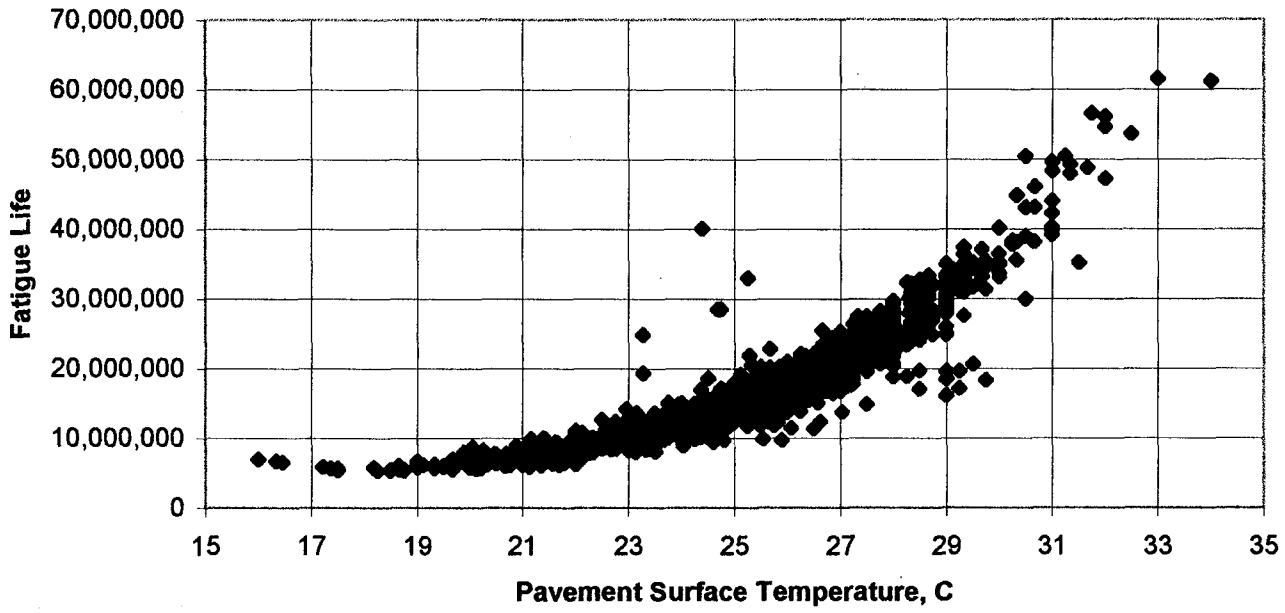

Figure B2 Simulated HVS Fatigue Life for Hourly Temperature Distributions

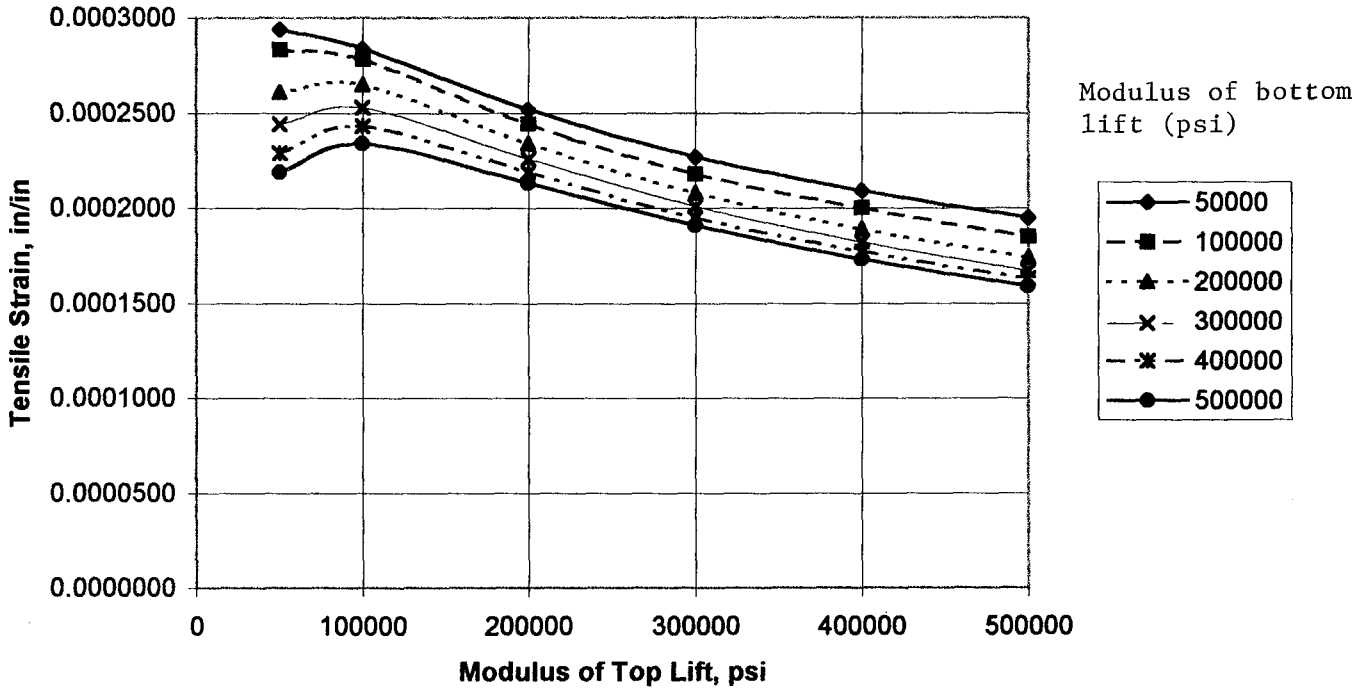

Figure B3 Tensile Strain as a Function of Modulus of Top Lift for Various Stiffnesses of the Bottom Lift (E for ATPB-345 MPa, 40 kN Load on Dual Tires)

For each temperature environment, the most damaging temperatures were in the approximate range of 25°C to 35°C (Figures 4.4a-d, Chapter 4). The fact that a greater fraction of the hourly temperatures were in this critical range at the RFS site than at the other three locations helps to explain why simulated damage accumulated more rapidly at RFS than at the other three locations.. The ranking of the four environments with respect to their susceptibility to fatigue distress remained the same as before.

Because of doubts about the location of the critical strain level and about possible confounding effects of the very large HVS load, additional ELSYM5 simulations were performed. The first set investigated the location of the critical strain level by examining additional locations on the underside of the bottom lift both parallel and perpendicular to the direction of loading. For the 100 kN (22,500 lb) test load, the critical strain was located just slightly off the load centerline; its magnitude, however, was essentially the same as the centerline strain. The second set investigated the possible effect of load magnitude. The question here was whether the increasing load radius associated with increasing loads might actually cause the critical tensile strain to decrease as a result of increases in the ratio of load radius to layer thickness. Computations in which the dual-tire loading was increased from 40 kN to 100 kN (8000 to 22,500 lbs) showed that this was not the case: increasing load magnitudes consistently resulted in increasing tensile strains.

The final analysis reexamined the HVS loading [100 kN (22,500 lb) on dual tires] but adjusted the ATPB modulus downward from 1200 MPa (174,165 psi) to 345 MPa (50,000 psi). The strain simulations are summarized in Figure B4, and Figures B5a-d identify the distributions of fatigue life and hourly temperature. As indicated by the following

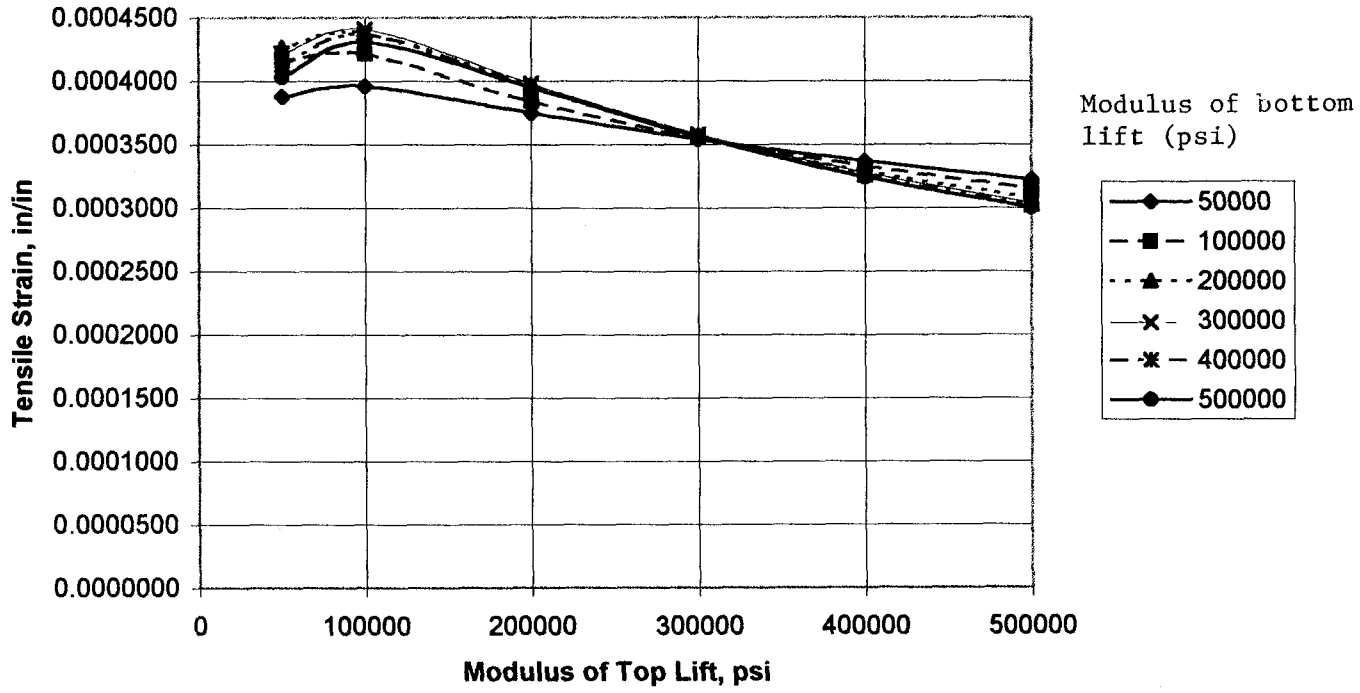

Figure B4 Tensile Strain as a Function of Modulus of Top Lift for Various Stiffnesses of the Bottom Lift (E for ATPB-345 MPa, 100 kN Load on Dual Tires)

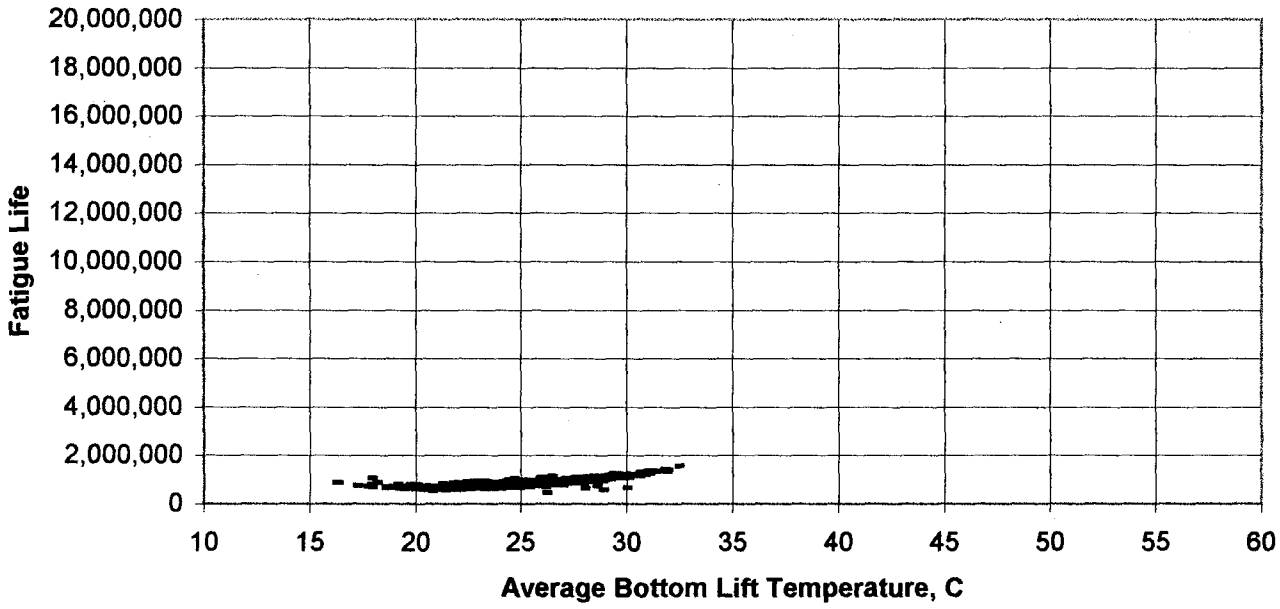

a. HVS test section at RFS

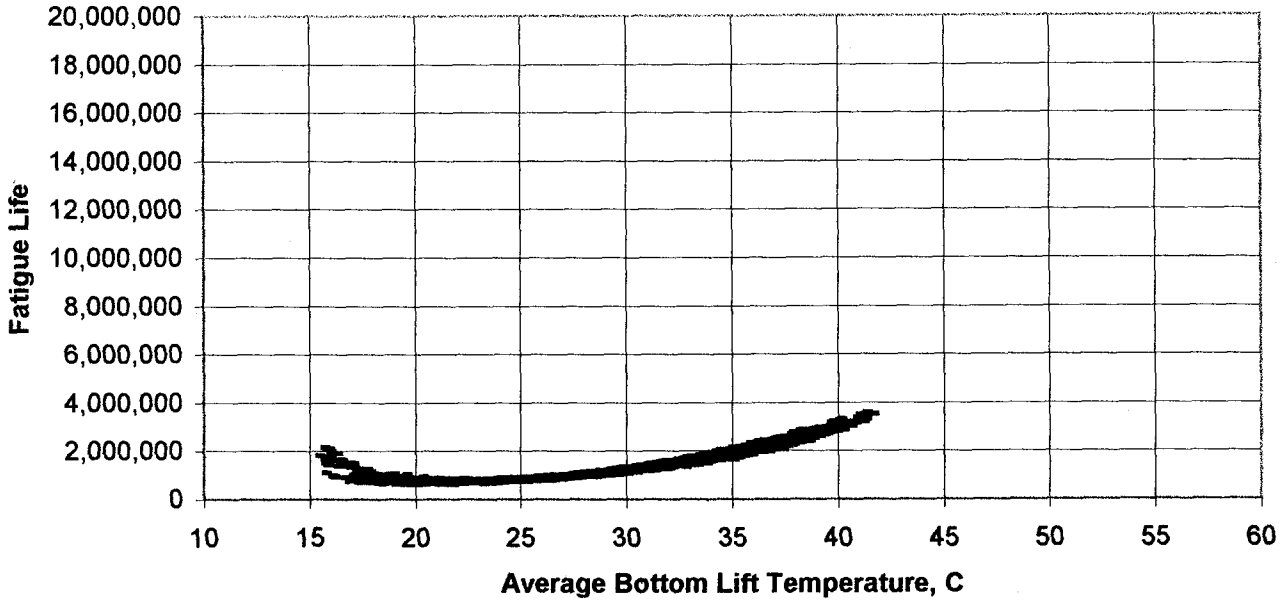

b. Coastal

Figure B5 Predicted Fatigue Life and Hourly Temperature of the Bottom Lift for Four California Environments

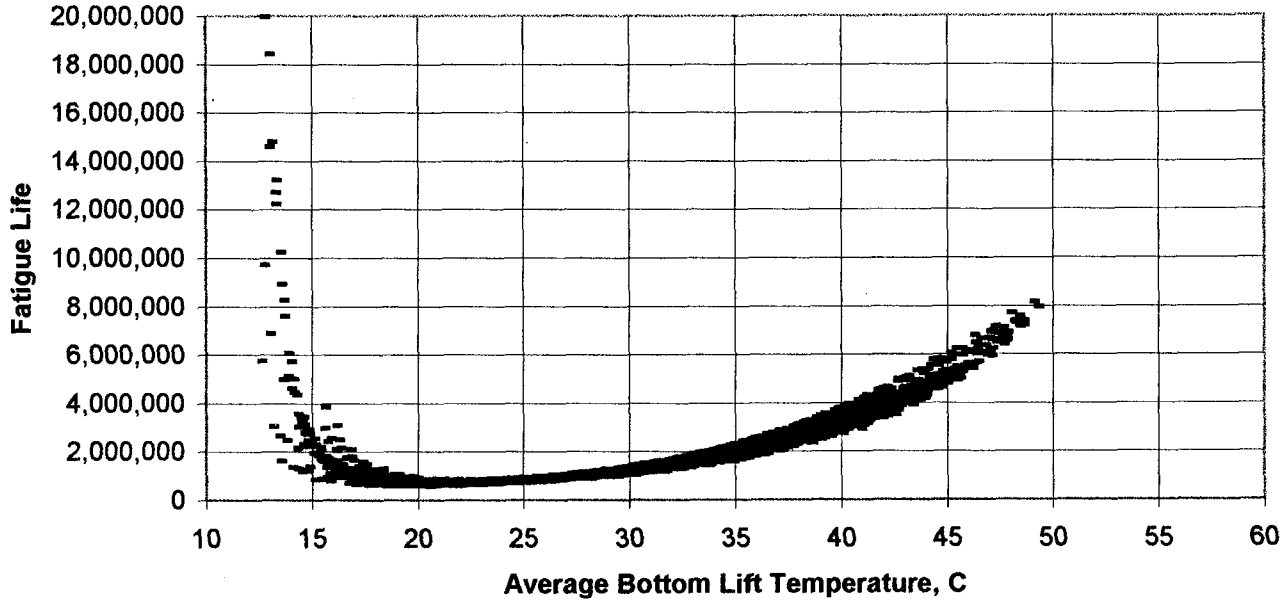

c. Mountain

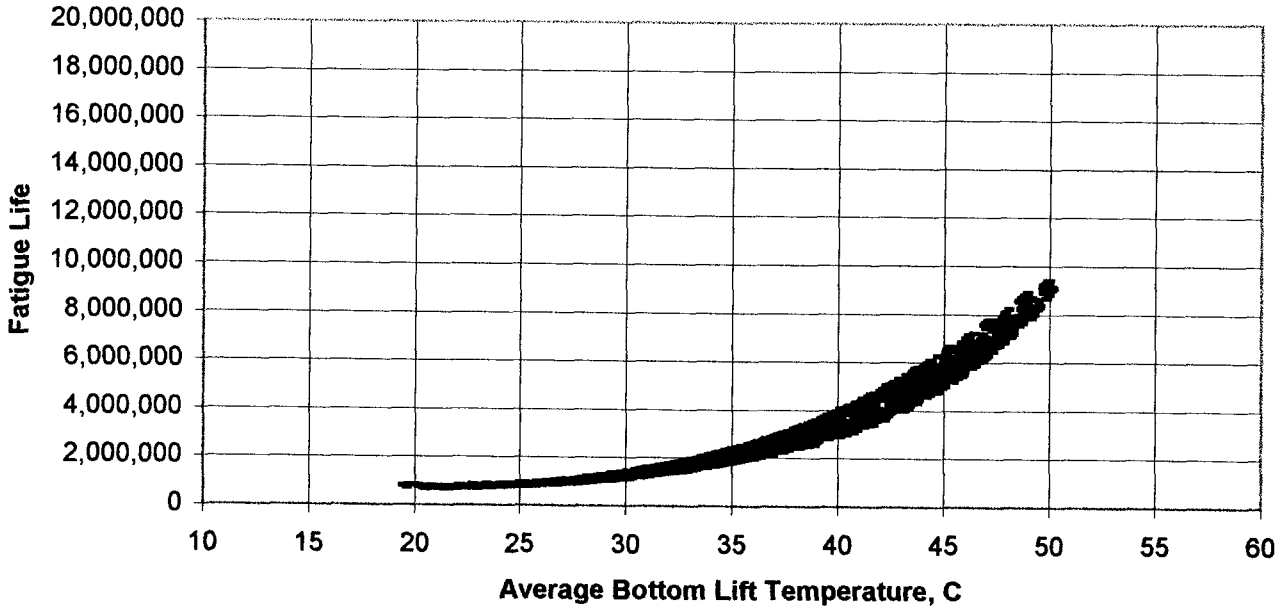

d. Desert

Figure B5 Predicted Fatigue Life and Hourly Temperature of the Bottom Lift for Four California Environments (cont.)

damage accumulations, the fatigue-susceptibility ranking of the four locations remained unchanged:

HVS	3.002
Coastal	2.343
Mountain	1.980
Desert	1.396

This analysis shows that the HVS test environment at RFS is likely to result in greater accumulation of fatigue distress than other environments in California. However, it should be emphasized that the analysis did not recognize the "frictionless" interface between top and bottom lifts and considered a "hypothetical" mixture rather than the actual mix used in test section 5OORF.

APPENDIX C

INFLUENCE OF STIFFNESS OF TOP LIFT OF THE ASPHALT CONCRETE ON SURFACE DEFLECTION

A very limited analytical study was performed to investigate the influence of stiffness of the top lift of the asphalt concrete layer on elastic surface deflection. For this model the stiffness values of the top lift were varied while the moduli values of all other layers were kept constant which means that the effect on surface deflections due to behavior changes in layers below the AC top lift was ignored.

The pavement section was modeled with the following stiffness properties:

AC top lift	1800-4600 MPa (261,000 - 667,600 psi)
AC bottom lift	4750 MPa (688,700 psi)
ATPB	1200 MPa (174,000 psi)
AB/ASB	189 MPa (27,400 psi)
Subgrade	69 MPa (10,000 psi)

The bond between the top and bottom lifts of the AC was assumed to be frictionless (based on observed debonding between lifts in the cores taken from the test section after the completion of the HVS loading). The range in moduli selected for the top lift was assumed to represent that which might be associated with the change in stiffness resulting from the fatigue cracking observed. The CIRCLY program was used to determine the surface deflection between the tires when loaded to 40 kN and 100 kN.

Results of the computations are shown in Figure C 1. It will be observed that for a range in stiffness of the top lift little change in the surface deflection is observed.. This is most likely due to the good support of the layers underneath the AC top lift. As the stiffness of the top lift changes, the effective combined modulus of the whole pavement structure is not significantly changed therefore the surface deflections are not influenced.

This observation corroborates somewhat with the elastic deflection values obtained both with the RSD and MDD. Although some changes in the in-depth elastic deflection

inside the pavement did occur, the surface deflection (the net effect of all in-depth deflections) did not significantly change from 500,000 load repetitions onwards. This was observed despite the fact that the top AC layer changed from an intact state to cracked.

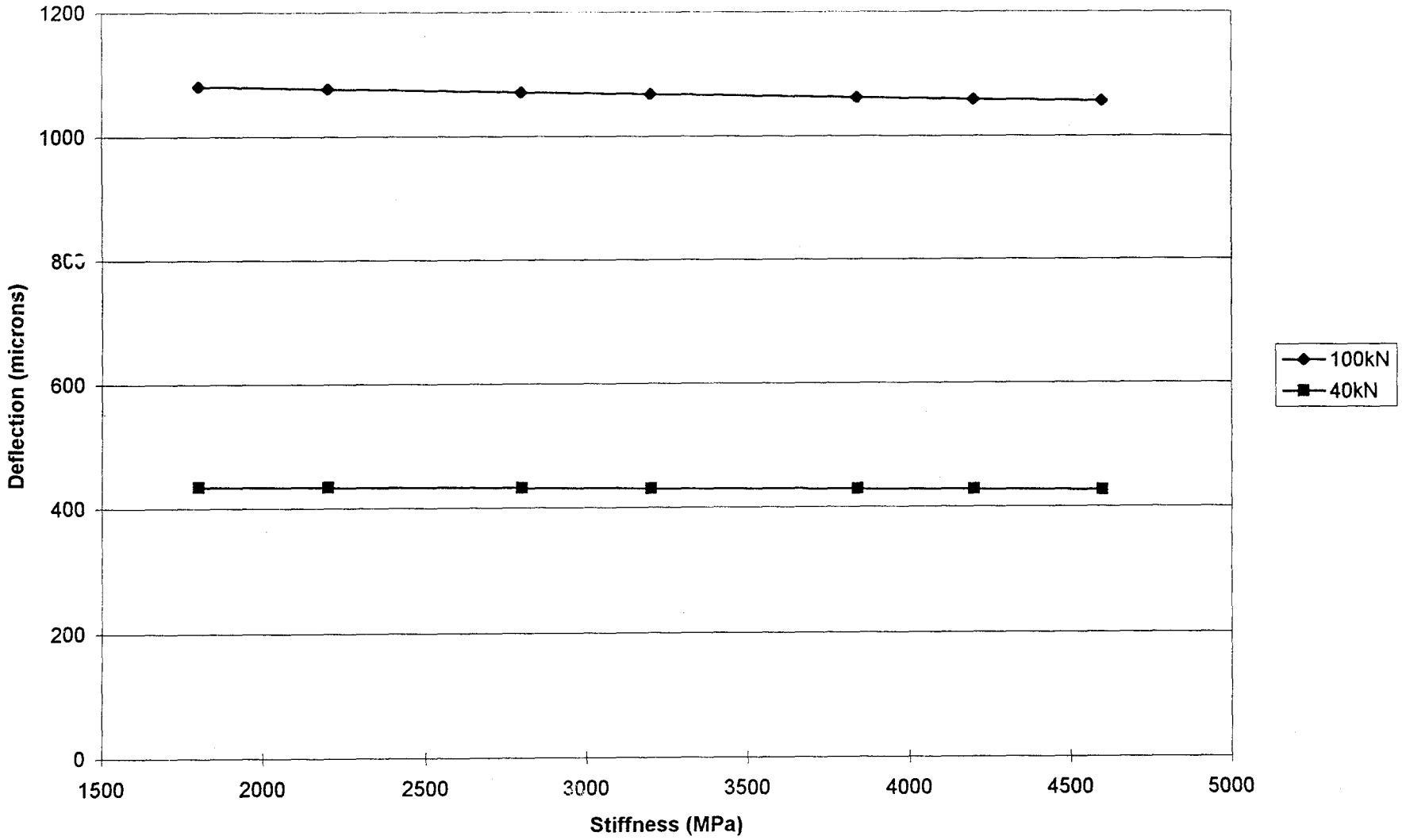

Figure C1 Effect of Stiffness of the Top Lift of AC on Surface Deflection